2019-06

MODELING THE IMPACTS OF CLIMATE CHANGE ON TROPICAL CYCLONE FORMATIONS IN THE WESTERN NORTH PACIFIC

Carter, Robert B.

Monterey, CA; Naval Postgraduate School

NAVAL POSTGRADUATE SCHOOL

MONTEREY, CALIFORNIA

THESIS

MODELING THE IMPACTS OF CLIMATE CHANGE ON TROPICAL CYCLONE FORMATIONS IN THE WESTERN NORTH PACIFIC

by

Robert B. Carter

June 2019

Thesis Advisor: Tom Murphree
Co-Advisor: David Meyer,
Statistical Solutions LLC

THIS PAGE INTENTIONALLY LEFT BLANK

REPORT DOCUMENTATION PAGE	*Form Approved OMB No. 0704-0188*

1. AGENCY USE ONLY *(Leave blank)*	**2. REPORT DATE** June 2019	**3. REPORT TYPE AND DATES COVERED** Master's thesis

4. TITLE AND SUBTITLE
MODELING THE IMPACTS OF CLIMATE CHANGE ON TROPICAL CYCLONE FORMATIONS IN THE WESTERN NORTH PACIFIC

5. FUNDING NUMBERS

6. AUTHOR(S) Robert B. Carter

7. PERFORMING ORGANIZATION NAME(S) AND ADDRESS(ES)
Naval Postgraduate School
Monterey, CA 93943-5000

8. PERFORMING ORGANIZATION REPORT NUMBER

9. SPONSORING / MONITORING AGENCY NAME(S) AND ADDRESS(ES)
N/A

10. SPONSORING / MONITORING AGENCY REPORT NUMBER

11. SUPPLEMENTARY NOTES The views expressed in this thesis are those of the author and do not reflect the official policy or position of the Department of Defense or the U.S. Government.

12a. DISTRIBUTION / AVAILABILITY STATEMENT
Approved for public release. Distribution is unlimited.

12b. DISTRIBUTION CODE
A

13. ABSTRACT (maximum 200 words)

A dynamical-statistical modeling approach was used to investigate climate change impacts on tropical cyclone (TC) formations in the western North Pacific (WNP). Reanalysis data and climate model projections were analyzed for 1981–2050 to identify both past and future impacts. The projections came from the Community Climate System Model version 4 (CCSM4). The primary analysis tool was a statistical model that uses information about large-scale environmental factors (LSEFs) to predict the probability of TC formation. This model was built using data on the LSEFs and TC formations during the last several decades. We forced the statistical model with the reanalysis LSEFs and with the climate model LSEFs outputs from the climate model to produce formation probability analyses for 1981–2018. The two methods for calculating the probabilities both showed increasing trends during this period for the central WNP region in which most WNP formations occur. These trends are consistent with the observed increase in TC formations in this region during this period. The climate model probabilities based on long-term mean, El Niño, and La Niña LSEFs for 1981–2018 were also consistent with observed TC formations. For future decades, the climate model projections showed multi-decadal increases in both TC formation probabilities and the WNP area in which TC formation is most probable. We recommend continued use of dynamical-statistical methods as observational data and climate models improve.

14. SUBJECT TERMS
tropical cyclone, climate change, statistical modelling, large scale environmental factors, LSEF, Western Pacific, Representative Concentration Pathway (RCP), climate system predictors, hindcast, tropical cyclone formation areas, Climate Forecast System Reanalysis, Climate Forecast System version 2, Coupled Model Intercomparison Project Phase 5, CMIP5, Community Climate System Model version 4

15. NUMBER OF PAGES
125

16. PRICE CODE

17. SECURITY CLASSIFICATION OF REPORT	**18. SECURITY CLASSIFICATION OF THIS PAGE**	**19. SECURITY CLASSIFICATION OF ABSTRACT**	**20. LIMITATION OF ABSTRACT**
Unclassified	Unclassified	Unclassified	UU

NSN 7540-01-280-5500

Standard Form 298 (Rev. 2-89)
Prescribed by ANSI Std. 239-18

THIS PAGE INTENTIONALLY LEFT BLANK

Approved for public release. Distribution is unlimited.

MODELING THE IMPACTS OF CLIMATE CHANGE ON TROPICAL CYCLONE FORMATIONS IN THE WESTERN NORTH PACIFIC

Robert B. Carter
Lieutenant Commander, United States Navy
BS, United States Naval Academy, 2006

Submitted in partial fulfillment of the
requirements for the degree of

MASTER OF SCIENCE IN METEOROLOGY AND PHYSICAL OCEANOGRAPHY

from the

NAVAL POSTGRADUATE SCHOOL
June 2019

Approved by: Tom Murphree
Advisor

David Meyer
Co-Advisor

Wendell A. Nuss
Chair, Department of Meteorology

THIS PAGE INTENTIONALLY LEFT BLANK

ABSTRACT

A dynamical-statistical modeling approach was used to investigate climate change impacts on tropical cyclone (TC) formations in the western North Pacific (WNP). Reanalysis data and climate model projections were analyzed for 1981–2050 to identify both past and future impacts. The projections came from the Community Climate System Model version 4 (CCSM4). The primary analysis tool was a statistical model that uses information about large-scale environmental factors (LSEFs) to predict the probability of TC formation. This model was built using data on the LSEFs and TC formations during the last several decades. We forced the statistical model with the reanalysis LSEFs and with the climate model LSEFs outputs from the climate model to produce formation probability analyses for 1981–2018. The two methods for calculating the probabilities both showed increasing trends during this period for the central WNP region in which most WNP formations occur. These trends are consistent with the observed increase in TC formations in this region during this period. The climate model probabilities based on long-term mean, El Niño, and La Niña LSEFs for 1981–2018 were also consistent with observed TC formations. For future decades, the climate model projections showed multi-decadal increases in both TC formation probabilities and the WNP area in which TC formation is most probable. We recommend continued use of dynamical-statistical methods as observational data and climate models improve.

THIS PAGE INTENTIONALLY LEFT BLANK

TABLE OF CONTENTS

THIS PAGE INTENTIONALLY LEFT BLANK

LIST OF FIGURES

LIST OF TABLES

THIS PAGE INTENTIONALLY LEFT BLANK

LIST OF ACRONYMS AND ABBREVIATIONS

ACE	accumulated cyclone energy
CCSM4	Community Climate System Model version 4
CFR	Central Formation Region
CFSR	Climate Forecast System Reanalysis
CFSV2	Climate Forecast System Version 2
CFSRV2	CFSR/CFSV2
CMIP5	Coupled Model Intercomparison Project Phase 5
CP	central Pacific
CPC	Climate Prediction Center
CSU	Colorado State University
DoD	Department of Defense
ECHAM	European Center Hamburg Global Climate Model
EMCWF	European Centre for Medium-Range Weather Forecasts
EN	El Niño
ENLN	El Niño/La Niña
IDL	international dateline
HADCRUT3	Hadley Centre–University of East Anglia Climatic Research Unit temperature time series since 1850
hPa	hectoPascal
HTCFS	hybrid tropical cyclone forecasting system
HURDAT2	National Hurricane Center's Central Pacific Hurricane Database
IRI	International Research Institute for Climate and Society
JASO	July, August, September, and October
JTWC	Joint Typhoon Warning Center
km	kilometer
LN	La Niña
LSEF	large-scale environmental factor
LTM	long term mean
m	meters
MEI	Multivariate ENSO Index

MJO	Madden-Julian Oscillation
NCAR	National Center for Atmospheric Research
NCEP	National Centers for Environmental Prediction
NHC	National Hurricane Center
NOAA	National Oceanic and Atmospheric Administration
NPS	Naval Postgraduate School
PCA	percent contoured area
POD	probability of detection
R1	NCEP/NCAR Reanalysis
RCP	Representative Concentration Pathway
RH	relative humidity
s	second
S2S	subseasonal to seasonal
SSLLC	Statistical Solutions LLC
SST	sea surface temperature
TC	tropical cyclone
WNP	western North Pacific

ACKNOWLEDGMENTS

Thank you, Dr. Murphree and David Meyer of Statistical Solutions LLC (SSLLC), for your guidance and expertise throughout the entire process of producing this thesis. Your time and efforts were invaluable to me and have piqued my interest in climate change and tropical cyclone research, which I hope to continue pursuing in the future.

Bruce Ford of Clear Science Incorporated, thank you for the tremendous support and time spent throughout this thesis mentoring me and teaching me technical programming concepts for my research. The progression of my thesis would not have happened without your support.

In this thesis, “we” refers to the team that conducted the research, which includes myself, Dr. Murphree, David Meyer, and Bruce Ford.

To my wife, Kaylene, whose love and support has kept me in the Navy and pursuing my career: you have been my support system throughout our eight years of marriage with your motivation and words of encouragement.

To the fellow Naval Postgraduate School (NPS) students in my cohort, Nicolaas Verhoeven, Ka Xiong, Travis Davis, Natasha Ried, Phil Smith, and Jillian Coughlin: I am grateful for the friendships we developed during my time in Monterey and hope that we will stay in touch as our careers progress.

Most importantly, all glory goes to my Heavenly Father, who guides me and helps me accomplish more than I could ever ask for.

THIS PAGE INTENTIONALLY LEFT BLANK

I. INTRODUCTION

Tropical cyclones (TCs) are one of the Earth's most unpredictable and destructive forces. Hurricane Katrina alone caused more than $160 billion in damages and was deemed the single most costly disaster in U.S. history (Patricola and Wehner 2018). TCs also affect the U.S. away from its borders, especially in the western North Pacific (WNP). The U.S. Navy has increased its presence in the WNP to protect allies and maintain peace in a tumultuous part of the world that has witnessed increased tensions with China and North Korea (Kuhn 2018). TC formation prediction and tracking is crucial to U.S. Navy operations.

As discussed in Gray (1975, 1977), TCs are influenced and affected by ocean and atmospheric temperatures over which they travel. Prior research has indicated that the average TC has a large energy requirement (4,000 calories per cm^2 per day) in the form of ocean sensible and latent heat (Gray 1975). There has been a direct link between an increase in sea surface temperature (SST) and the intensity of tropical cyclones (Emanuel et al. 2008). Observational data from the past few decades has shown that SST is on the rise, mainly due to anthropogenic reasons and Earth's climate variations (Cheng et al. 2019, Dowdy 2014). The Intergovernmental Panel on Climate Change (IPCC) (International Panel on Climate Change 2019) reports have concluded that this observed rise in global temperatures, both in the sea and atmosphere, is likely due to anthropogenic forcing in terms of increasing greenhouse gas concentrations such as carbon dioxide, methane, and other aerosols (Wang et al. 2011). The big question is: Is the world witnessing—or will it witness—more frequent and stronger TCs than in the past? The answer is uncertain, but the ocean and atmosphere are warming, which directly affects TCs as shown in modeling simulations conducted by, for example, Bengtsson et al. (2007), Knutson et al. (2015), and Nakamura et al. (2017). The more knowledge obtained concerning TCs and a warming climate, the more ready the U.S. government, and specifically the U.S. Navy, will be in future decades to prepare and hopefully avoid major catastrophic events, loss of life, and loss of operational readiness in the future.

The potential impacts of climate change on TC activity have been addressed in many prior studies such as Emanuel et al. (2008), Kossin et al. (2016), Meehl et al. (2012), Meyer and Murphree (2015), Meyer (2007), Sharmila and Walsh (2018), and Wang et al. (2011). TC activity has been studied with respect to track, intensity, poleward shifts, precipitation amounts, and cyclogenesis parameters, but the indications so far provide relatively little clear consensus as to what will change in a future warmer world with respect to TC activity (Colbert et al. 2015). However, for the globe as a whole, there are indications that TC numbers may not change much, and may decrease, but the number of very intense TCs may increase (Bengtsson et al. 2007, Bhatia et al. 2018, Emanuel et al. 2008, Knutson et al. 2015, Patricola and Wehner 2018).

In this paper, climate change is investigated on how likely it is to affect TC activity, especially TC formations, with an emphasis on TC activity in the western North Pacific.

A. SCIENTIFIC AND OPERATIONAL MOTIVATIONS FOR RESEARCH

The planning of U.S. Naval operations depends on weather and climate forecasts, especially to keep bases, ships, and aircraft operating in safe conditions. Climate information with lead times of years to decades is important in order to address the long-range goals and plans of operations in an ever-changing environment. As of right now, the Fleet Weather Center San Diego in coordination with the Naval Oceanography Antisubmarine Warfare Center Yokosuka only provides limited TC formation and hazard products coming from the Joint Typhoon Warning Center (JTWC) with a forecasting lead time on the order of days while pushing the National Weather Service's Climate Prediction Center Global Tropical Hazard and Benefits Outlook with a lead time of two weeks in the future (JTWC 2019). JTWC has addressed the need for longer lead time TC outlooks and has created a global TC formation outlook product with a two-week lead time. U.S. naval operations are planned months to years in the future, and a better understanding of the TC outlook for the future years and decades would aid U.S. Navy's focus in protecting its allies, allowing freedom of navigation, all the while maintaining a strong presence in this area with limited interruptions.

B. PRIOR RESEARCH

1. Parameters for TC Formation

A TC is defined as a closed cyclonic circulation weather event that forms over tropical oceans with a low-pressure center and low-level disturbance in the atmosphere that causes high winds, torrential rain, and storm surge (Montgomery and Farrell 1993). In the WNP, there are three categories characterizing this intensity: (1) tropical depression with rotational winds up to 17 ms^{-1}; (2) tropical storm with rotational winds up to 33 ms^{-1}; and (3) typhoon with rotational winds above 33 ms^{-1} (Montgomery and Farrell 1993).

In order to assess the role future TCs will have on Earth, TC predictors such as large scale environmental factors (LSEFs) can be used to provide a good understanding of where TCs may form (Gray 1975). Although LSEFs provide a basis for TC formation prediction, they do not provide all the information needed to predict TC formation. TCs can be affected by climate variations in the form of El Niño (EN), La Niña (LN), and the Madden Julian Oscillation (MJO), of which research by Johnson (2011) has been conducted to relate these variations to changes in TC formation areas.

Gray (1977) used statistical analysis of many years of data to determine the main factors associated with TC genesis in the WNP during the period from 1946–1973. Gray (1977) concluded that six parameters could be directly related to TC genesis: low level relative vorticity, Coriolis, vertical wind shear, SST, the vertical equivalent potential temperature gradient between the surface and 500 hPa, and middle tropospheric relative humidity. Mundhenk (2009) and Johnson (2011) used the following LSEFs to predict WNP TC formations: 850 hPa relative vorticity, SST, 200 hPa–850 hPa vertical wind shear, and 200 hPa divergence. Although these LSEFs Mundhenk (2009) and Johnson (2011) used are necessary for the prediction of TC genesis, they are not totally sufficient based on observational studies (Meyer and Murphree 2015). The LSEFs can be useful indicators of future TC formations, but they are limited because they are not necessarily sufficient indicators (Gray 1975, Johnson 2011, Meyer and Murphree 2015). A forecast based on the LSEFs may not be able to account for all the factors that affect TC formations and therefore may result in a failure to forecast TCs and contribute to false alarm forecasts (Gray 1975,

Meyer and Murphree 2015). Given this information, the LSEFs used in prior studies predicted the formation of 95% of all WNP TCs from 1981–2006 (Johnson 2011).

2. El Niño and La Niña Impacts on TC Formations

EN and LN events alter TC formation locations. Figure 1 shows an example from Ford (2000) of the effects of El Niña and La Niña (ENLN) on 200 hPa–850 hPa vertical wind shear, TC formation, and TC tracks occurring from August–November between the years 1957–1998. EN and LN set up anomalous circulations (indicated by the red and blue ovals) that alter the steering flow and make TCs either recurve or straight running. Ford showed that TCs are more or less likely to shift in locations of zero shear as a result of these anomalous circulations. Shifts in location of zero shear indicate shifts in areas of favorable TC formation. TC Formation locations indicate a change in response to changes in vertical wind shear. In EN events, there is a TC formation shift to the east and a higher probability of TC recurving tracks towards Japan. In LN events, TC formation shifts more to the western North Pacific and more TC tracks are straight running towards China (Ford 2000).

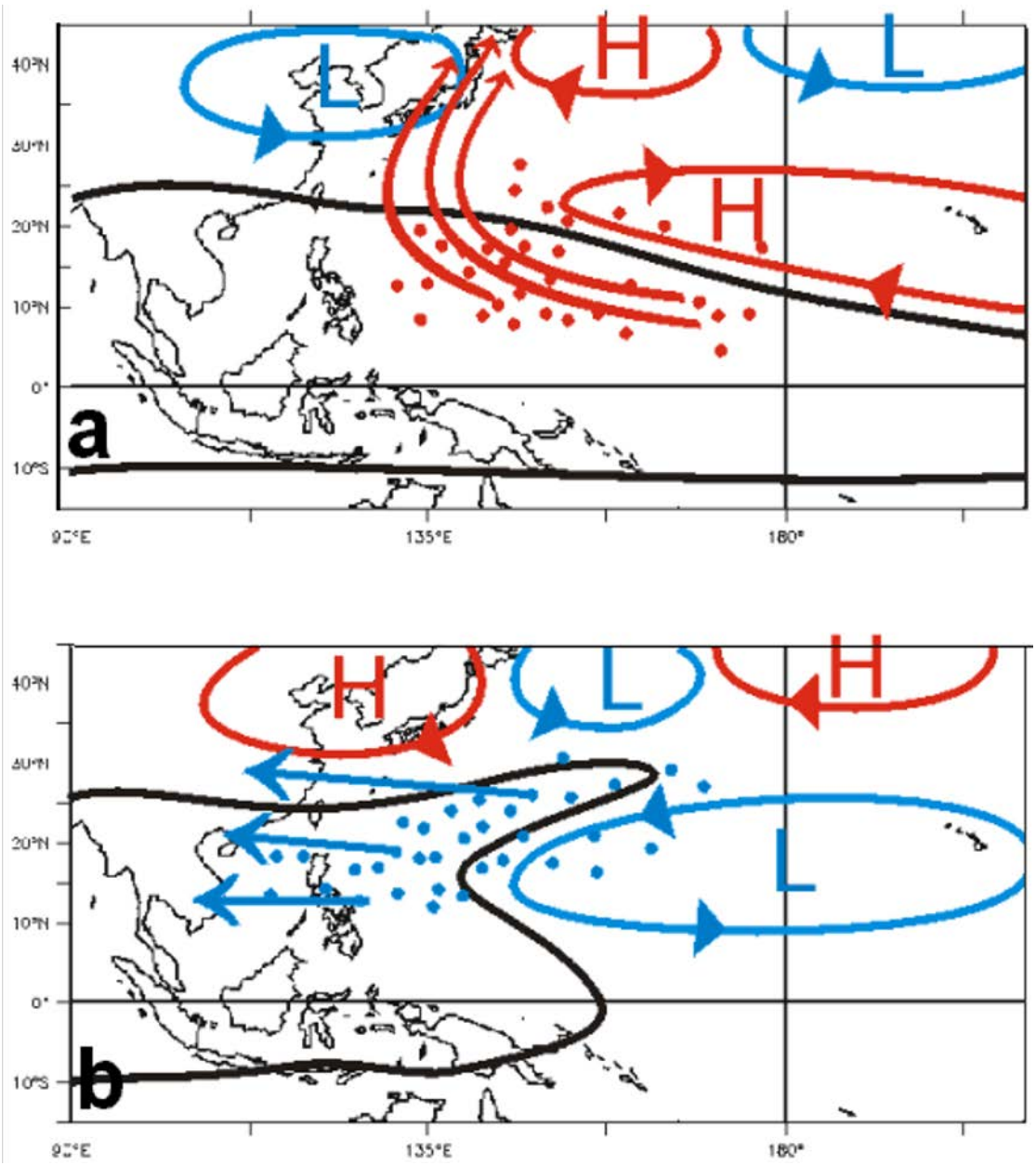

Figure 1. Schematic representations of the effects of (a) EN and (b) LN on TC formation areas and tracks based on data for August–November 1957–1998. Black line is zero wind shear line for winds at 200 hPa minus winds at 850 hPa. Red and blue ovals marked with "H" and "L" represent anomalous upper tropospheric heights with arrow heads indicating corresponding anomalous winds. Red and blue dots represent TC formation locations, and red and blue arrows represent corresponding TC tracks. Source: Ford (2000).

Additionally, other Ford (2000) results that are not shown in Figure 1 indicate that changes in other LSEFs also affect formation locations; and ENLN do not affect TC numbers but do affect TC formation locations and tracks.

Johnson (2011) compared TC formations during these ENLN events to the long-term mean (LTM) formations using the hybrid tropical cyclone forecasting system (HTCFS). The HTCFS that Johnson (2011) used was version one and was developed using TC and LSEF data for the years 1981–2010. HTCFS is a logistic regression model that includes second order polynomial terms with all predictors (Meyer and Murphree 2015). It was determined to a 99% confidence level using backward stepwise logistic regression that the TC formation probability was a function of SST and SST squared, shear and shear squared, divergence, relative vorticity, and three secondary interaction terms (Meyer and Murphree 2015). The LSEF data for the HTCFS version one came from the National Center for Environmental Prediction (NCEP)/National Center for Atmospheric Research (NCAR) reanalysis 1 data set (R1). When the LSEFs SST, 200 hPa – 850 hPa vertical wind shear, 850 hPa relative vorticity, and 200 hPa divergence LSEFs are used in the HTCFS, TC formation probability is calculated.

Figure 2 shows the results of Johnson (2011) LTM for July, August, September, October (JASO) of 1981–2010 for TC formation probability. The warmer colors represent higher TC formation probabilities and are overlaid with the JTWC best track TC formations. The band of higher TC formation probability goes from 110°E–160°E and 10°N–20°N, encompassing the South China Sea (SCS) and east of the Philippines.

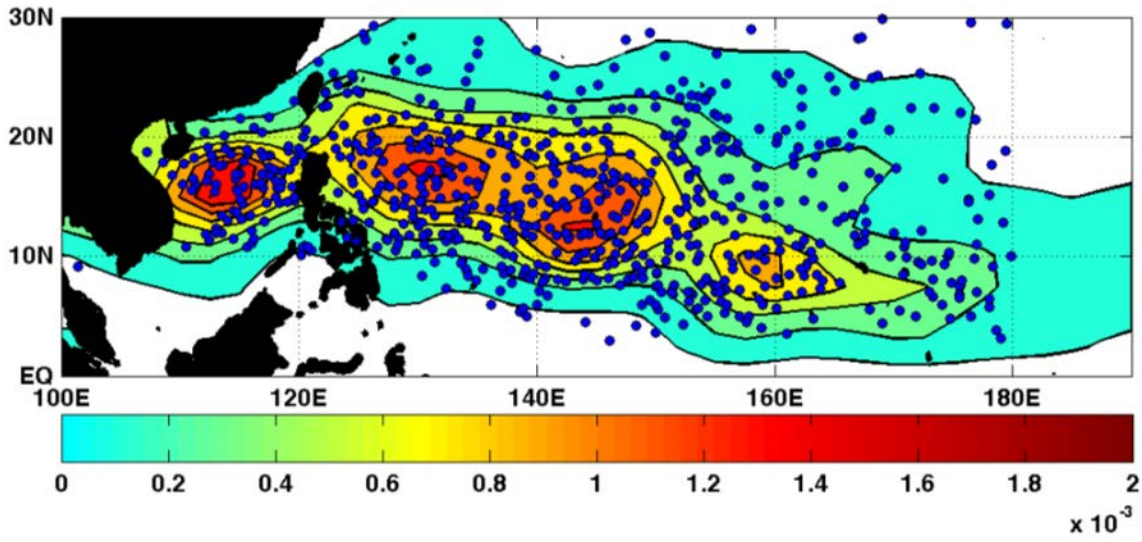

Figure 2. LTM TC formation probabilities for JASO 1981–2010 (color shading) overlaid with locations of TC formations during this period (blue dots). Formations east of 180°E are not shown. Source: Johnson (2011).

Figure 3 shows TC formation areas during JASO of EN years 1982, 1986, 1987, 1991, 1993, 1994, 1997, 2009 and JASO of LN years 1982, 1986, 1987, 1991, 1993, 1994, 1997, and 2009. EN years shift higher TC formation probabilities to the southern and eastern portion of the WNP, closer to the equator and international dateline (IDL) while LN years caused the TC formation probability region to shift to the northern and western parts of the WNP, in the subtropics of Japan. The variations in the LSEFs with EN when compared to the LTM included: a shift in higher SSTs to the east, stronger low level relative vorticity in the South China Sea (SCS) extending east of the Philippines, stronger easterly zonal wind shear across the WNP, and stronger upper level divergence over the maritime continent and central WNP (Johnson 2011). For LN events, the variations in the LSEFs included: a shift in higher SSTs to the west, weaker low level relative vorticity in the South China Sea (SCS) extending east of the Philippines towards the east, weaker easterly zonal wind shear across the WNP, and weaker upper-level divergence over the maritime continent and central WNP (Johnson 2011).

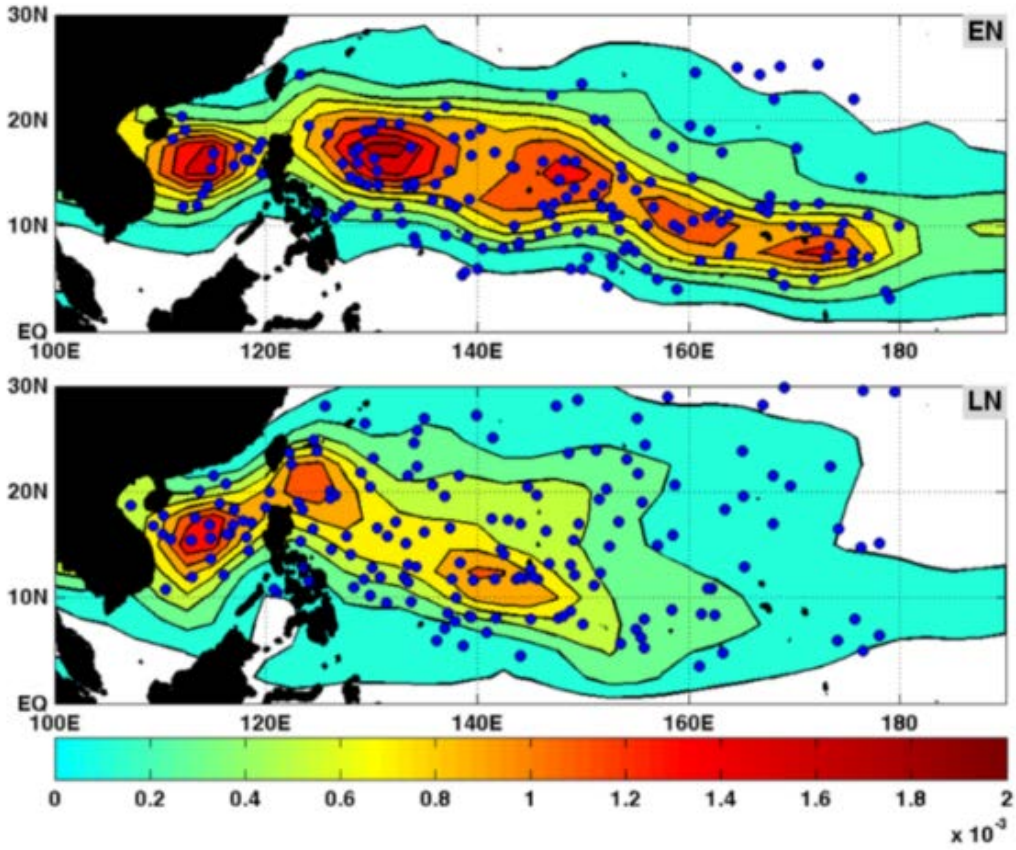

Figure 3. EN (top panel) and LN (bottom panel) TC formation probabilities for JASO 1981–2010 (color shading) overlaid with locations of TC formations during this period (blue dots). Formations east of 180°E are not shown. Source: Johnson (2011).

Figure 4 shows the EN and LN anomalies when compared to the LTM for JASO of 1981–2006 (Johnson 2011). The differences shown here reiterate that EN events tend to cause TC formation probability to shift eastward in the WNP. For LN events, there is a TC formation probability shift to the western part of the WNP that includes the SCS.

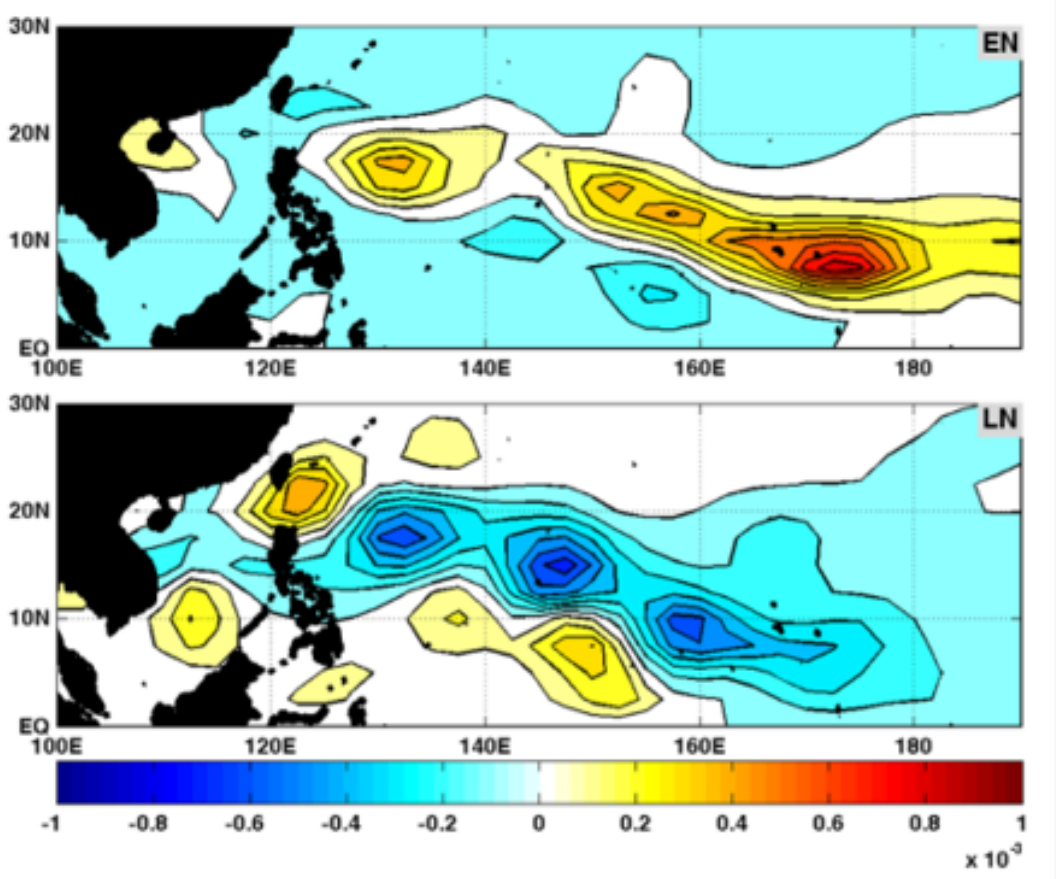

Figure 4. EN (top panel) and LN (bottom panel) TC formation probability anomalies (color shading) for JASO 1981–2010. Source: Johnson (2011).

3. Climate Change Impacts on TCs

In recent years, prior studies have investigated how TC activity has changed over the last several decades and how TC activity is likely to change in future decades due to climate change. The topic of climate change has also been of interest in the news, in part due to recent discussions involving political beliefs in climate change (Friedman and Astor 2019). The outputs from climate model projections of Earth's future climate under different greenhouse gas emissions scenarios that represent different possible future emissions and greenhouse gas concentrations in the atmosphere have been analyzed to look for indications of changes in TC activity due to climate change (i.e., Bhatia 2018, Bengtsson et al. 2007, Colbert et al. 2014, Dowdy 2014, Emanuel et al. 2008, Knutson and Tuleya 2008, Knutson et al. 2015, Kossin et al. 2016, Patricola and Wehner 2018, Wang et al.

2016). Many, but not all of these future greenhouse gas emissions scenarios in the papers mentioned are based on one of the Representative Concentration Pathways (RCPs). RCPs are scenarios that describe future atmospheric greenhouse gas concentrations based on assumptions about future emissions of greenhouse gasses (International Panel on Climate Change DDC 2019). RCPs are used in modeling future climate change associated with greenhouse gas concentrations (International Panel on Climate Change DDC 2019). The primary RCPs are named: RCP 2.6, RCP 4.5, RCP 6.0, and RCP 8.5 (for more information on the RCPs, see Chapter I, Section B.6).

Climate change studies have identified several potential changes in TC activity in the past several decades in the past that may be due to climate change while using observational data, reanalysis data, and climate models (especially changes in TC intensities, TC formation numbers, and TC tracks), as well as potential future activity changes due to future climate change. The impacts of climate change on TC activity (including formations, intensities, and tracks) may be affected by multiple factors that make the tropical environmental more favorable or less favorable for TC activity. One of these factors is atmospheric stability, which is affected by the vertical distribution of temperature and moisture in the atmosphere (e.g., Knutson and Tuleya 2008). Climate change may lead to increases in tropical atmospheric temperature and moisture in ways that stabilize the tropical atmosphere. If so, these atmospheric changes would tend to suppress TC activity for example, reduce the number of TC formations and/or TC intensity and offset other environmental changes that would tend to enhance TC activity (such as SST increases). There has not been a clear consensus on how climate change has affected TC statistics owing to their natural variability being large and the changes in TC observation methodologies over time (Patricola and Wehner 2018).

Prior studies have investigated how the number of TC formations in individual TC formation regions may change as Earth warms (Bengtsson et al. 2007, Colbert et al. 2014, Dowdy 2014, Emanuel et al. 2008, Knutson et al. 2015). As an example, Figure 5 from Emanuel et al. (2008) shows the changes in TC formation frequency during 1980–2000 to the last twenty years of the twenty second century in each TC formation region using thermodynamic and kinematic statistics derived from global climate models to produce

synthetic TCs to characterize TC genesis. The results from six of the seven models showed a rise in the frequency of TCs in the WNP when comparing the last 20 years of the twentieth century and the last 20 years of the 22nd century (Emanuel et al. 2008).

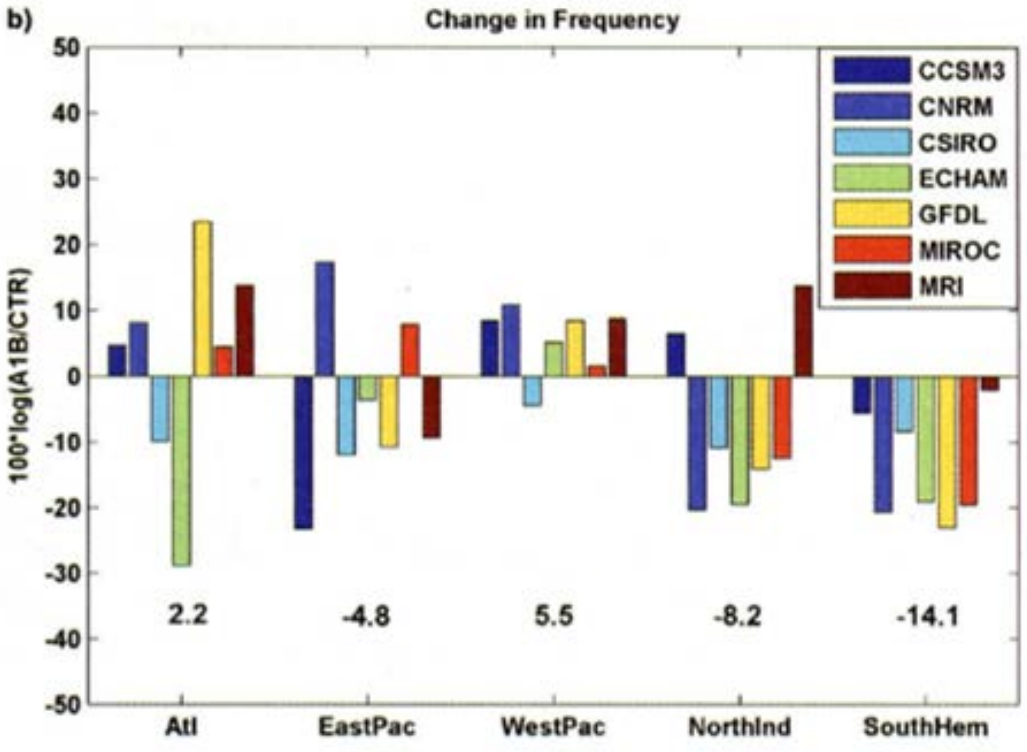

Figure 5. Percentage change in the frequency in occurrence of all TC events from 1980–2000 to the last 20 years of the 22nd century that achieve a peak wind speed of at least 21 m/s. Note the increase in TC activity in the WNP from 6 of the 7 model runs. Source: Emanuel et al. (2008).

Knutson et al. (2015) also used modeling to investigate potential changes in TC activity in a future warmer world using the RCP 4.5 scenario. They found an overall decrease in the number of TCs globally by the late 21st century, but increases in some basins, including the WNP. Their findings indicate a reduced global TC genesis frequency in four of the six TC basins (North Atlantic, northwest Pacific, south Indian, and southwest Pacific) while indicating an increase for the northeast Pacific and north Indian Ocean basins (Knutson et al. 2015). Bengtsson et al. (2007) using the coupled European Center Hamburg

Global Climate Model (ECHAM) saw a decrease in the number of TCs in every basin except for the eastern Pacific. Colbert et al. (2015) noted projected decreases in WNP TC formation near the Philippines (negative 3–5 TCs per decade through 2100) and an increase in projected TC formation over the central WNP (1–3 more TCs per decade through 2100) using ensemble mean projections from the Coupled Model Intercomparison Project Phase 3 and Phase 5 (CMIP5) models. The changes in TC formation numbers were attributed into an apparent reduction in the easterlies in the 21st century. Dowdy (2014) conducted a time series representation of TC numbers in the Southern Hemisphere Australian region using the National Climate Center of the Australian Bureau of Meteorology historical TC database from 1970–2010 and also saw a decrease in TCs in that region. In this research, he removed the natural variations in TCs represented by ENLN. As shown in the results of Bengtsson et al. (2007), Colbert et al. (2015), and Knutson et al. (2015), there is no clear consensus as to whether the number of TCs in the WNP region are increasing or decreasing. Most of the research indicates that the WNP should see an increase in TC activity.

Prior studies have also investigated how TC intensity in individual TC formation regions may change as Earth warms (Bengtsson et al. 2007, Bhatia 2018, Emanuel et al. 2008, Knutson et al. 2015, Patricola and Wehner 2018). Knutson et al. (2015) used the Geophysical Fluid Dynamics Laboratory high resolution atmospheric model with a 50 km grid and RCP 4.5 to conclude that in a warmer climate, TCs globally will increase in the 21st century by 24% for category 4 and 5 storms. Interestingly, this research also indicates a projected decrease in TC intensity in parts of the northwest Pacific Ocean. Bengtsson et al. (2007) points out that he received mixed results towards the maximum wind speed intensity of TCs in each basin based on the horizontal atmospheric resolution on the coupled ECHAM from T63 to T319. The WNP saw more intense TCs when the atmospheric model resolution was increased only to T319 in the 20th and 21st centuries (Bengtsson et al. 2007). Emanuel et al. (2008) while using the coupled air-sea model Coupled Hurricane Intensity Prediction System (CHIPS) saw an overall increase in TC intensity in the WNP in the 21st century when compared to the 20th century.

Prior studies have additionally investigated how TC tracks in individual TC formation regions may change as Earth warms (Kossin et al. 2016, Sharmila and Walsh

2018, Wang et al. 2011). For example, Figure 6 shows the Kossin et al. (2016) model results when using CMIP5 with the largest emissions projection RCP 8.5. Kossin et al. (2016) research showed decreased TC exposure meaning less TCs formed near the Philippines and South China Sea (SCS) and increased TC exposure in regions of the East China Sea to include Japan and the Ryukyu Islands, indicating a poleward migration in the WNP from July through November 1980–2013.

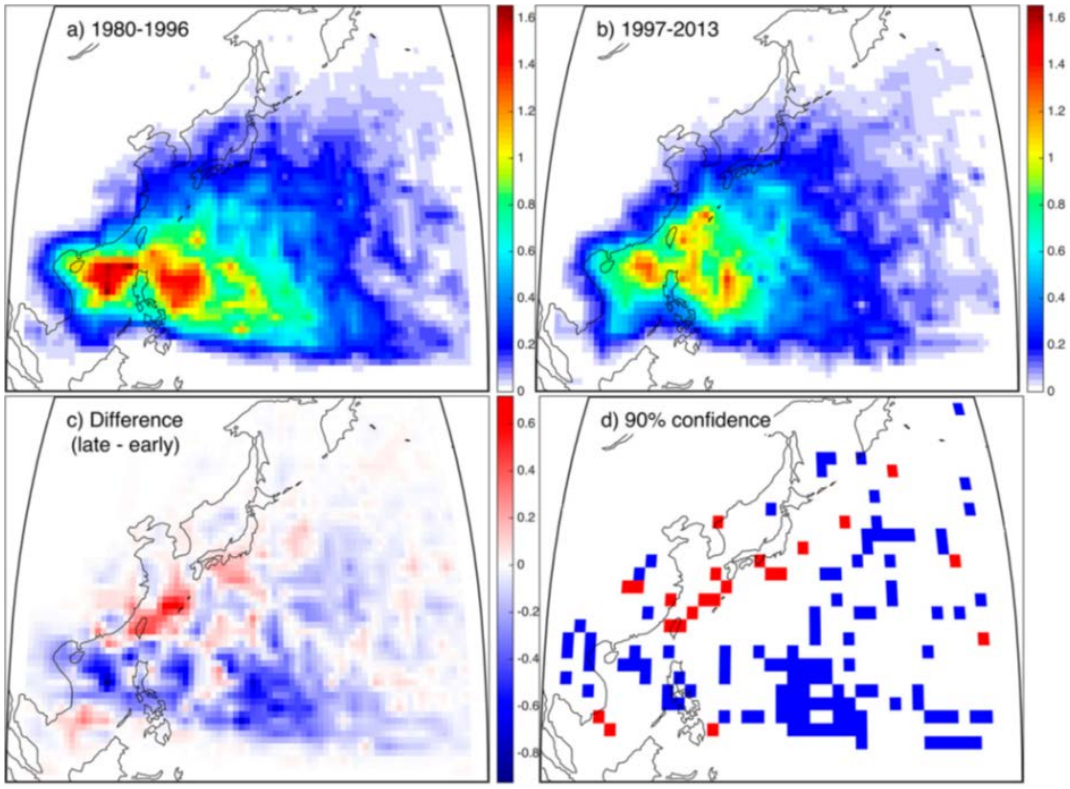

Figure 6. Observed WNP TC track density differences. From July to November of (a) 1980–1996, (b) 1997–2013, (c) difference of 1997–2013 subtracted from 1980–1996, and (d) regions where the difference was significant at the 90% confidence level based on the student t test. Source: Kossin et al. (2016).

Wang et al. (2011) conducted an analysis of TC formation and track patterns in the WNP, specifically the SCS utilizing JTWC best track data with a spatial resolution of a 2° longitude by 2° latitude grid, coupled with the utilization of singular value decomposition of observational data from the IPCC Assessment Report version 4. The experiment was

conducted over July, August, and September from 1965–2009 using reanalysis data and projected into the future until 2040. Conclusions from Wang et al. detected decreased westward TC tracks in the SCS during this timeframe due to changes in large scale steering flows and SST rise. The problem with this research was that Wang et al. had to assume there was little TC formation location change in the future and warned that caution should be taken when interpreting the projections.

4. Knowns and Unknowns for TC Formation in a Warmer World

There are many unknowns when it comes to TC formation and properties in the future. These include uncertainties about how anthropogenic forcing is quantified and how well the RCP scenarios represent future human activities (Overpeck et al. 2011). It is hard to anticipate future anthropogenic emissions due to uncertainties about human population changes, changes in agricultural practices, and changes in industrial production (Koneswaran and Nierenberg 2008). Anthropogenic forcing levels are estimates based on statistical analysis of data and are coarse projections, meaning grid spacing and data are over a large area, for example a 2° longitude by 2° latitude grid for the future world (Van Vuuren et al. 2011).

What is known is that global SST upper ocean temperatures have been increasing in most ocean basins (Deser et al. 2010). TCs depend heavily on the SST and upper ocean heat content to form, and many studies have shown that increasing ocean temperatures are likely to lead to an increase in TC formations and intensity (Bengtsson et al. 2007).

5. Strengths and Weaknesses of Climate Change Modeling

Strengths of climate change modeling are the future projection coupled models such as the Community Climate System Model version 4 (CCSM4) are based on past historical data and provide many possible representative projections for future Earth conditions (Overpeck et al. 2011). Reanalysis data, created from model observational datasets and assimilating observations into a dynamical model, have proven to be reliable for climate research (Overpeck et al. 2011). The biggest strength of climate change modeling is that it starts the conversation as to what could happen in the future.

Weaknesses in climate change projections based on climate models deal with a variety of issues linked directly to input data. There is not one source of TC tracks and standards used to assess climate change, leading to diverse TC formation areas and tracks (Song et al. 2010). Additionally, there has been a limited period of consistent observations in the atmosphere, leading to a small sample size of approximately 50 years (Song et al. 2010). Future climate models have a difficult time parameterizing convection, a necessity in predicting TC formation (Patricola and Wehner 2018). Although models are getting better with time, coarse resolutions mean that the models cannot fully represent smaller mesoscale activities in the climate system (Meehl et al. 2012). Additionally, climate data is vast in volume and complexity, and sometimes data is considered intellectual property with access being restricted from other scientists mainly because of governmental interests (Overpeck et al. 2011).

6. Future Earth Climate and Representative Concentration Pathways

Table 1 shows the four common RCPs used for representation of potential future climate states (RCPs 8.5, 6.0, 4.5, 2.6) and how the RCPs are differentiated through their anthropogenic forcing levels along with their stabilization timeframes. RCPs are the product of collaboration and assessment of the future climate by modelers, climate scientists, ecosystem modelers, and emissions experts to provide plausible descriptions of future climates and encompass socioeconomic change, technological change, energy and land use, and greenhouse gas emissions (Van Vuuren et al. 2011).

Table 1. Overview of RCPs and forcing levels. Adapted from Van Vuuren et al. (2011).

RCP 8.5	Rising radiaitive forcing pathway leading to 8.5 W m^{-2} (~1370 ppm CO2 equivalent) by 2100
RCP 6.0	Stabalization without overshoot pathway to 6 W m^{-2} (~850 ppm CO2 equivalent) at stabalization after 2100
RCP 4.5	Stabalization without overshoot pathway to 4.5 W m^{-2} (~850 ppm CO2 equivalent) at stabalization after 2100
RCP 2.6	Peak in radiative forcing at 3 W m^{-2} (~490 ppm CO2 equivalent) before 2100 and then decline to 2.6 W m^{-2} by 2100

Figure 7 shows differences in the four RCPs with regards to the carbon dioxide (CO2) emissions amounts for each RCP scenario. Note that RCP 8.5 has both the highest CO2 emissions and concentrations that increase past the year 2100, while RCP 2.6 has declining CO2 emissions starting in the year 2010. In this study, climate model projections based on the RCP 8.5 scenario were used to investigate TC formation changes in the WNP out to the year 2050.

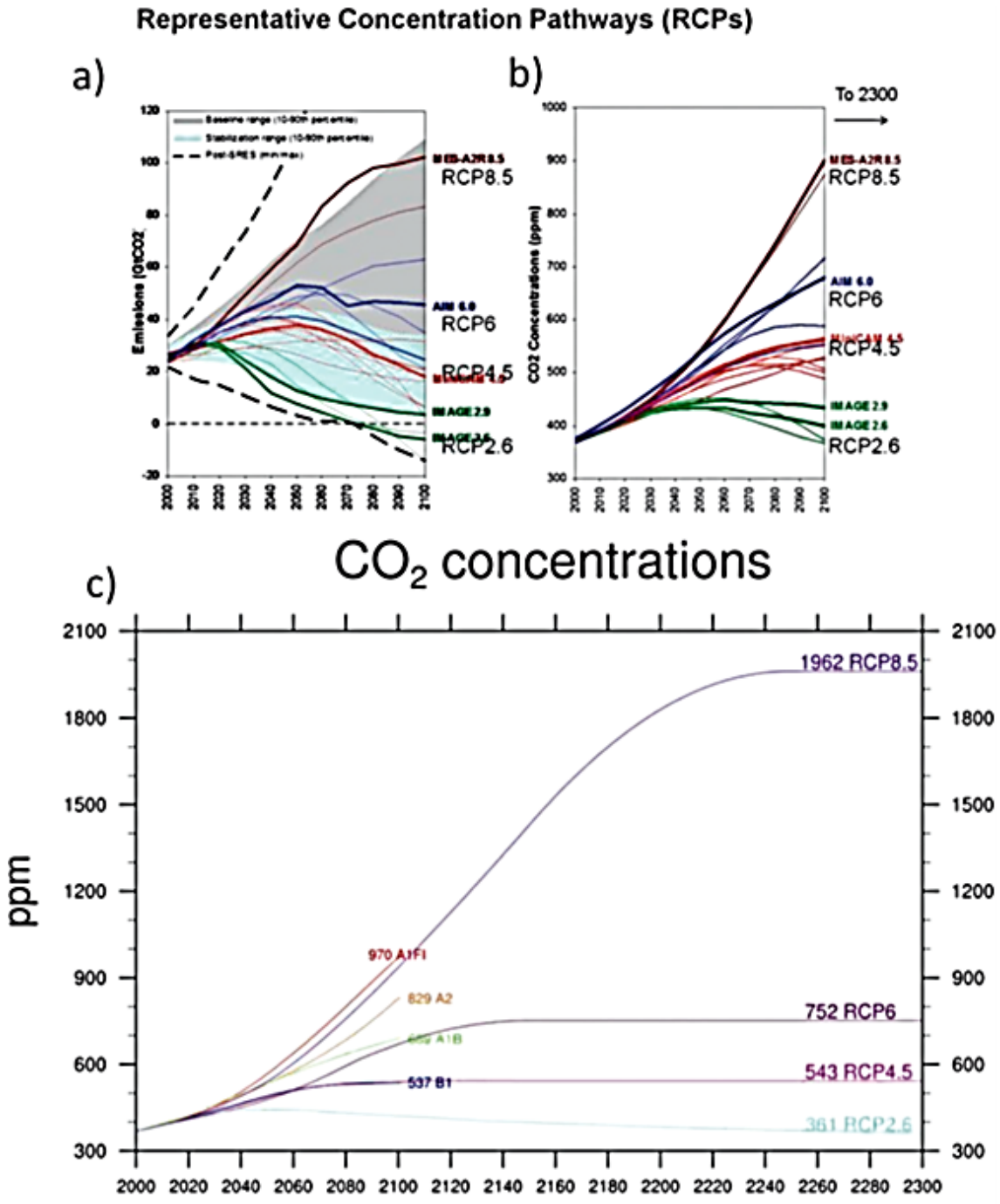

Figure 7. RCP emission scenarios. For: (a) Carbon dioxide emissions for each of the RCP scenarios, (b) Carbon dioxide concentrations derived from the emissions in (a), (c) Carbon dioxide concentrations from (b) with extensions to 2300. Source: Meehl et al. (2012).

Figure 8 from Gent et al. (2011) shows the time series of globally averaged surface temperature anomalies with CCSM3, CCSM4, and observations from the Meteorological Office Hadley Center (HADCRUT3). Note the difference in surface temperature for the red line representing CCSM4 versus the black line representing observational data. By 2005, there is a difference of about 0.4°C between CCSM4 and the HADCRUT3 observations, which indicates an SST bias with CCSM4 (Gent et al. 2011, Meehl et al. 2012). Gent et al. (2011) cites potential reasons for the SST bias, but of note is that the bias is a global trend that is also evident in the WNP.

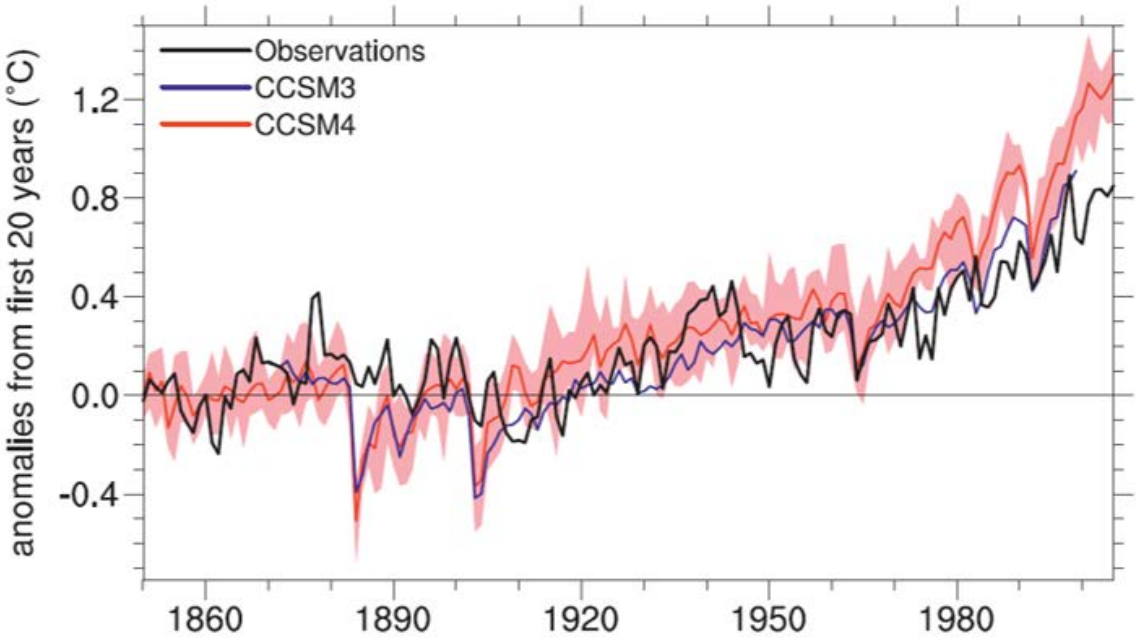

Figure 8. Globally averaged surface temperature anomalies for 1850–2005, from three sources. (1) CCSM3 (blue), HADCRUT3 observations (black), and CCSM4 (red) with red shading representing the CCSM4 ensemble spread. For each time series, the base period for the calculating the anomalies is the first 20 years of the time series. Source: Gent et al. (2011).

7. Subseasonal to Seasonal TC Formation Forecasting

Several universities and weather prediction centers provide subseasonal to seasonal (S2S) TC forecasts for TC basins around the globe. These include S2S outlooks provided by the Climate Prediction Center (CPC), Colorado State University (CSU), NPS/Statistical

Solutions LLC, and JTWC (NOAA CPC 2019, Colorado State University 2019, Statistical Solutions LLC 2019, JTWC 2019).

S2S TC forecasts have lead times of several days to several months and valid periods of approximately one week to six months. An example of a subseasonal TC forecast is the CPC Global Tropical Hazards/Benefits Assessment that issues predictions for TC formation for periods of one and two weeks with a valid time of one week (NOAA CPC, 2019). JTWC is experimenting with a 14-day TC formation outlook in the Indian Ocean basin that may be extended into the Pacific.

S2S forecasts of TCs are produced by three main types of forecasting systems: dynamical, statistical, and hybrid dynamical-statistical.

a. Dynamical Forecasting Systems

Dynamical forecast systems use real time data to initialize prediction models based on dynamical equations from physics and chemistry. These systems can be skillful in predicting a wide range of processes occurring over global domains at S2S lead times; however, they tend to be less accurate in their forecasts of relatively small scale processes, such as those involved in TCs (van den Dool 2007). Dynamical models tend to be more accurate in forecasting large scale features in the atmosphere that evolve slowly (van den Dool 2007). The European Center for Medium-range Weather Forecasting (EMCWF) along with the International Research Institute for Climate and Society produce dynamical model forecasts of TC activity for selected TC basins (European Centre for Medium-Range Weather Forecasts 2019, International Research Institute for Climate and Society 2019). EMCWF uses a coupled global circulation model to forecast TC activity, including the number of named storms and accumulated cyclone energy (ACE) in all TC basins around the globe (Camargo et al. 2007).

b. Statistical Forecasting Systems

Statistical forecasting systems are widely used in S2S forecasting and can predict climate variations that are known to impact TC formation in a given region (e.g., ENLN, MJO). Examples of statistical models include products from the National Oceanic and

Atmospheric Administration (NOAA) CPC and the National Hurricane Center (NHC). The CPC and NHC issue a North Atlantic basin hurricane seasonal outlook that forecasts the seasonal number of named storms, hurricanes, and major hurricanes (NOAA CPC 2019, National Hurricane Center 2019). Additionally, the City University of Hong Kong issues a statistical forecast of the annual number of TCs in the WNP (City University of Hong Kong Laboratory of Atmospheric Research 2019).

c. Hybrid Dynamical-Statistical Forecasting System

Hybrid-dynamical statistical forecasting systems merge dynamical and statistical systems to apply the strengths of each. For example, a hybrid system might emphasize dynamical methods for forecasting larger scale processes and statistical methods for smaller scale processes (cf. van den dool 2007). In this research, a hybrid system was applied to analyze past TC activity and project future TC activity. This system was created by NPS and SSLLC (Meyer and Murphree 2015). This hybrid system uses dynamical model forecasts of LSEFs that strongly determine TC activity to force a statistical model that describes the probability of TC activity based on the environment described by the forecasted LSEFs This system can be thought of as one in which the output from the dynamical forecasts are statistically post-processed. The forecasts are probabilistic forecasts of TC activity.

8. Hybrid TC Forecasting System

Mundhenk (2009) and Meyer and Murphree (2015) describe the development and testing of a hybrid system based on a statistical model that predicts TC formation probabilities when forced with S2S forecasts of LSEFs for TC formation from the NCEP Climate Forecast System (CFS or CFSV2, Saha et al. 2006, Saha et al. 2014) dynamical S2S forecasting system. This system, which is referred to in this study as the HTCFS, applies statistical post-processing of the dynamical forecasts of the LSEFs to generate probabilistic forecasts of TC formations at S2S lead times. The HTCFS is ran in ensemble mode, based on ensembles of the LSEF forecasts and lagged average ensembling of the HTCFS forecasts (Meyer and Murphree 2015). The statistical model in the HTCFS is a logistic regression model that was built using best track data and LSEF data from the NCEP

Climate Forecast System Reanalysis (CFSR, Saha et al. 2010) for 1979-2011 and CFSV2 analyses and very short lead forecasts for the post-2011 years. In this study, the combined CFSR and CFSV2 datasets are referred to as CFSRV2. The LSEFs used in the HTCFS are: SST, 200 hPa–850 hPa vertical wind shear, 850 hPa relative vorticity, and 200 hPa divergence (Murphree and Meyer 2015). Mundhenk (2009) and Meyer and Murphree (2015) identified values for these LSEFs that are most associated with, and thus most favorable for, TC formation. These values are: (a) SST above 26°C, (b) weak vertical wind shear between upper and lower levels (200 hPa–850 hPa), (c) positive relative vorticity at 850 hPa (indicating cyclonic circulation in the lower troposphere), and (d) positive divergence at 200 hPa (indicating upward vertical motion in the underlying troposphere).

Figure 9 shows representative examples of TC formation forecasts from the HTCFS. The TC formations that occurred during the forecast valid periods (the purple dots in Figure 9) are used to assess the accuracy of the forecasts.

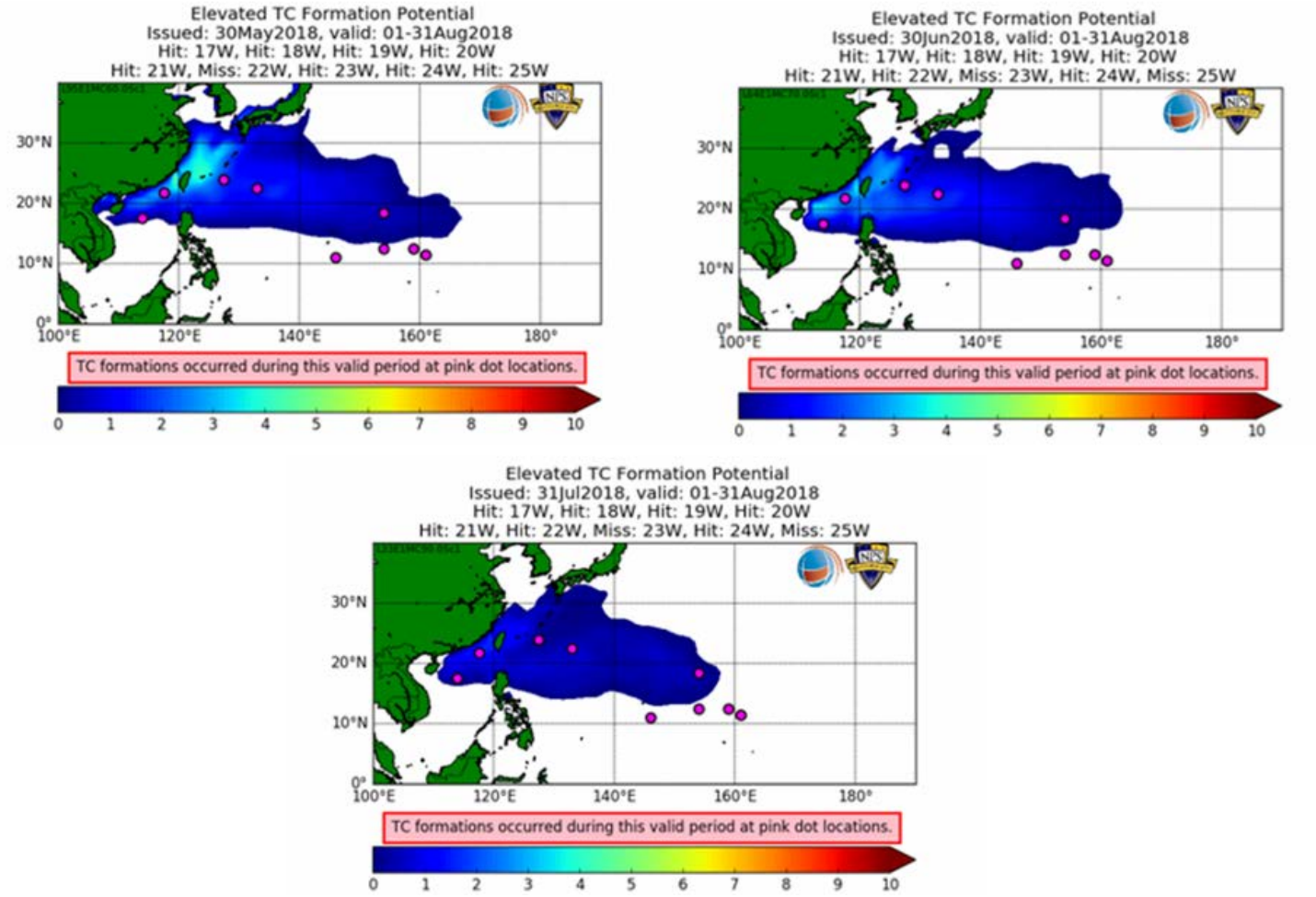

Figure 9. TC formation probability forecasts (color shading) produced by the HTCFS for August 2018 at lead times of: 90 days (top left), 60 days (top right), and 30 days (bottom) overlaid with actual TC formations (purple dots). Source: Statistical Solutions LLC (2019).

Figure 10 shows representative skill scores by lead time for HTCFS forecasts of TC formation probabilities in the WNP. Probability of detection (POD) describes the percent of actual TCs that were correctly forecasted. Larger values of POD indicate greater skill. Percent contoured area (PCA) describes the percent of the entire WNP basin for which elevated probabilities of formation were forecasted. Smaller values of PCA indicate greater skill. Mundhenk (2009) and Meyer and Murphree (2015) showed that HTCFS is skillful at all lead times based on a wide range of skill measures. Johnson (2011) showed that the statistical model in HTCFS was skillful in representing the impacts of MJO and ENLN events on the LSEFs and on TC formations.

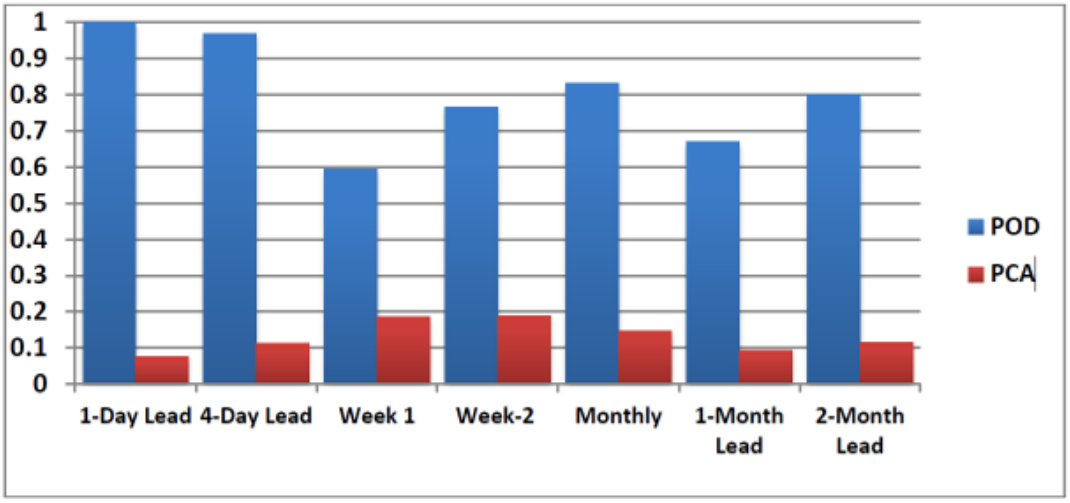

Figure 10. Skill metrics for HTCFS forecasts of TC formation probabilities for WNP TCs in 2013 by forecast lead times. POD shown by blue bars and PCA shown by red bars. Source: Meyer and Murphree (2015).

C. RESEARCH

1. Gaps in Prior Research

A number of prior studies of how climate change may affect TC activity have focused on using dynamic models and on just some of the LSEFs, such as SST. Many of these studies mainly described TC activity from a global perspective with relatively coarse grid spacing and limited focus on specific basins. Several studies that investigated

individual basins found large differences between basins (e.g., Gent et al. 2011, Meehl et al. 2012. Many of the prior studies have focused on future changes in TC intensities, with relatively few focusing on changes in the number, location, and seasonal timing of TC formations. Exceptions to this include Kossin et al. (2016) and Sharmila and Walsh (2018), which found a poleward shift occurring northward with regard to TC tracks and formation areas. Many of the conclusions from individual studies and from syntheses of many studies are inconclusive or contradictory.

2. Overall Approach to Addressing Those Gaps

These gaps were addressed in our research. One basin (the WNP) was analyzed with a relatively small grid spacing (1° longitude by 1° latitude). Climate change projections of LSEFs from a dynamical climate model (CCSM4) were used to force a statistical model and generate probabilistic projections of TC formations in future decades. The four LSEFs individually were investigated to assess the past and future LSEF contributions to the overall TC formation probabilities in the WNP. The ability of the climate model (CCSM4) was assessed on how well it simulated LSEFs and TC formation probabilities during the past four decades. Climate model projections of future LSEFs were used to assess the probability of TC formation in the next several decades.

3. Research Questions

Our goal in this study was to achieve a better understanding of how TC formation areas will change in the WNP up to 30 years in the future as a result of human induced global warming and global climate change. To accomplish this, the HTCFS was forced with LSEF projections from CCSM4 for the 2021–2050 period. Our main research questions were:

1. Do CCSM4 simulations of the LSEFs for 1981–2018 provide a realistic description of TC formations for this period when those LSEFs are used to force the HTCFS?

2. What do the CCSM4 results for 1981–2018 indicate about the ability of CCSM4 to accurately represent TC formations in the next three decades, 2021–2050?

3. What do the CCSM4 projections of the LSEFs for 2021–2050 indicate about environmental changes, and TC formations, that are likely to occur in the WNP as a result of human induced climate change?

4. Thesis Organization

Chapter II addresses our study region and time period, followed by an overview of the data and methods used. Chapter III presents a summary of our findings, including LTM, ENLN CCSM4 results, time series for both CCSM4 and CFSRV2 results, bias analysis results for CCSM4 and CFSRV2, future time series CCSM4 results, and future CCSM4 results. Chapter IV presents conclusions and recommendations for further research.

THIS PAGE INTENTIONALLY LEFT BLANK

II. DATA AND METHODS

A. STUDY REGION AND PERIOD

The study region for this research was the WNP. This area is of particular significance due to: (a) extensive Department of Defense (DoD) operations in the WNP; and (b) high level of TC activity in the WNP where approximately 30% of Earth's TCs form (Meyer and Murphree 2015). The WNP region is defined as the area occurring within 100°E–150°W and 0°N–50°N. This area accounts for all TCs in the WNP region and also accounts for part of the central Pacific (CP) to encompass TCs that may track into the WNP.

Our study period for assessing LSEFs and TC formations during the most recent decades was JASO from 1981–2018 (a 38-year period), which was called the past study period. The period 1981–2018 was chosen based on the availability of climate projection outputs and reanalysis data. The study focused on the JASO period of each year due to the relatively high number of TCs during these months. Figure 11 shows the number of TCs in the WNP during each month, January–December, during the 1981–2018 study period. There were 1,182 TC formations during these 38 years, with 796 of these formations occurring during JASO (67%).

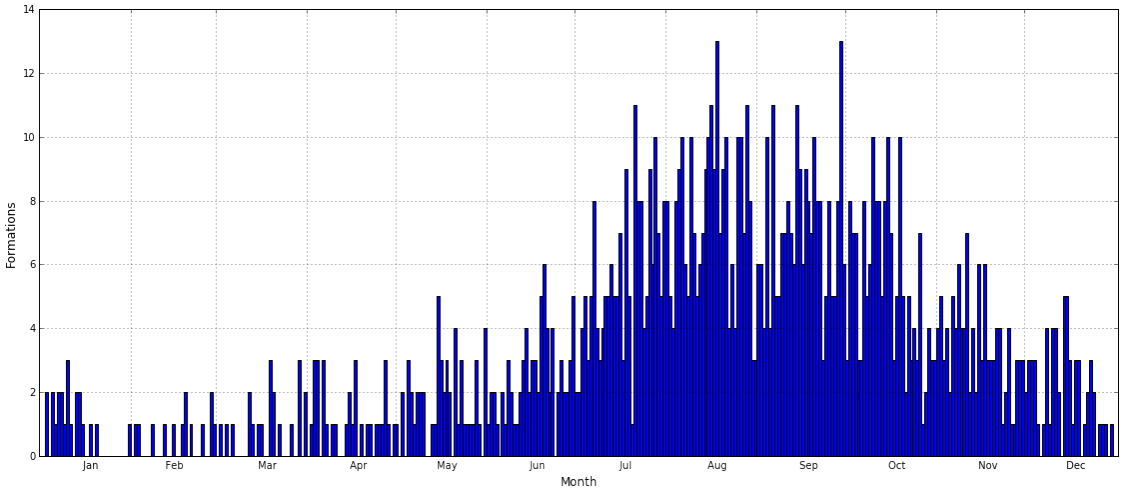

Figure 11. Number of TC formations (y-axis) for the WNP region by month (x-axis) during 1981–2018 for the WNP (100°E–180°E, 0°N–50°N). TC formation numbers from JTWC best track data for 1981–2017 and from NRL TC Page (NRL Monterey 2019) for 2018.

Figure 12 shows WNP study region overlaid with TC formation locations representing the formation locations for the 796 TC formations during JASO of 1981–2018 using JTWC best track data and the National Hurricane Center central Pacific hurricane database (HURDAT2) (JTWC 2018, NOAA NHC 2019). For the year 2018, the Naval Research Laboratory (NRL) Monterey TC Page was utilized for the WNP since JTWC and HURDAT2 best track data was not available (NRL Monterey 2019).

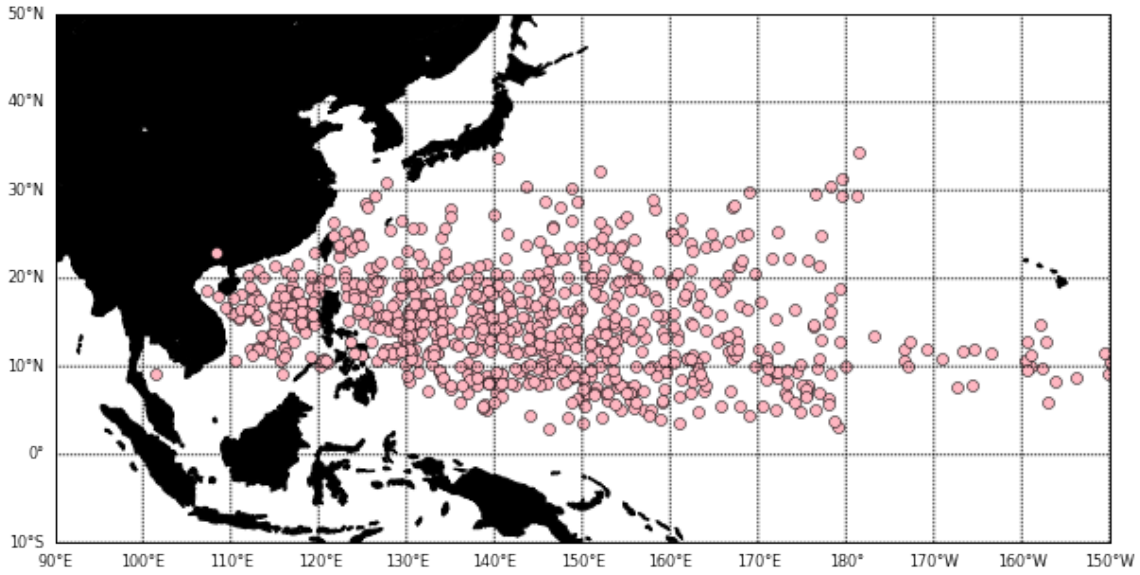

Figure 12. WNP study region overlaid with locations of TC formations for JASO 1981–2018 (pink dots). TC formation locations are based on JTWC and HURDAT2 best track data for 1981–2017 and from NRL TC Page for 2018.

This study identified within the WNP a central area in which TC formations in JASO were concentrated. This area of the WNP was named the central formation region (CFR), which is the area bounded by 127°E–165°E and 08°N–21°N. Of all the 775 TCs in the WNP study region bounded by 100°E–180°E and 0°N–50°N, during JASO 1981–2018, 395 (51%) of them occurred in the CFR (for more information, see Appendix Table 3). The CFR was used to represent past and future variations in the LSEFs, TC formations, and TC probabilities. The CFR was chosen rather than the entire WNP to: (a) focus on the most active part of the WNP in our investigations of multi-decadal changes; (b) study these multi-decadal changes in a relatively uniform sub-region of the WNP that also has a large number of TCs; and (c) minimize the complications that arise when averaging together information from the many diverse sub-regions of the WNP. In this study, the focus was mainly on TC formations during JASO, the most active part of the WNP TC season. TC formations during the whole TC season (June–November) or the entire calendar year were not investigated. Therefore, there are both spatial and temporal complications to consider

when comparing prior results for the whole WNP and a whole season or calendar year with our results for the CFR for only JASO.

Figure 13 shows the CFR overlaid on a map of the WNP study region and with the TC formations from JASO of 1981–2018 from JTWC and HURDAT2 best track data. For the year 2018, the NRL Monterey TC Page was utilized since JTWC and HURDAT2 best track data was not available.

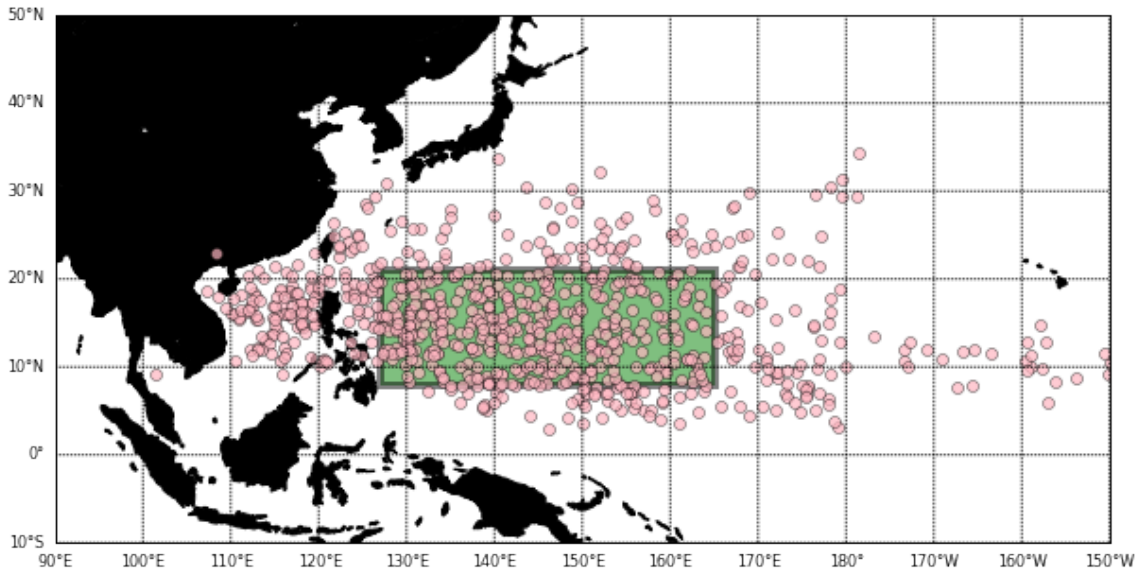

Figure 13. WNP study region overlaid with locations of TC formations for JASO 1981–2018 (pink dots) and with the CFR region shown by the green area within the black rectangle. TC formation locations are based on JTWC and HURDAT2 best track data for 1981–2017 and from NRL TC Page (NRL Monterey 2019) for 2018.

B. DATA SETS AND SOURCES

1. JTWC Best Track

JTWC best track data was used for TC formation locations in the area within the WNP region from 100°E–180°E and 0°N–50°N (JTWC 2018). JTWC TC formations are historical accounts for each storm and data points consist of six hourly reports directly from the JTWC best track data archive formulated from the first noted time and location for each

storm. JTWC intensity estimates for TCs use one-minute mean sustained wind speeds. JTWC best track data is not a reanalysis dataset, and may contain temporal variations in available observational data and with TC formation analysis procedures over the course of the study period. With TC formation analysis, it was expected that there would be a relatively small error on the order of 1°–2° and 1–2 days or less based on the assessments of real time analysis and best track analysis (Johnson 2011). For each TC, the first time and position data in the JTWC best track dataset was used as the TC formation time and location.

2. HURDAT2

HURDAT2 was used for TC formation locations in the area within the WNP region from 180°W–150°W and 0°N–50°N. HURDAT2 makes use of all available TC observations in the CP and may not have been in real time. This database includes observations made at six hourly intervals and observations made at times other than six hourly intervals to aid in intensity and landfall criteria, and the inclusion of non-developing tropical depressions (Landsea and Franklin 2013). With TC formation analysis, it is expected that there would be a relatively small error on the order of 1°–2° and 1–2 days or less based on the assessments of real time analysis and best track analysis (Johnson 2011). For each TC, the first time and position data in the HURDAT2 best track dataset was used as the TC formation time and location.

3. 2018 TC Data

For the years 1981–2017, JTWC best track and HURDAT2 data was available for the WNP area of research. However, 2018 data has not yet been published. Therefore, the NRL Monterey TC Page, a storage site for raw TC data in the WNP, was utilized for 2018. The first noted time and place for each TC from the NRL Monterey TC Page was used.

4. CFSR and CFSV2

CFSR and CFSV2 data, combined and called CFSRV2, was used as a primary source for LSEF data for JASO of 1981–2018 (NOAA National Center for Environmental Information 2018). This data was a combination of two different data sets, the CFSR for

JASO of 1981–2011 and CFSV2 for JASO of 2012–2018. Evaluation of these forecasts, referred to in this thesis as CFSRV2, shows that they provide a good continuity of the climate record and skillful estimates for subseasonal and seasonal predictions (Saha et al. 2010, Saha et al. 2014). CFSRV2 is a fully coupled atmospheric-ocean-land model used through NCEP and was a source for LSEF data consisting of; SST, 200 hPa – 850 hPa vertical wind shear, 850 hPa relative vorticity, and 200 hPa divergence. CFSRV2 has a global resolution of 0.5° longitude by 0.5° latitude. CFSRV2 data was used since the HTCFS was validated through CFSRV2 results. For this research, all CFSRV2 data was interpolated into a 1° longitude by 1° latitude grid in the WNP.

5. CCSM4

The CMIP5 set of experiments, including the CCSM4 future projection results, are simulations of the 21st and 22nd century climates using RCP forcing scenarios (see Chapter I, Section B.6). The Climate Data Gateway at NCAR, compiled projection results from CCSM4 (Climate Data Gateway at NCAR 2018). CCSM4 is a climate modeling system that includes models of the atmosphere, land, ocean, and sea ice. The CCSM4 historical runs covered the period 1850-2005. The CCSM4 projections using different RCP scenarios covered the period 2006-2300. The CCSM4 results have a horizontal resolution of 0.9° longitude by 1.25° latitude. The CCSM4 historical and projection have some shortcomings, including, for example, difficulty capturing the indirect effects of aerosols, which could be a factor in CCSM4 producing globally averaged SSTs that are warmer than observed SSTs (Meehl et al. 2012).

CCSM4 historical and projection results were used to produce LSEFs for our study. These LSEFs were: SST, 200 hPa – 850 hPa vertical wind shear, 850 hPa relative vorticity, and 200 hPa divergence. CCSM4 historical results were used for JASO 1981–2005 and the CCSM4 projection results for JASO 2006–2050. For some purposes, CCSM4 historical results for JASO 1981–2005 were combined with CCSM4 projection results based on RCP 8.5 forcing for JASO 2006–2018 (for example, for use in assessing CCSM4 biases). For this research, the CCSM4 results were interpolated onto a 1° longitude by 1° latitude. For this thesis, CCSM4 future projection results were used based on the RCP 8.5 scenario.

C. CALCULATION OF LSEF VARIABLES

1. LSEF Calculations

The CFSRV2 and CCSM4 results did not directly provide some of the LSEFs—in particular, 200 hPa–850 hPa vertical wind shear, 850 hPa relative vorticity, and 200 hPa divergence. Therefore, the LSEFs were calculated from the CFSRV2 and CCSM4 winds at 850 hPa and 200 hPa using the equations shown in Table 2. Monthly averages for each variable were created for July, August, September, and October of each year during our study period. From those monthly averages, four-month averages were calculated for JASO of each year in our study period and averages for several multi-year periods.

Table 2. LSEF calculation formulas for vertical wind shear (top box, levels measured in hPa), relative vorticity (middle box), and divergence (bottom box).

Vertical Wind Shear =	$(u200 - u850) + (v200 - v850)$
Relative Vorticity =	$\frac{\partial v}{\partial x} - \frac{\partial u}{\partial y}$
Divergence =	$\frac{\partial u}{\partial x} + \frac{\partial v}{\partial y}$

2. Anomaly Calculations

A standard way to represent climate variations is to calculate climate anomalies, which are differences between values for a specific period and values for a LTM base period, with the LTM values being subtracted from the specific period values. The following equation shows an example of how anomalies were calculated, in this case, the anomaly for the 200 hPa divergence during JASO for EN periods (cf. Johnson 2011):

$$200\ hPa\ Divergence\ Anomaly = EN\ 200\ hPa\ Divergence_{JASO} - LTM\ 200\ hPa\ Divergence_{JASO}.$$

LSEF anomalies associated with ENLN, CCSM4 bias analyses, and CCSM4 projections were analyzed. Additionally, anomalies were used when comparing TC formation probabilities to highlight differences in values when compared to the LTM. For ENLN anomalies, the base period was JASO of 1981–2005. The EN periods were JASO of 1982, 1986, 1988, 1991, 1994, and 1997. The LN periods were JASO of 1984, 1988, 1995, 1998, 1999, and 2000. For CCSM4 bias differences (or anomalies), the base period was JASO 1981-2018. For CCSM4 projection anomalies, the base period was JASO 1981–2018. For investigations of future CCSM4 projections, decadal averages were computed and analyzed for JASO of 2021–2030, 2031–2040, and 2041–2050.

D. APPLICATION OF HTCFS: TC FORMATION PROBABILITY

The HTCFS has demonstrated skill in detecting the probability (Mundhenk 2009, Johnson 2011, and Meyer and Murphree 2015). Therefore, we chose to use this model to calculate TC formation probabilities with this thesis.

The HTCFS was used to calculate TC formation probabilities for the LTM, ENLN, CCSM4 bias analyses, and CCSM4 projections. The model produced TC probabilities based in the JASO averaged and interpolated LSEF data for 1981–2050. HTCFS generated probabilities between 0.003 and 0.02 were focused on for the years 1981–2018. For the years 2021–2050, TC formation probabilities increased throughout the WNP, and to capture these higher probabilities, probabilities between 0.006 to 0.04 were focused on, or two times the typical values during the years 1981–2018. JTWC Best Track, HURDAT2 best track, and NRL Monterey TC Page TC formation data were used to validate the accuracy of the data for 1981–2018. Accurate TC formation probabilities for 1981–2018 were indicated by many TC formation locations lying within the highest TC formation probability regions, with the highest concentration of TC formation locations occurring in the areas with the highest probabilities.

Figure 14 shows the adaption of the HTCFS process for seasonal and subseasonal TC probability forecasting (Meyer and Murphree 2015) that was used for climate change projections of TC formation probabilities. In this process, the statistical model from

HTCFS was used and forced with CCSM4 projections of the LSEFs. in response to this forcing, the statistical model produced TC formation probability projections.

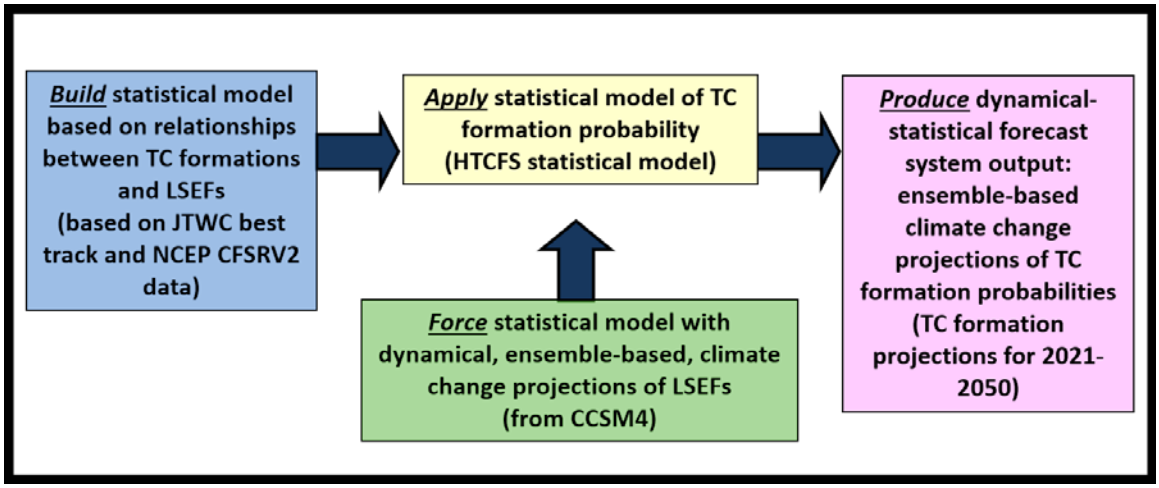

Figure 14. Overview of the process used to produce probabilistic climate change projections of TC formations. Adapted from Meyer and Murphree (2015).

The HTCFS statistical model was built using historical LSEF and historical TC data (Meyer and Murphree 2015). The ideal statistical model to have used in our study would have been one built using LSEF projections and TC formation projections. Climate models (such as CCSM4) provide LSEF projections but not TC projections. So, the ideal statistical model does not exist and was not available for our study. Without having the ideal model, it could not be determined how different the model used was from the ideal model, and how important this limitation was on the research methods might be. If the differences were small, then the limitations would likely have little impact on our results. If the differences were large, then the limitations might be problematic. It was expected that the potential impacts of this limitation are smaller for shorter range projections (e.g., smaller when projecting TC formation probabilities for 2021-2030 than for 2091-2100), since the near term future LSEFs and TC formations are more likely to be similar to those for the past several decades. This is one reason that we chose to apply our dynamical-statistical approach for only the next 30 years (2021-2050).

E. TIME SERIES ANALYSES

1. LTM

LTM LSEFs and TC formation probabilities were calculated for CCSM4 historical results for JASO of 1981–2005 so that it would encompass the entire CCSM4 historical results for 25 years. Statistical probabilities that were considered relevant with the HTCFS were TC formation probabilities between 0.003 and 0.02. These LTM results were used as our basis for comparison against ENLN data.

2. ENLN

To test the CCSM4 historical results, LSEFs and TC formation probabilities were calculated for ENLN years in JASO of 1981–2005. Assurance was needed that the CCSM4 historical dataset picked up known climate variations in the past such as ENLN in order to further validate its usage as a reliable future climate predictor. The EN years were: 1982, 1986, 1988, 1991, 1994, and 1997. The LN years were: 1984, 1988, 1995, 1998, 1999, and 2000. These ENLN years were verified as strong to moderate EN and LN years by the Multivariate ENSO Index (MEI) provided by the NOAA Climate Prediction Center (NOAA ESRL 2019). TC formation probability was formed for ENLN from the averaging of their respective JASO months and then averaging over the six years. Statistical probabilities that were considered relevant with the HTCFS were TC formation probabilities between 0.003 and 0.02. Further analysis compared the ENLN anomalies to the LTM.

3. Past Time Series 1981–2018

In order to see further trends in LSEF and TC formation probability, time series for CFSRV2 and CCSM4 were created for JASO of 1981–2018 in the CFR (see Chapter II, Section A). CCSM4 results were used for the years 1981–2018, which came from the 1981-2005 historical period and from the 2006-2018 portion of the CCSM4 RCP 8.5 projection results. Comparing CCSM4 results with CFSRV2 results allowed us to better gauge the validity of the CCSM4 data. In addition, annual TC formation numbers were evaluated for both the WNP (100°E–180°E, 0°N–50°N) and the CFR for JASO of 1981–2018 based on

JTWC best track data for 1981–2017 and the NRL Monterey TC Page for 2018. For our time series results, a least squares polynomial best fit line was used to highlight the long-term time series trends in the LSEFs and TC formation probabilities.

4. CCSM4 Biases

Climate model projections, including those from CCSM4, have biases (e.g., Gent et al. 2011, Meehl et al. 2012). However, corrections of those biases has received relatively little attention in prior studies. Biases were investigated in the CCSM4 LSEFs and TC formation probabilities by comparing these LSEFs and probabilities to those based on CFSRV2 data. In particular, CCSM4 minus CFSRV2 calculated differences for JASO 1981-2018. For 1981-2005, CCSM4 historical results were used and for 2006-2018, CCSM4 RCP 8.5 results were used.

5. Future Time Series 2018–2050

Future trends in LSEF and TC formation probability were evaluated through time series analysis in the CFR for CCSM4 future result projections for JASO of 2019–2050. For our time series results, a least squares polynomial best fit line was used to highlight the long-term time series trends in the LSEFs and TC formation probabilities.

6. Future CCSM4 2021–2050

The CCSM4 RCP 8.5 projection results were used for decadal analysis of future LSEFs and TC formation probabilities. The decades analyzed were JASO of: 2021–2030, 2031–2040, and 2041–2050. CCSM4 future projection anomaly calculations were made with CCSM4 results for JASO of 1981–2018. Of note is the change to TC formation probability scales with future projections to adequately capture higher TC formation probabilities. Statistical probabilities that were considered relevant with the HTCFS for CCSM4 future projections were TC formation probabilities between 0.006 and 0.04, two times the TC formation probabilities used with CCSM4 results from JASO of 1981–2018.

THIS PAGE INTENTIONALLY LEFT BLANK

III. RESULTS

Two of our initial objectives were to assess the ability of the CCSM4 outputs to: (1) describe the LSEFs for the past study period (JASO 1981-2005); and (2) describe the TC formation probabilities for the historical period when the CCSM4 derived LSEFs were used to force the NPS TC formation statistical model. To do this, the LTM LSEFs and the ENLN mean LSEFs were analyzed using CCSM4 output for JASO 1981–2005. These LSEFs were then used to force the statistical model.

A. WNP CCSM4 LTM 1981–2005

1. LSEFs

Figure 15 shows the LTM LSEFs for JASO 1981–2005 for the WNP based on the CCSM4 historical dataset.

Figure 15a shows the SST LSEF. The SST spatial pattern in the WNP is warmer temperatures near the equator to 20°N (26°C–29°C) and cooler temperatures towards to poles. (Note the large area of temperatures exceeding 28°C in the central portion of the WNP (130°E–180°E, 0°N–20°N). This is an area that is supportive for TC formation because of SST temperatures exceeding 26° as stated in Chapter I, Section B.8. Note also that SSTs shown in Figure 14a are approximately 0.25°C–0.5°C greater overall than those used by Johnson (2011) in the WNP. The largest differences are located in the central part of the WNP. This is likely an indication of a bias in the CCSM4 with SST. This is consistent with the surface temperature biases found in CCSM4 by Gent et al. (2011) and Meehl et al. (2012). See Chapter I, Section 6 for more discussion of biases in SST.

Figure 15b shows the 200 hPa–850 hPa vertical wind shear magnitude LSEF. Of note is the large area of low vertical wind shear with a southeast to northwest orientation (120E°–150°W, 0°N–20N°). This is an area that is expected to be favorable for TC formation with a shear magnitude between 0–8 ms^{-1}, below the threshold found by Meyer and Murphree (2015). The SCS shows an unsupportive area for TC formation with vertical wind shear between 16–20 ms^{-1}. The vertical wind shear values are consistent with results

from Johnson (2011), even though Johnson used a different method for calculating wind shear (zonal and meridional wind shear).

Figure 15c shows the relative vorticity at 850 hPa LSEF. Note the large area of positive vorticity throughout the WNP (100°E–150°W, 10°N–20°N). This is an area that is supportive for TC formation throughout the WNP. Note the area of negative relative vorticity to the east and west of Taiwan (100°E–150°W, 20°N–30°N) that is unsupportive of TC formation. These results are consistent with the results from Johnson (2011).

Figure 15d shows the divergence at 200 hPa LSEF. Note the large area of positive divergence throughout the WNP (100°E–150°W, 0°N–20°N). This is an area that is supportive for TC formation throughout the WNP. Note the area of low positive and negative divergence to the east and west of Taiwan (100°E–150°W, 20°N–30°N) that is unsupportive of TC formation. These results are consistent with the results from Johnson (2011).

Based on the LTM LSEFs, the area in the WNP that is favorable for TC formation would be from 100°E–150°W and 10°N–20°N since there are high SST, low vertical wind shear, positive 850 hPa relative vorticity, and positive 200 hPa divergence. The area that is unfavorable for TC formation would be from 100°E–150°W and 20°N–30°N since there are lower SSTs, high vertical wind shear, neutral to negative 850 hPa relative vorticity, and neutral to negative 200 hPa divergence.

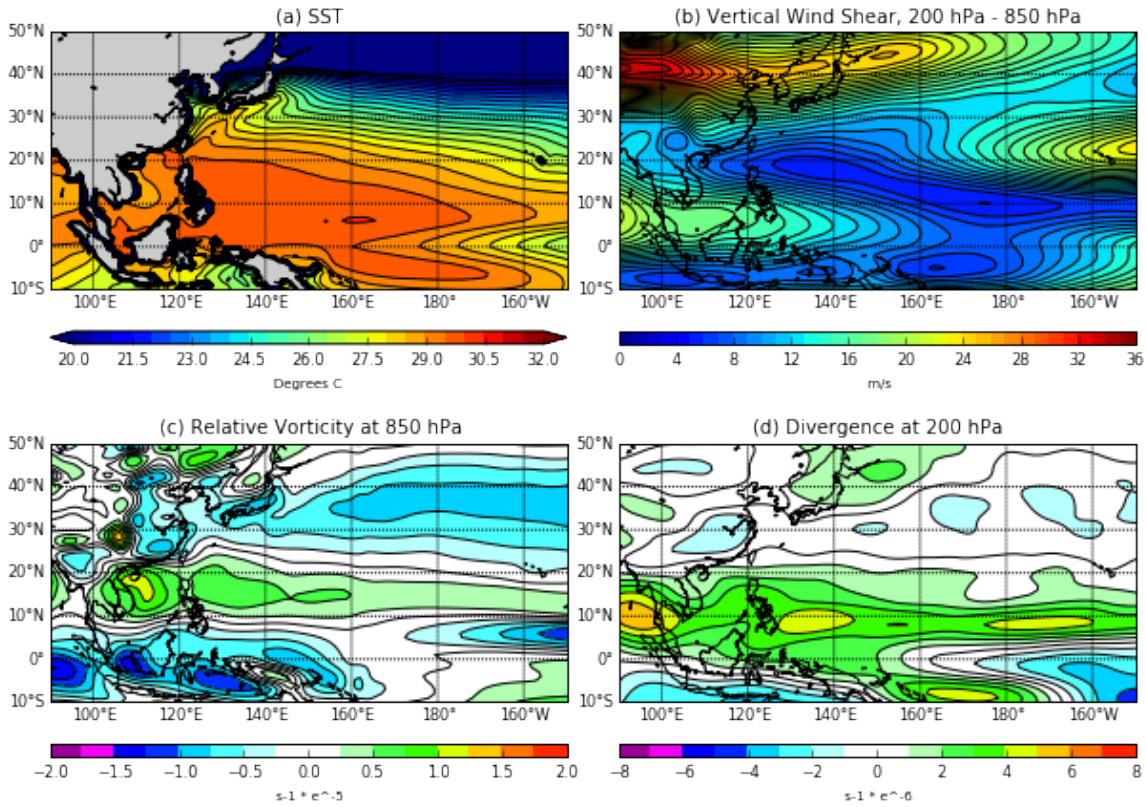

Figure 15. LTM LSEFs for JASO 1981–2005 based on CCSM4 historical results. (a) SST (°C); (b) vertical wind shear (m s^{-1}); (c) relative vorticity (s^{-1}); (d) divergence (s^{-1}).

2. WNP LTM TC Formation Probability

Figure 16 shows the LTM TC formation probability for JASO 1981–2005 for the WNP based on the CCSM4 dataset. The pink dots in this figure represent the TC formation locations in the study region for JASO 1981–2005. The calculation of the probabilities and the sources of the TC formation data are discussed in Chapter II, Section D.1. Note that the highest probabilities are located in the northern SCS, Luzon Strait, and Philippine Sea, and in the Kuroshio region near the Ryukyu Islands and southeast of southern Japan (120°W–150°E, 05°N–25°N) . This area of high probability is approximately co-located with favorable LTM LSEFs. Note that the TC formation locations are mostly located within the TC probability regions. However, the region of highest probability appears to lie 05°N–10°N of the area of highest formation density. A number of TC formation locations east of 160°E and north of 20°N fall outside the high probability region. In addition, the

probabilities are high in the region of the Kuroshio (130°E–140°E, 28°N–33°N), but there were relatively few TC formations in that region. The poor match near the Kuroshio may be because the SST temperatures are too high in that region (Gent et al. 2011, Meehl et al. 2012). Note the poor correlation of TC formation locations and TC formation probability in the subtropical region of the WNP (150°W–170°W, 05°N–08°N) due to formations not historically being a high formation area. The poor match mentioned above concerning the TC formation locations not located in the TC formation probability area east of the dateline may be due to the differences in the JTWC and HURDAT2 datasets with their reporting procedures or the TCs in this region being outliers due to the lack of favorable LSEFs needed in this region being characteristically worse.

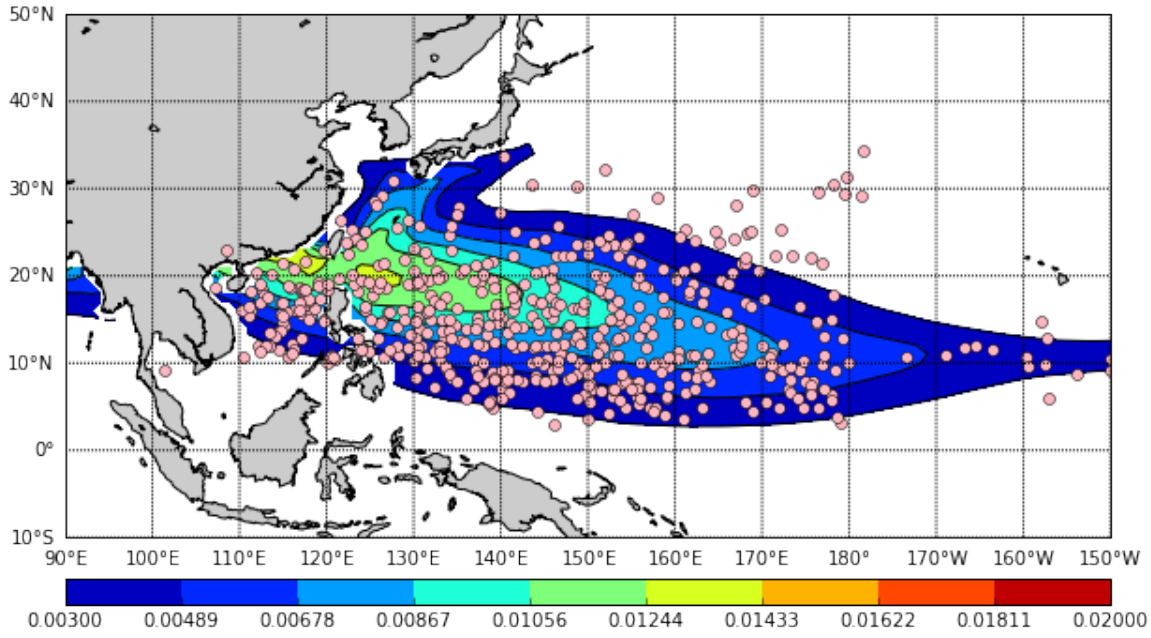

Figure 16. LTM TC formation probabilities for JASO 1981–2005 based on CCSM4 historical results (color shading) overlaid with locations of TC formations during this period (pink dots). TC formation locations are based on the JTWC Best Track and HURDAT2 datasets.

B. WNP CCSM4 EN

1. EN LSEFs

Figure 17 shows the EN LSEFs for JASO for the WNP based on the CCSM4 historical results. The EN years used are listed in Chapter II, Section E.2.

Figure 17a shows the SST LSEF. The spatial pattern for SSTs in the WNP is warmer temperatures near the equator to 20°N (26°C–29°C) and cooler temperatures towards to poles. Note the large area of SST exceeding 28°C in the eastern portion of the WNP (160°E–180°W, 05°N –12°N). This is an area that is expected to be supportive for TC formation because of SST temperatures exceeding 26°C as stated in Chapter I, Section B.8. Overall, the favorable TC formation areas of the WNP are 100°E–160°W and 0°N–20°N. These findings are consistent with the changes associated with an EN season and in agreement with Johnson (2011).

Figure 17b shows the 200 hPa – 850 hPa vertical wind shear magnitude LSEF. Of note is the large area of low vertical wind shear is favorable for TC formation and has a southeast to northwest orientation (120°E–150°W, 0°N–20°N). This is an area that is expected to be favorable for TC formation with a shear magnitude between 0–8 ms^{-1}, below the threshold found by Meyer and Murphree (2015). The SCS shows an unsupportive area for TC formation with vertical wind shear between 16–20 ms^{-1}. The vertical wind shear values are similar to the LTM and are consistent with results from Johnson (2011),

Figure 17c shows the relative vorticity at 850 hPa LSEF. Note the large area of positive relative vorticity throughout the WNP (100°E–150°W, 10°–20°N). This is an area that is supportive for TC formation throughout the WNP. Note the area of negative relative vorticity to the east and west of Taiwan (100°E–150°W, 20°N–30°N) that is unsupportive of TC formation. These results are similar to the LTM and are consistent with the results from Johnson (2011).

Figure 17d shows the divergence at 200 hPa LSEF. Note the large area of positive divergence throughout the WNP (100°E–150°W, 05°N–15°N). This is an area that is supportive for TC formation throughout the WNP. Note the area of low positive and negative divergence to the east and west of Taiwan (100°E–150°W, 20°N–30°N) that is

unsupportive of TC formation. These results are similar to the LTM and are consistent with the results from Johnson (2011).

Based on the EN LSEFs, the area in the WNP that is favorable for TC formation would be from 100°E–150°W and 05°N–20°N since there are high SSTs, low vertical wind shear, positive 850 hPa relative vorticity, and positive 200 hPa divergence. The area that is unfavorable for TC formation would be from 100°E–150°W and 20°N–30°N since there are lower SSTs, high vertical wind shear, neutral to negative 850 hPa relative vorticity, and neutral to negative 200 hPa divergence. These results are similar to the results found with the LTM LSEFs and have similar favorable TC formation locations.

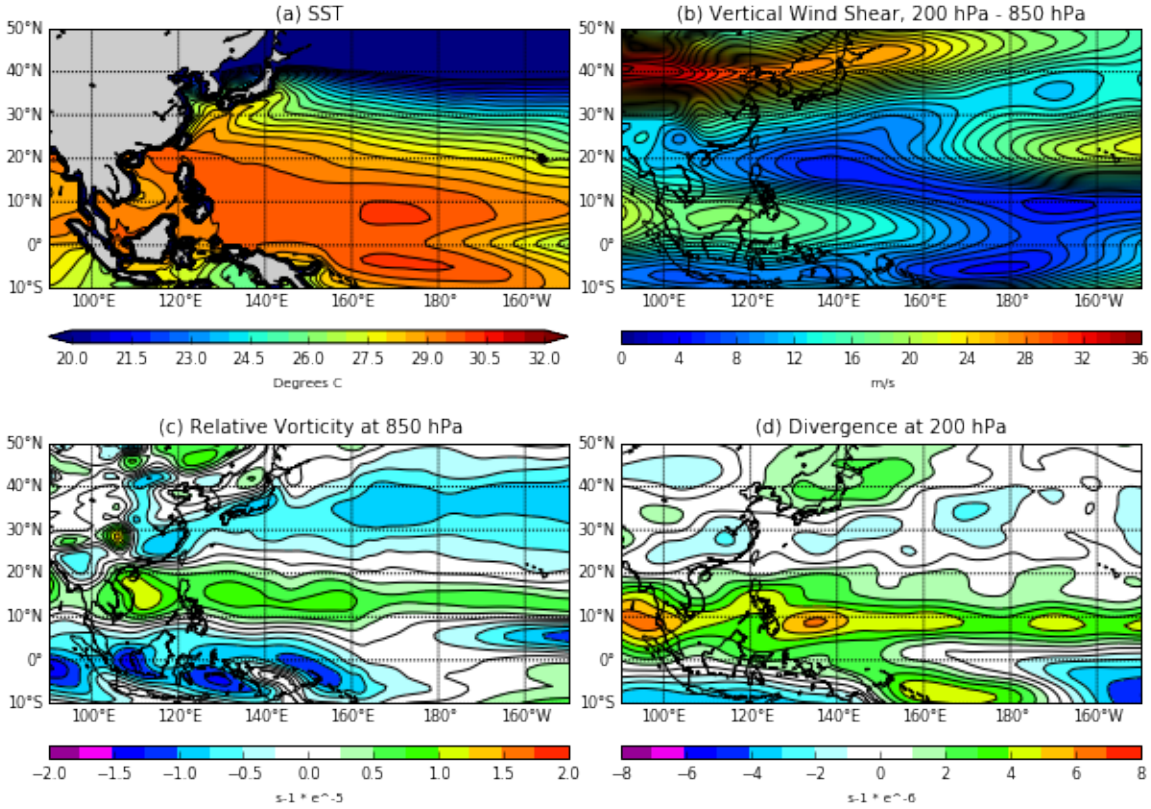

Figure 17. LSEFs for JASO of EN years (1982, 1986, 1987, 1991, 1997, 2002) based on CCSM4 historical results. (a) SST (°C); (b) vertical wind shear (m s^{-1}); (c) relative vorticity (s^{-1}); (d) divergence (s^{-1}).

2. EN TC Formation Probability

Figure 18 shows the EN JASO TC formation probability in the WNP based on the CCSM4 historical results. The pink dots in this figure represent all of the TC formations in the study region for EN JASO. During these EN JASO years, there were 125 TCs. The calculation of the TC formation probabilities and the sources of the TC formation data are discussed in Chapter II, Section D.1. Note that the highest probabilities are located in the northern SCS, Luzon Strait, and Philippine Sea, and in the Kuroshio region near the Ryukyu Islands and south of southern Japan (120°W–150°E, 05°N–25°N). This area of high probability is approximately co-located with favorable LTM LSEFs. Note that the TC formation locations are mostly located within the TC probability regions. However, the region of highest probability appears to lie 05°N–10°N and 20°E of the area of highest formation density. In addition, the probabilities are high in the region of the Kuroshio (120°E–130°E, 25°N–32°N), but there were no TC formations in that region. The poor match near the Kuroshio may be because the SST temperatures with CCSM4 are too high in that region (Gent et al. 2011, Meehl et al. 2012).

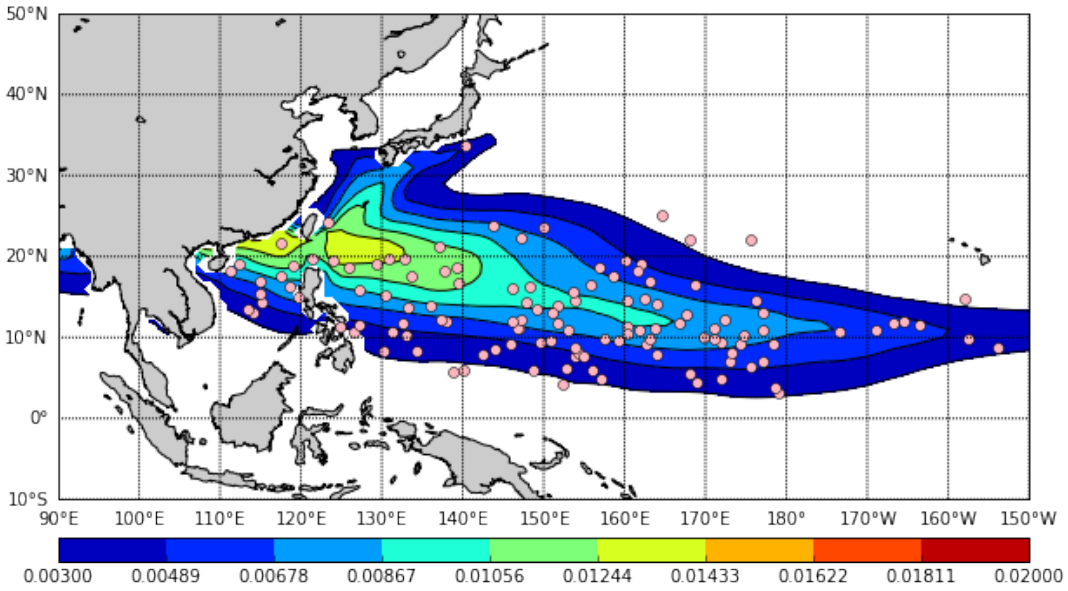

Figure 18. TC formation probabilities for JASO for EN years (1982, 1986, 1987, 1991, 1997, 2002) based on CCSM4 historical results (color shading) overlaid with locations of TC formations during this period (pink dots). TC formation locations are based on the JTWC Best Track and HURDAT2 datasets.

3. EN and LTM Anomalies

To highlight the differences between EN and the LTM, Figure 19 shows the EN LSEF anomalies for JASO for the WNP based on the CCSM4 historical results. Figure 19a shows the SST anomaly. Note the anomalously warm water in the eastern portion of the WNP (160°E–150°W, 0°N–15°N). This anomaly in SST is a good indicator as to why the TC formation probability movement is to the east with EN when compared to the LTM. Figure 19b shows the 200 hPa – 850 hPa vertical wind shear magnitude anomaly. Note the positive difference with wind shear in the western portion of the WNP (120°E–160°E, 0°N–10°N). Figure 19c shows the relative vorticity 850 hPa anomaly. Note the large positive difference in the entire portion of the WNP (100°E–150°W, 05°N–15°N). Figure 19d shows the divergence at 200 hPa anomaly. Note the large positive difference in the eastern portion of the WNP (100°E–170°W, 05°N–10°N).

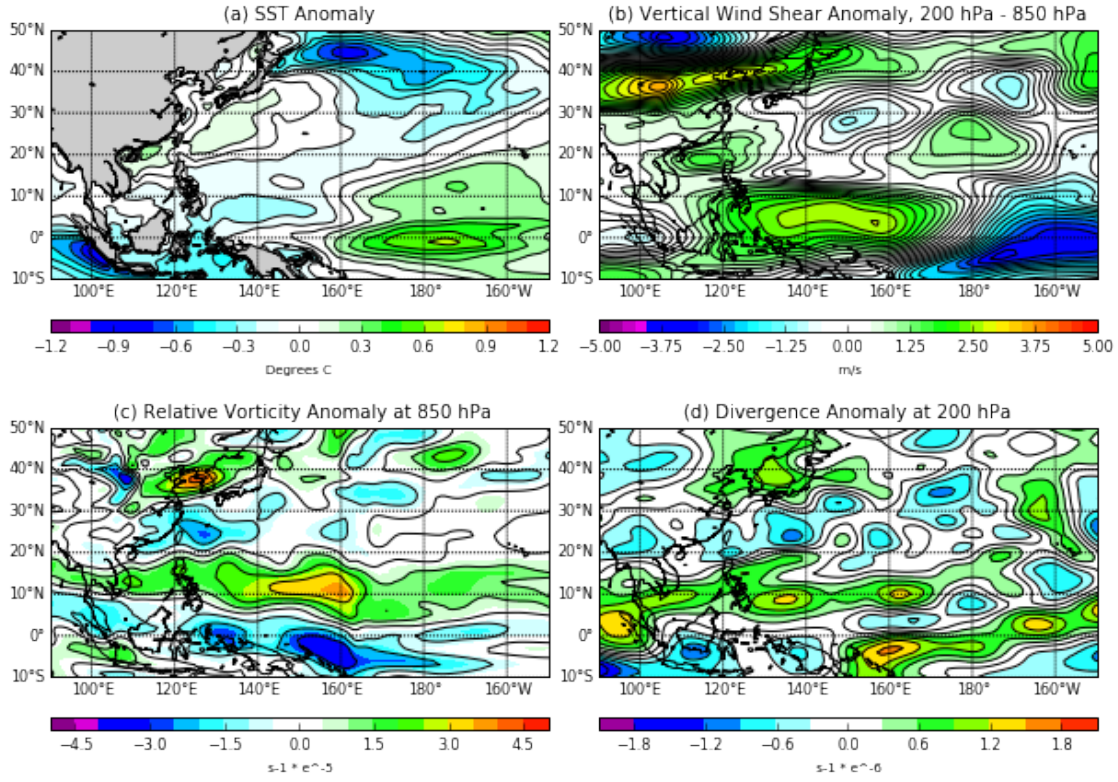

Figure 19. EN LSEF anomalies for JASO of 1981–2005 based on CCSM4 historical results. (a) SST (°C); (b) vertical wind shear (m s^{-1}); (c) relative vorticity (s^{-1}); (d) divergence (s^{-1}).

Figure 20 shows the EN TC formation probability anomalies for JASO of 1981–2005 for the WNP based on the LSEFs from the CCSM4 historical results. Of note are the anonymously high probabilities in the eastern part of the WNP (160°E–150°W, 0°N–15°N). During an EN season, it is expected that more TCs to form in the eastern part of the WNP These results are consistent with Johnson (2011).

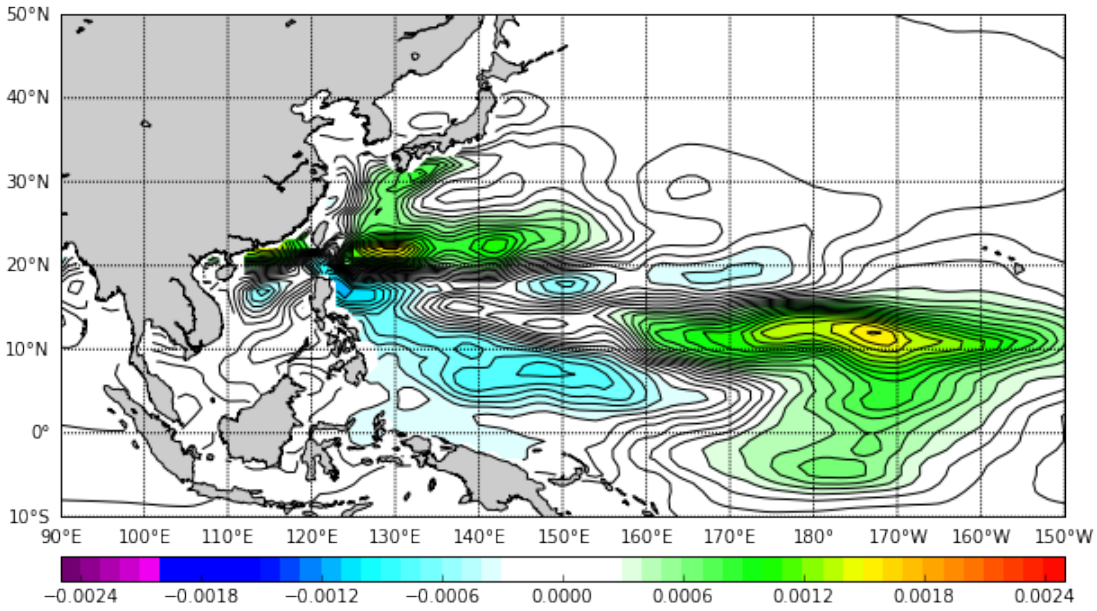

Figure 20. EN TC formation probability anomalies for JASO of 1981–2005 based on CCSM4 historical results.

C. WNP CCSM4 LN

1. LN LSEFs

Figure 21 shows the LN LSEFs for JASO for the WNP based on the CCSM4 dataset. The LN years used are listed in Chapter II, Section E.2.

Figure 21a shows the SST LSEF. The spatial pattern for SSTs in the WNP is warmer temperatures near the equator to 20°N (26°C–29°C) and cooler temperatures towards to poles. Note the large area of SST exceeding 28°C in the central and eastern portion of the WNP (130°E–155°W, 02°N –15°N). This is an area that is expected to be supportive for TC formation because of SST temperatures exceeding 26°C as stated in

Chapter I, Section B.8. Overall, the favorable TC formation areas of the WNP are 100°E–180°E, 05°N–20°N. These findings are consistent with the changes associated with an LN season and in agreement with Johnson (2011).

Figure 21b shows the 200 hPa – 850 hPa vertical wind shear magnitude LSEF. Vertical wind shear is favorable for TC formation and has a southeast to northwest orientation between the equator and 20°N. The TC favorable area has a shear magnitude between 0–8 ms^{-1} and has shifted more west when compared to the LTM.

Figure 21c shows the relative vorticity at 850 hPa LSEF. Note the large area of positive relative vorticity in the eastern portion of the WNP (100°E–130°W, 10°N–20°N). This is an area that is supportive for TC formation in the WNP. Note the area of negative relative vorticity to the east and west of Taiwan (100°E–150°W, 20°N–30°N) that is unsupportive of TC formation. These results are similar to are consistent with the results from Johnson (2011).

Figure 21d shows the divergence at 200 hPa LSEF. Note the large area of positive divergence throughout the WNP (100°E–150°W, 0°N–20°N). This is an area that is supportive for TC formation throughout the WNP. These results are consistent with the results from Johnson (2011).

Based on the LN LSEFs, the area in the WNP that is favorable for TC formation would be from 100°E–180°E and 05°N–20°N since there are high SSTs, low vertical wind shear, positive 850 hPa relative vorticity, and positive 200 hPa divergence. The area that is unfavorable for TC formation would be from 100°E–150°W and 20°–30°N and in the eastern WNP from 180°W150°W and 10°N–20°N since there are lower SSTs, high vertical wind shear, neutral to negative 850 hPa relative vorticity, and neutral to negative 200 hPa divergence.

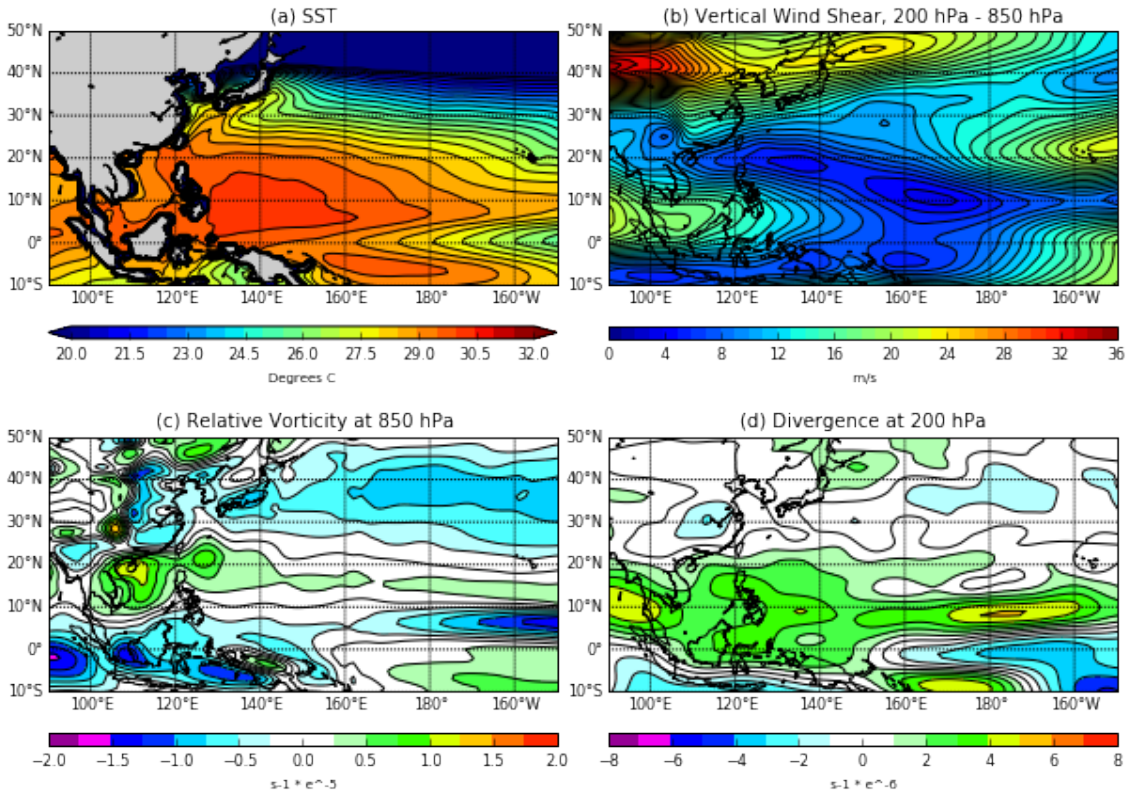

Figure 21. LSEFs for JASO of LN years (1984,1988,1995,1998,1999,2000) based on CCSM4 historical results. (a) SST (°C); (b) vertical wind shear (m s^{-1}); (c) relative vorticity (s^{-1}); (d) divergence (s^{-1}).

2. LN TC Formation Probability

Figure 22 shows the LN JASO TC formation probability in the WNP based on the CCSM4 historical results. The pink dots in this figure represent all of the TC formations in the study region for LN JASO. During these LN JASO years, there were 140 TCs. The calculation of the TC formation probabilities and the sources of the TC formation data are discussed in Chapter II, Section D.1. Note that the highest probabilities are located in the northern SCS, Luzon Strait, Philippine Sea, central WNP, and in the Kuroshio region near the Ryukyu Islands and south of southern Japan (115°W–170°E, 05°N–25°N) . This area of high probability is approximately co-located with favorable LN LSEFs. Note that the TC formation locations are mostly within the TC probability regions. However, the region of highest probability appears to lie 05°S of the area of highest formation density. In

addition, the probabilities are high in the region of the Kuroshio (120°E–130°E, 25°N–32°N), but there were few TC formations in that region. The poor match near the Kuroshio may be because the SST temperatures with CCSM4 historical results are too high in that region (Gent et al. 2011, Meehl et al. 2012).

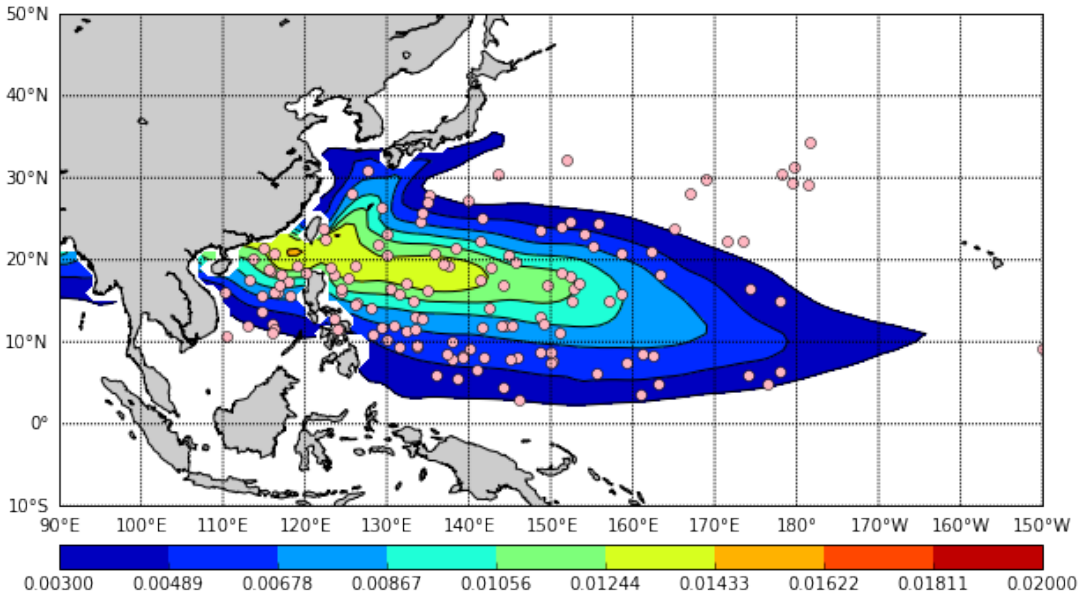

Figure 22. TC formation probabilities for JASO for LN years (1984, 1988, 1995, 1998, 1999, 2000) based on CCSM4 historical results (color shading) overlaid with locations of TC formations during this period (pink dots). TC formation locations are based on the JTWC Best Track and HURDAT2 datasets.

3. LN and LTM Anomalies

To highlight the differences between LN and the LTM, Figure 23 shows the LN LSEF anomalies for JASO for the WNP based on the CCSM4 historical dataset.

Figure 23a shows the SST anomaly. Note the region of anonymously cool water in the eastern portion of the WNP (150°E–150°W, 0°N–10°N). Additionally, there is an anomalously warm area of water in the central and eastern WNP (120°E–160°E, 0°N–20°N). This anomaly in SST is a good indicator as to why the TC formation probability

movement is to the west with LN when compared to the LTM. These results are consistent with Johnson (2011).

Figure 23b shows the 200 hPa – 850 hPa vertical wind shear magnitude anomaly. Note the positive difference with wind shear in the eastern portion of the WNP (180°W–150°W, 0°N–15°N).

Figure 23c shows the relative vorticity at 850 hPa anomaly. Note the large positive difference in the northern SCS and east of the Luzon Strait (110°E–160°E, 20°N–30°N). Additionally, there is an area of negative values across the WNP for relative vorticity (120°E–150°W, 10°N–20°N).

Figure 23d shows the divergence at 200 hPa anomaly. Note the band of negative differences in the western and central portion of the WNP (100°E–170°W, 05°N–20°N).

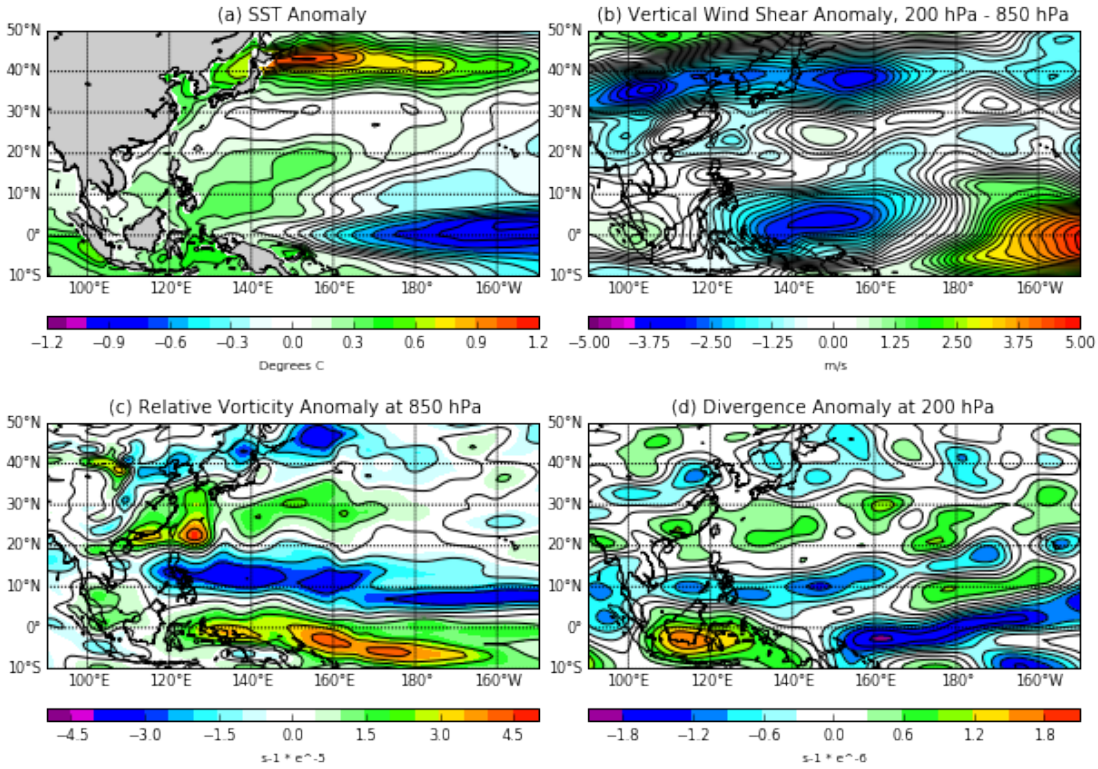

Figure 23. LN LSEF anomalies for JASO of 1981–2005 based on CCSM4 historical results. (a) SST (°C); (b) vertical wind shear (m s^{-1}); (c) relative vorticity (s^{-1}); (d) divergence (s^{-1}).

Figure 24 shows the LN TC formation probability anomalies for JASO for the WNP based on the LSEFs from the CCSM4 historical results. Of note are the anonymously high probabilities in the western and central parts of the WNP (110°E–165°E, 0°N–22°N). During an LN season, it is expected more TCs to form in the western and central part of the WNP. These results are consistent with Johnson (2011).

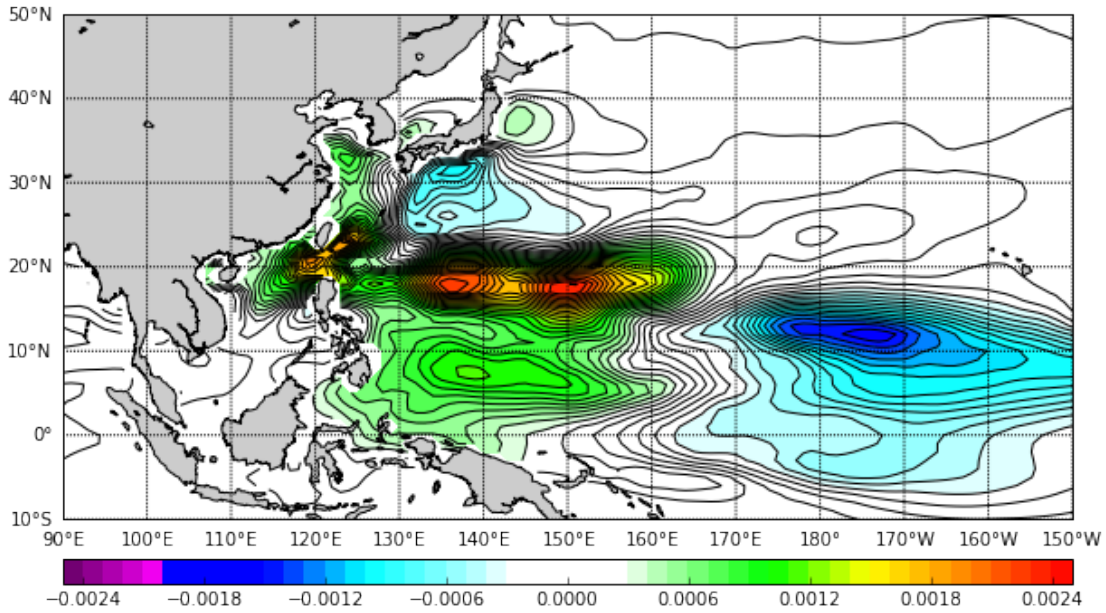

Figure 24. LN TC formation probability anomalies for JASO of 1981–2005 based on CCSM4 historical results.

D. LSEF AND TC FORMATION PROBABILITY TIME SERIES FOR CFR 1981–2018

A time series analyses was conducted for the CFR (see Chapter II, Section A) to understand how the LSEFs and TC formation probabilities changed during JASO of 1981–2018. For the time series analyses, CFSRV2 and CCSM4 LSEF and TC formation probability results were compared to better understand the results, especially the CCSM4 results. For this section, CCSM4 results were used for the years 1981–2018, which came from the 1981–2005 historical period and from the CCSM4 RCP 8.5 results for 2006–2018. Comparing CCSM4 results with CFSRV2 results allowed us to better assess the accuracy of the CCSM4 results. For the time series figures, a least squares polynomial best fit line

(dashed line) was used to highlight the long-term time series trends in the LSEFs and TC formation probabilities.

1. CFR CFSRV2 and CCSM4 LSEFs

Figure 25 shows the time series for LSEFs in the CFR for JASO of 1981–2018 based on the CCSM4 and CFSRV2 results.

Figure 25a shows the SST LSEFs. Note the increasing trends for SST for both the CCSM4 and CFSRV2 data sets. CCSM4 has an overall higher SST consistent with the overall bias of about 0.4°C mentioned in Chapter I, Section B.6. In general, these trends are positive and supportive of increased probability of TC formation during this period.

Figure 25b shows the 200 hPa – 850 hPa vertical wind shear magnitude LSEFs. Note that shear decreasing throughout the time series is a similar trend seen with CCSM4 and CFSRV2. CCSM4 has a lower overall wind shear magnitude over the time period when compared to CFSRV2. Although both shear magnitudes for CFSRV2 and CCSM4 are below the threshold for inhibiting TC formation (Johnson 2011, Murphree and Meyer 2015), CCSM4 shear values are lower and therefore more favorable for TC formation.

Figure 25c shows the relative vorticity at 850 hPa LSEFs. Relative vorticity shows an increasing trend throughout the time series for both CCSM4 and CFSRV2. CCSM4 relative vorticity magnitudes are higher than those of CFSRV2. For both time series, the values are positive and thus supportive of TC formation.

Figure 25d shows the divergence at 200 hPa LSEFs. Divergence differs between CCSM4 and CFSRV2, with CCSM4 showing an increasing trend while CFSRV2 shows a decreasing trend throughout the time series. CCSM4 values are positive and thus supportive of TC formation.

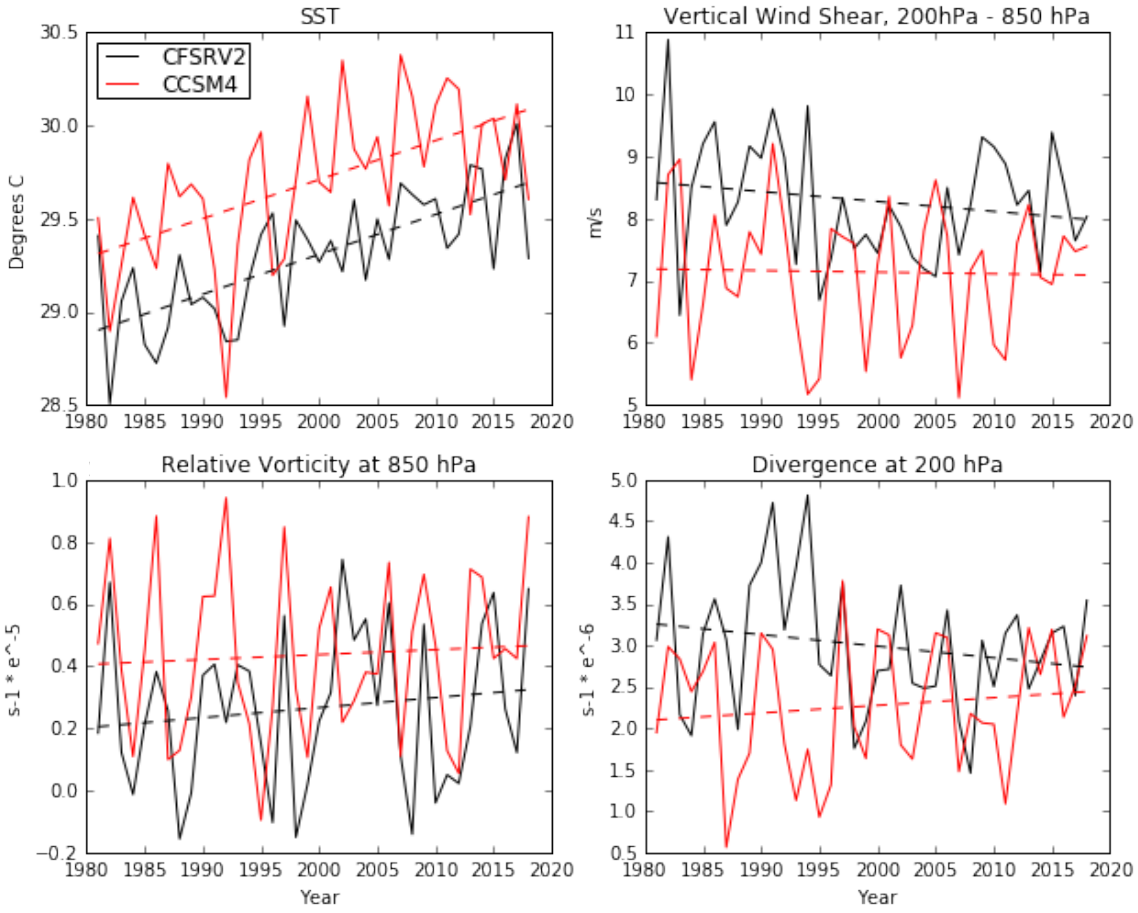

Figure 25. LSEFs for the CFR for JASO of 1981–2018 based on CCSM4 results (red) and CFSRV2 results (black) with best fit trend lines (dashed). (a) SST (°C); (b) vertical wind shear (m s^{-1}); (c) relative vorticity (s^{-1}); (d) divergence (s^{-1}).

Overall in the time series shown in Figure 25, CCSM4 is more supportive of TC formation in the CFR than CFSRV2 with respect to all four LSEFs: SST, vertical wind shear, relative vorticity, and divergence in the CFR. This indicates that the corresponding TC formation probabilities in the CFR based on the CCSM4 LSEFs should be greater than those based on the CFSRV2 LSEFs.

2. TC Formation Numbers in the WNP and CFR

Figure 26 shows the TC formation numbers for JASO of each year during 1981–2018 for the WNP (100°E–180°E, 0°N–50°N) and for the CFR (127°E–165°E, 08°N–

21°N). For the year 2018, the NRL Monterey TC Page was used as discussed in Chapter II, Section B.3. There is a decreasing trend in TCs per year in the WNP and an increasing trend in TCs in the CFR. For the WNP there was a decrease of 0.25 TCs per decade, with a decrease of one TC over the entire period. Kossin et al (2016) and Colbert et al. (2015) also found decreases in TC formations in the WNP. For the CFR, there was an increase of 0.75 TCs per decade, with an increase of three TCs over the entire period. Overall, there was an approximate decrease in TC formations in the WNP by 5% and an increase in the CFR TC formations by 33% for JASO of 1981–2018. These results indicate that TC formation locations may have shifted into the CFR from other sub-regions of the WNP. However, the TC formation numbers have a standard deviation of 4.07 TCs in the WNP and 2.75 TCs in the CFR. These are relatively large standard deviations and indicate a relatively high level of uncertainty about the trends for both the WNP and CFR. For more information regarding the values used in Figure 26, see Appendix Table 3.

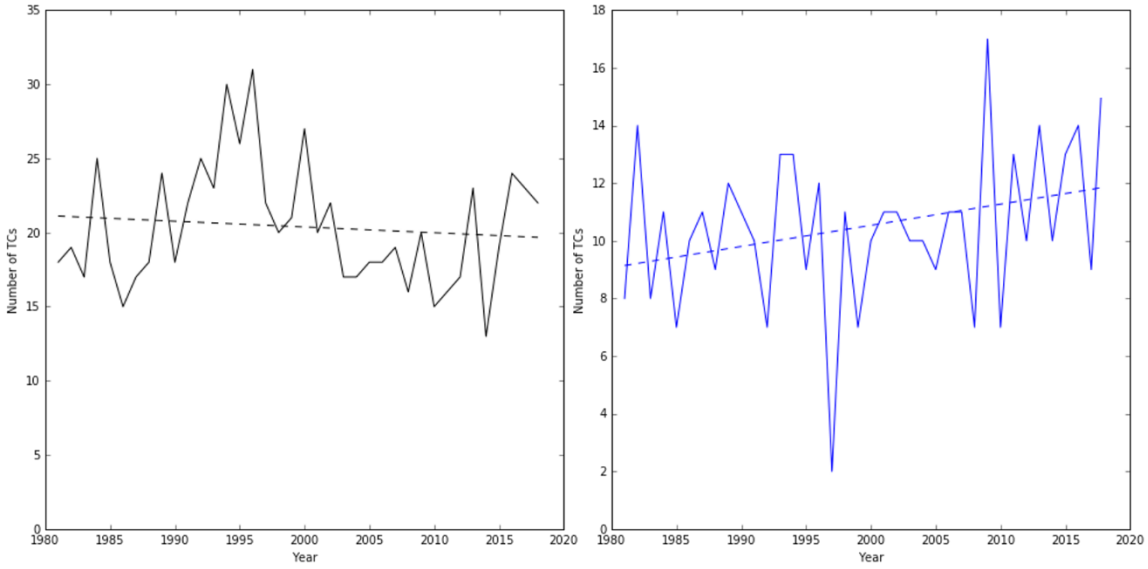

Figure 26. Number of TCs per year in the WNP (black, left) and CFR (blue, right) in JASO for 1981–2018 based on JTWC best track data and the NRL TC Page with best fit trend lines (dashed).

The increase in TC numbers suggests that the CFR TC formation probabilities also increased during 1981–2018. To test this, the corresponding TC formation probabilities were calculated, which are shown in the next section.

3. CFR CFSRV2 and CCSM4 TC Formation Probability

Figure 27 shows the TC formation probability time series in the CFR for JASO of 1981–2018 for CCSM4 and CFSRV2. Note the increasing trend for both CCSM4 and CFSRV2 during this period. CCSM4 TC formation probabilities are higher due to more favorable conditions with LSEFs (see Figure 25, Chapter III, Section D.1). This increasing trend is consistent with the increasing trend in the numbers of TCs in the CFR (see Chapter III, Section D.2).

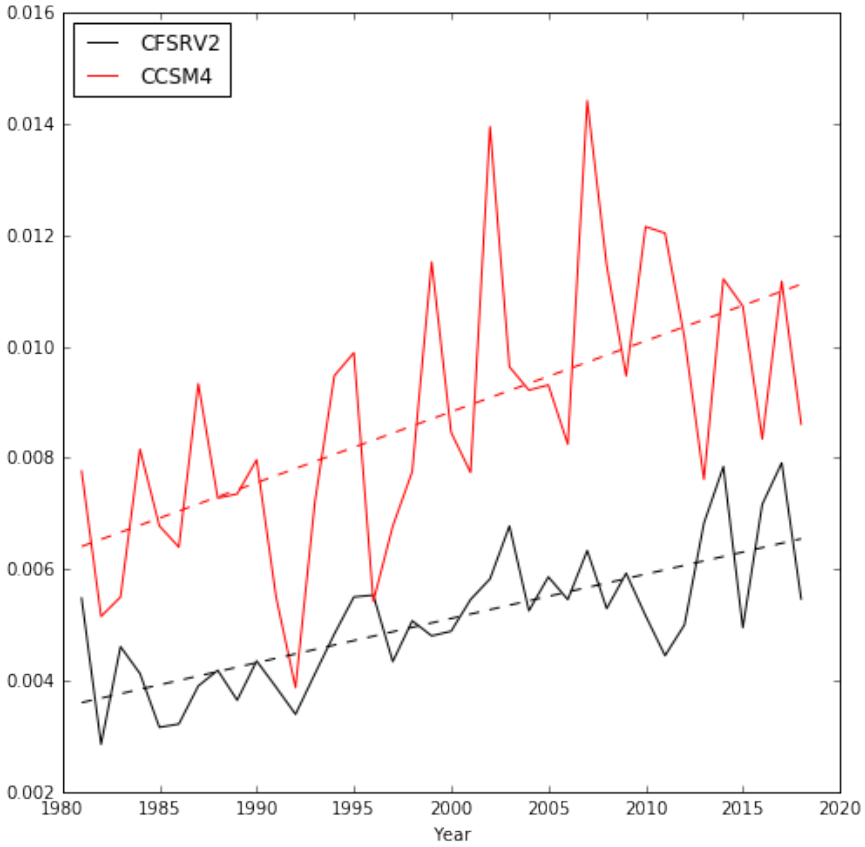

Figure 27. TC formation probabilities for the CFR for JASO 1981–2018 based on CCSM4 results (red) and CFSRV2 results (black) with best fit trend lines (dashed).

E. CCSM4 BIASES

Biases were assessed in the CCSM4 results for JASO 1981–2018 using the methods described in Chapter II, Section E.4. This assessment was motivated by prior studies (e.g., Gent et al. 2011) and our own results shown in prior sections of this chapter. The possibility of using the 1981–2018 differences between CFSRV2 and CCSM4 LSEFs and TC formation probabilities to develop bias corrections to the CCSM4 LSEF and TC formation probabilities was investigated. The objective was to determine if such bias corrections could feasibly be used to improve the CCSM4 LSEF and TC formation probability projections for 2021–2050.

1. CFSRV2 LTM LSEFs and TC Formation Probability 1981–2018

Figure 28 shows the CFSRV2 LSEFs for JASO 1981–2018 from the results in the WNP.

Figure 28a shows the SST LSEF. The SST spatial pattern in the WNP is warmer temperatures from near the equator to 20°N (26°C–29°C) and cooler temperatures in higher latitudes. Note the large area of temperatures exceeding 28°C in the central portion of the WNP (120°E–170°W, 0°N–22°N). This is an area that is supportive for TC formation because the SSTs exceed 26°C (see Chapter I, Section B.8).

Figure 28b shows the 200 hPa – 850 hPa vertical wind shear magnitude LSEF. Of note is the large area of low vertical wind shear with a northwest to southeast orientation (120E°–180°E, 0°N–25°N). This is an area that is expected to be supportive for TC formation with a shear magnitude between 0–8 ms^{-1}, below the threshold found by Meyer and Murphree (2015). The SCS and the eastern WNP (160E°–150°W, 15°N–25°N) show an unsupportive area for TC formation with vertical wind shear between 16–24 ms^{-1}.

Figure 28c shows the relative vorticity at 850 hPa LSEF. Note the area of positive relative vorticity throughout the WNP (100°E–150°W, 10°N–20°N). This is an area that is supportive for TC formation.

Figure 28d shows the divergence at 200 hPa LSEF. Note the large area of positive divergence throughout the WNP (100°E–150°W, 05°N–20°N). This is an area that is supportive for TC formation throughout the WNP.

Based on the CFSRV2 LSEFs, the area in the WNP that is favorable for TC formation would be from 120°E–180°E and 05°N–20°N since there are high SSTs, low vertical wind shear, positive 850 hPa relative vorticity, and positive 200 hPa divergence. The area that is unfavorable for TC formation would be in the SCS and in the eastern part of the WNP at 160°E–150°W and 10°N–20°N since there are lower SSTs, high vertical wind shear, neutral to negative 850 hPa relative vorticity, and neutral to negative 200 hPa divergence.

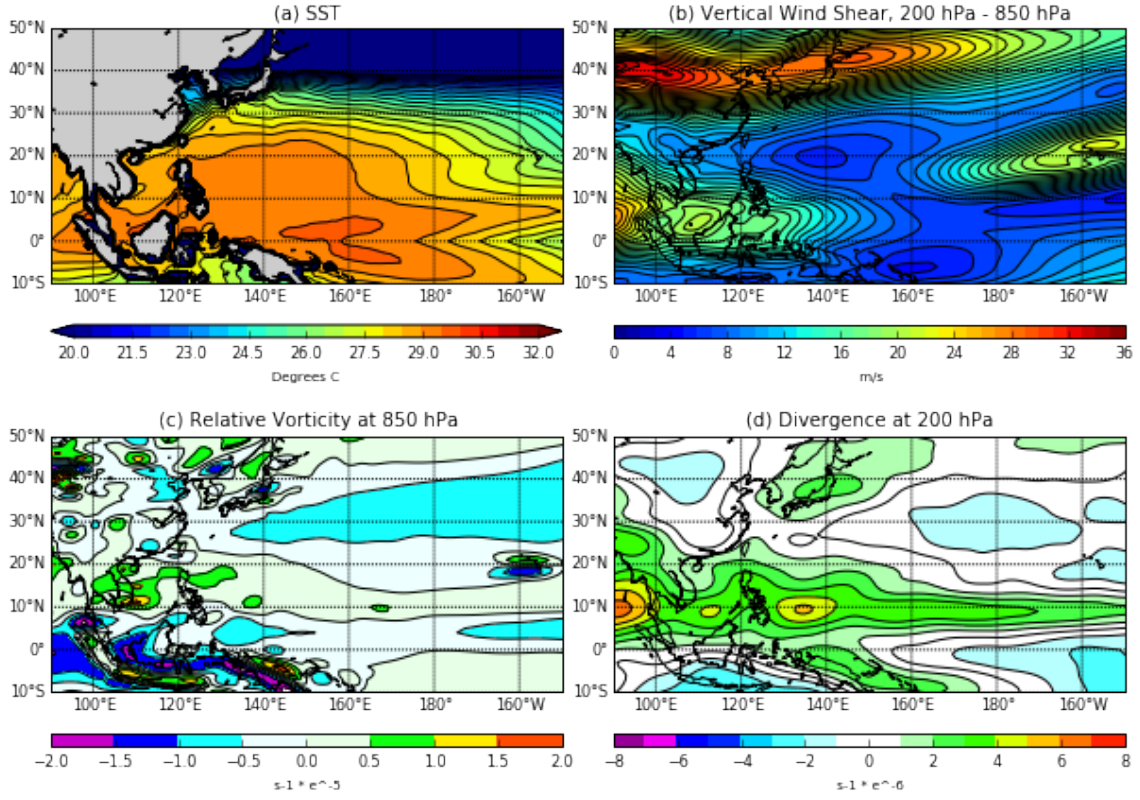

Figure 28. LSEFs for JASO 1981–2018 based on CFSRV2 results. (a) SST (°C); (b) vertical wind shear (m s^{-1}); (c) relative vorticity (s^{-1}); (d) divergence (s^{-1}).

Figure 29 shows the CFSRV2 JASO 1981–2018 TC formation probability in the WNP based on the CCSM4 dataset. The pink dots in this figure represent all of the TC formation locations in the study region for JASO 1981-2018. During this period, there were 1,145 TCs. The highest probabilities are centered near 110°W–160°E and 10°N–25°N. Note that the TC formation locations are mostly located within the higher TC probability regions. However, many of the TC formations east of 170°E occurred outside the area of relatively high probabilities. This poor match may be due to the differences in the JTWC and HURDAT2 datasets with their reporting procedures, or to the TCs in this region being outliers in terms of the favorable LSEFs represented by the statistical model used.

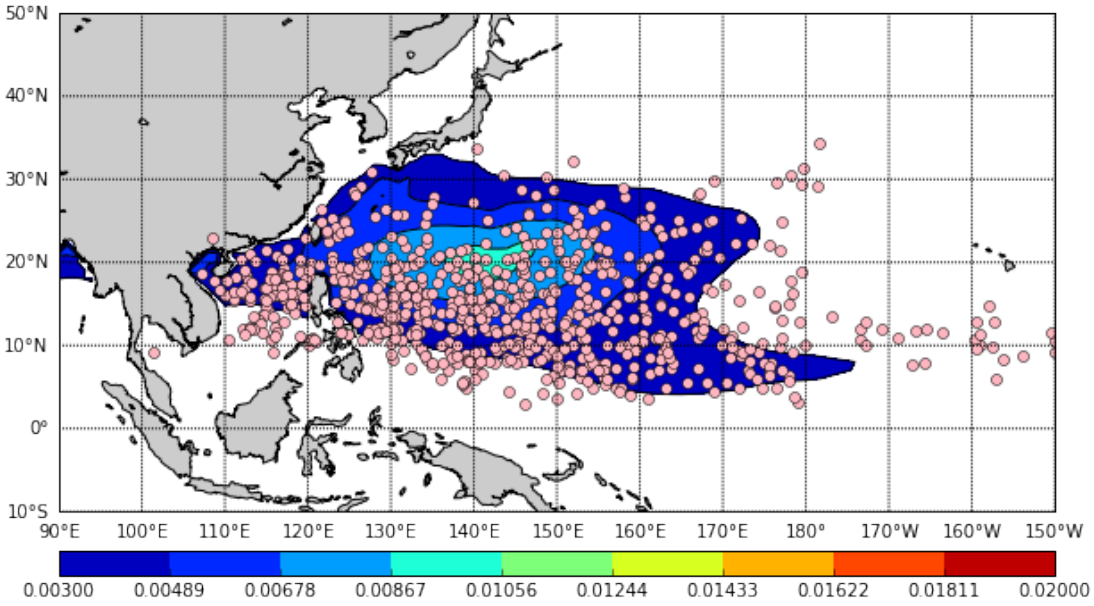

Figure 29. TC formation probabilities for JASO 1981–2018 based on CFSRV2 results (color shading) overlaid with locations of TC formations during this period (pink dots). TC formation locations are based on the JTWC Best Track and HURDAT2 datasets.

2. CCSM4 LSEFs and TC Formation Probability

Figure 30 shows the LTM LSEFs for JASO 1981–2018 for the WNP based on CCSM4 results.

Figure 30a shows the SST LSEF. The SST spatial pattern in the WNP is warmer temperatures near the equator to 20°N (26°C–29°C) and cooler temperatures towards to poles. (Note the large area of temperatures exceeding 29°C in the central portion of the WNP (140°E–170°E, 05°N–10°N). The supportive area for TC formation is 110°E–150°W and 05°N–20°N. This is an area that is supportive for TC formation because of SST temperatures exceeding 26° (see Chapter I, Section B.8).

Figure 30b shows the 200 hPa – 850 hPa vertical wind shear magnitude LSEF. Of note is the large area of low vertical wind shear with a southeast to northwest orientation (120E°–150°W, 0°N–20N°). This is an area that is expected to be favorable for TC formation with a shear magnitude between 0–8 ms^{-1}, below the threshold found by Meyer and Murphree (2015). The SCS shows an unsupportive area for TC formation with vertical wind shear between 16–20 ms^{-1}.

Figure 30c shows the relative vorticity at 850 hPa LSEF. Note the large area of positive vorticity throughout the SCS and WNP (100°E–150°W, 10°N–20°N). This is an area that is supportive for TC formation throughout the WNP.

Figure 30d shows the divergence at 200 hPa LSEF. Note the large area of positive divergence throughout the WNP (100°E–150°W, 0°N–20°N). This is an area that is supportive for TC formation throughout the WNP.

Based on these LSEFs, the area in the WNP that is favorable for TC formation would be from 100°E–150°W and 10°N–20°N since there are high SST, low vertical wind shear, positive 850 hPa relative vorticity, and positive 200 hPa divergence. The area that is unfavorable for TC formation is from 100°E–150°W and 20°N–30°N since there are lower SSTs, high vertical wind shear, neutral to negative 850 hPa relative vorticity, and neutral to negative 200 hPa divergence.

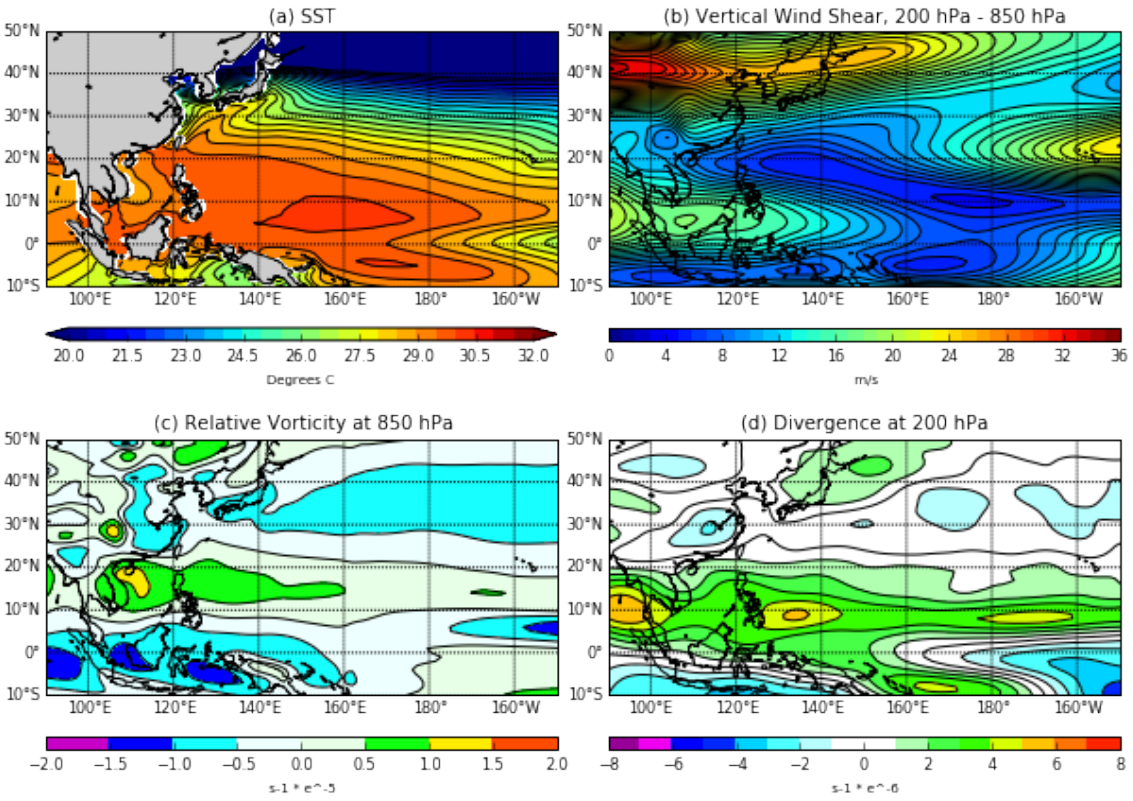

Figure 30. LSEFs for JASO 1981–2018 based on CCSM4 results. (a) SST (°C); (b) vertical wind shear (m s^{-1}); (c) relative vorticity (s^{-1}); (d) divergence (s^{-1}).

Figure 31 shows the LTM TC formation probability for JASO 1981–2018 for the WNP based on the CCSM4 dataset. The pink dots in this figure represent all of the TC formations in the study region for JASO years. During these years, there were 1,145 TCs. The calculation of the probabilities and the sources of the TC formation data are discussed in Chapter II, Section D.1. Note that the highest probabilities are located in the northern SCS, Luzon Strait, and Philippine Sea, and southeast of southern Japan (110°E–150°W, 05°N–25°N). This area of high probability is approximately co-located with favorable LTM LSEFs. Note that the TC formation locations are mostly located within the TC probability regions. However, the region of highest probability appears to lie 5°N–10°N of the area of highest formation density. A number of TC formation locations east of 160°E and north of 20°N fall outside the high probability region. In addition, the probabilities are high in the region of the Kuroshio (130°E–140°E, 28°N–33°N), but there were relatively

few TC formations in that region. The poor match near the Kuroshio may be because the SST temperatures are too high in that region (Gent et al. 2011, Meehl et al. 2012). Note the poor correspondence between TC formation locations and TC formation probabilities in the subtropical region of the WNP (150°W–170°W, 05°N–08°N). The poor match mentioned above concerning the TC formation locations not located in the TC formation probability area east of the dateline may be due to the differences in the JTWC and HURDAT2 datasets with their reporting procedures or the TCs in this region being outliers because of the lack of favorable LSEFs in this region.

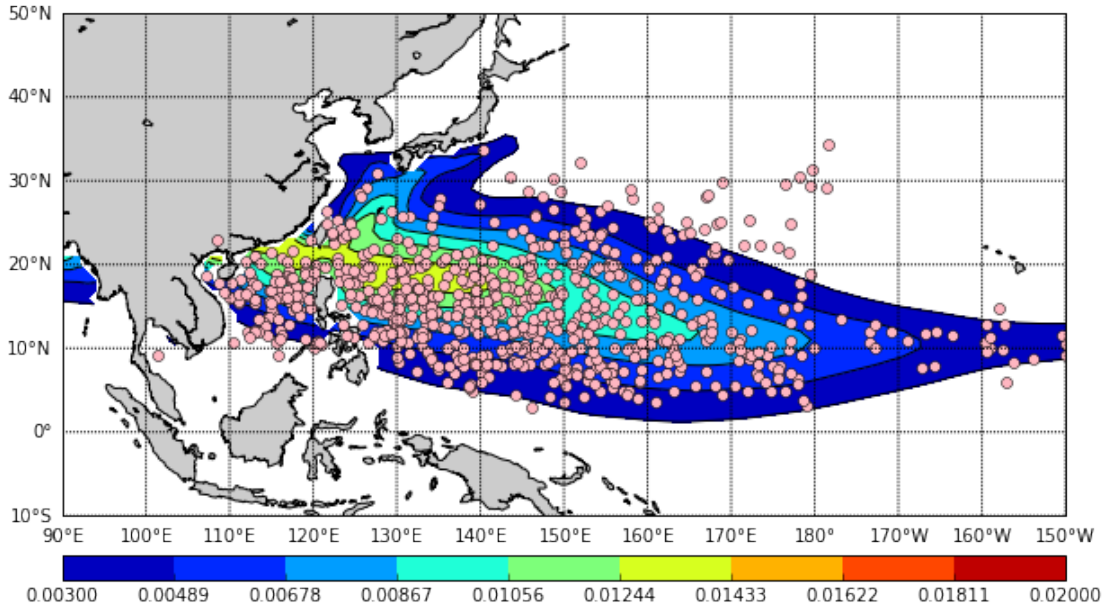

Figure 31. TC formation probabilities for JASO 1981–2018 based on CCSM4 results (color shading) overlaid with locations of TC formations during this period (pink dots). TC formation locations are based on the JTWC Best Track and HURDAT2 datasets.

3. Differences between CCSM4 and CFSRV2

One way to identify biases in the CCSM4 LSEF projections is by evaluating the differences between the LSEFs in CFSRV2 and CCSM4 for JASO of 1981–2018 (CCSM4 results minus CFSRV2 results). Figure 31 shows the LSEF differences for JASO 1981–2018 between CCSM4 and CFSRV2.

Figure 32a shows the SST LSEF differences. CCSM4 has a warmer temperature by about 1.5°C from 120°E–150°W and 05°N–20°N. The higher CCSM4 SST would support more TC formations within the WNP.

Figure 32b shows the 200 hPa – 850 hPa vertical wind shear magnitude LSEF differences. CCSM4 shows a lower vertical wind shear from 145°E–160°W and 10°N–20°N. CCSM4 vertical wind shear shows more support for TC formations than CFSRV2.

Figure 32c shows the relative vorticity at 850 hPa LSEF differences. CCSM4 shows a higher relative vorticity from 110°E–170°W and 10°N–30°N. CCSM4 relative vorticity shows more support for TC formations than CFSRV2.

Figure 32d shows the divergence at 200 hPa LSEF differences. Of note is that CCSM4 has higher divergence in the eastern part of the WNP from 160°E–150°W and 05°N–20°N.

Based on the LSEFs differences when comparing CCSM4 and CFSRV2, it is expected that there will be higher TC formation probabilities and larger TC formation areas with CCSM4 results due to the more favorable LSEF conditions. CCSM4 for the most part across the WNP has more favorable TC formation conditions since there are higher SSTs, lower vertical wind shear areas, more positive relative vorticity areas, and higher divergence areas. Of note is the much more favorable conditions for TC formation in the eastern part of the WNP for CCSM4.

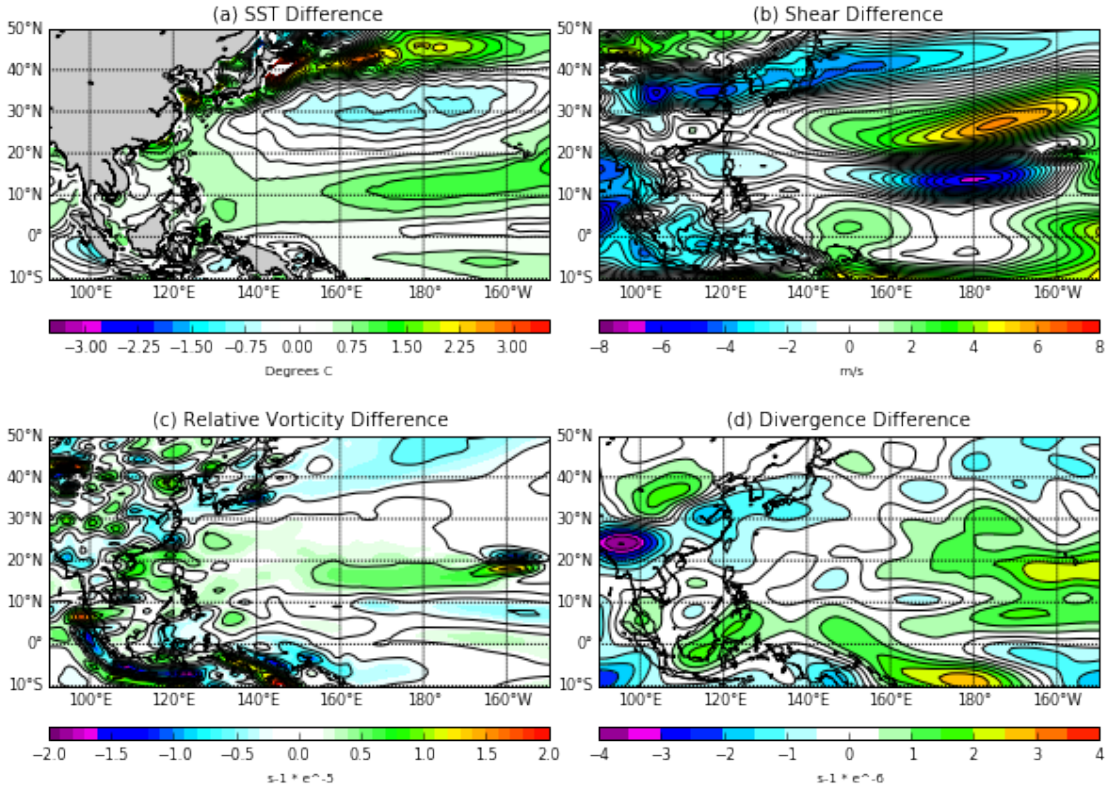

Figure 32. LSEF anomalies for JASO of 1981–2018 based on CCSM4 and CFSRV2 results. (a) SST (°C); (b) vertical wind shear (m s^{-1}); (c) relative vorticity (s^{-1}); (d) divergence (s^{-1}).

Another way to analyze biases in the CCSM4 formation probability projections is by evaluating the differences between the TC formation probabilities based on CFSRV2 and CCSM4 results for JASO 1981–2018 (CCSM4 results minus CFSRV2 results). Figure 33 shows the differences in CCSM4 and CFSRV2 TC formation probability for JASO of 1981–2018. Note the band of higher CCSM4 TC formation probabilities across the WNP from 100°E–150°W and 05°N–20°N.

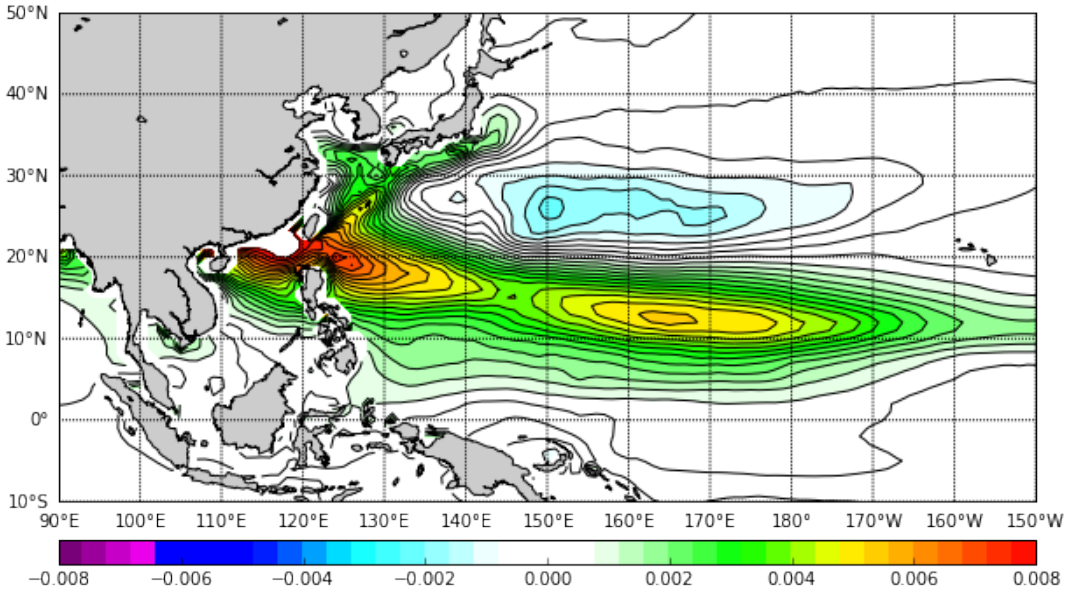

Figure 33. TC formation probability anomalies for JASO 1981–2018 based on CCSM4 and CFSRV2 results.

In this section, CCSM4 biases were assessed. This assessment was motivated by the differences between CFSRV2 and CCSM4 for JASO 1981–2018 in: (a) LSEFs; and (b) TC formation probabilities (see Chapter III, Section D). Overall, notable differences were found between CCSM4 and CFSRV2 results, and thus apparent biases. However, it was determined that bias correction would complicated and unlikely to provide an overall improvement of the CCSM4 projection results or our confidence in those results. Thus, bias corrections were not applied.

F. LSEF AND TC FORMATION PROBABILITY TIME SERIES FOR CFR 2019–2050

To investigate future LSEFS and TC formation probabilities, CFR LSEF and probability time series analysis were extended to include JASO 2019–2050. For this extension, LSEF values were used based on CCSM4 RCP 8.5 projections. Best fit lines (dashed) were used to highlight the long term trends in the LSEFs and TC formation probabilities. The statistical model limitation discussed in Chapter II, Section D, should be considered when assessing our results for future years.

1. LSEFs

Figure 34 shows the time series for LSEFs in the CFR for JASO of 1981–2050 based on the CCSM4 with CFSRV2 datasets from 1981–2018 used as a reference.

Figure 34a shows the SST LSEFs. Note the increasing trends for SST for CCSM4. CCSM4 has an overall higher SST which may have to do with the overall bias of 0.4°C mentioned in Chapter I, Section B.6. Additionally, a 4% rise in SST was observed over the 38-year time series. In general, these trends are expected to be supportive for TC formation probability rise throughout this timeframe.

Figure 34b shows the 200 hPa – 850 hPa vertical wind shear magnitude LSEFs. Note that shear is decreasing slightly throughout the time period with CCSM4. Lower vertical wind shear is supportive of TC formation.

Figure 34c shows the relative vorticity at 850hPa LSEFs. Relative vorticity stays constant throughout the time period and similar trends are seen for both CCSM4 and CFSRV2.

Figure 34d shows the divergence at 200hPa LSEFs. This differs between CCSM4 and CFSRV2, with CCSM4 showing an increasing trend while CFSRV2 shows a decreasing trend.

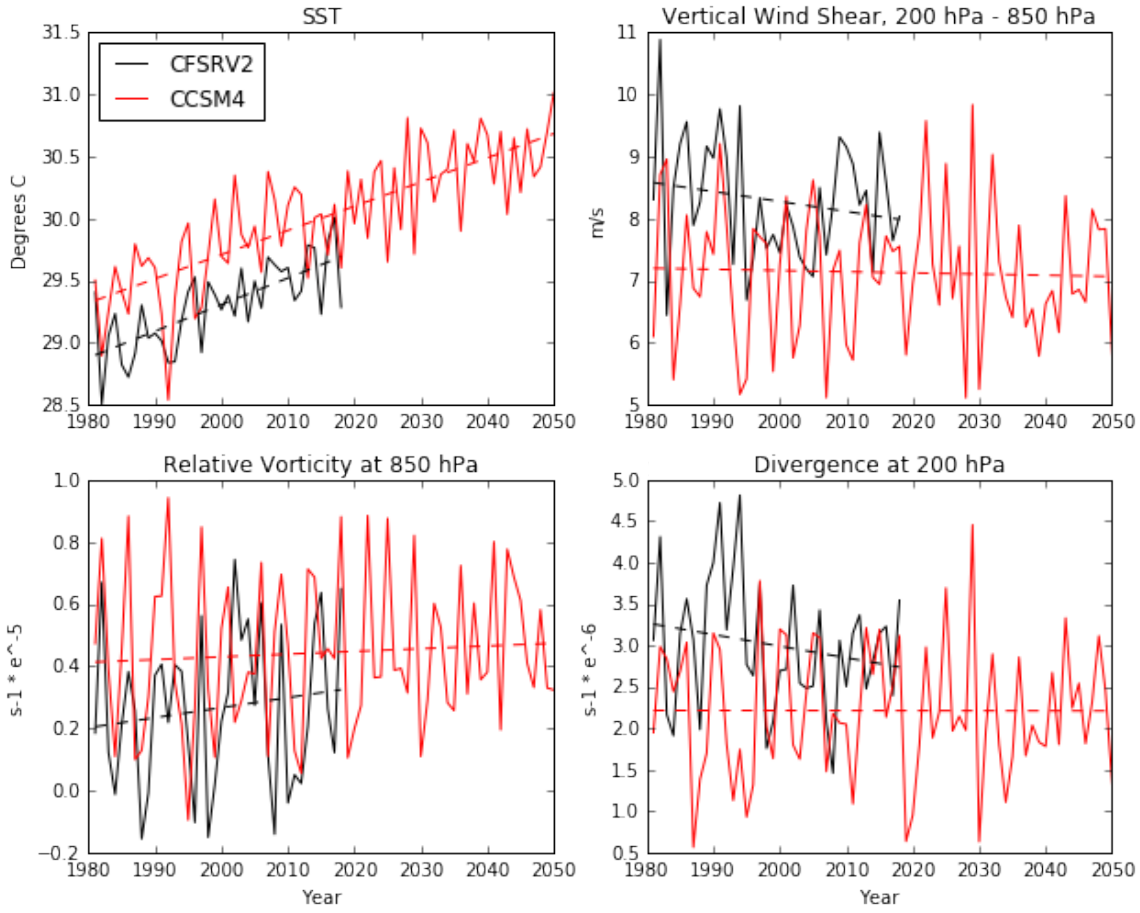

Figure 34. LSEFs for the CFR for JASO 1981–2050 based on CCSM4 projections (red) and CFSRV2 results (black) with best fit trend lines (dashed). (a) SST (°C); (b) vertical wind shear (m s^{-1}); (c) relative vorticity (s^{-1}); (d) divergence (s^{-1}).

Figure 34 shows that all four LSEFs are projected by CCSM4 to be as supportive, or more supportive, of TC formation in the CFR in 2019–2050 than during 1981–2018. The CCSM4 projected TC formation probabilities for JASO of 2019–2050 indicate that formations will be more likely than they were for JASO 1981–2018.

2. TC Formation Probability

Figure 35 shows the TC formation probability time series in the CFR for JASO of 1981–2050 for CCSM4 and for JASO of 1981–2018 CFSRV2. During these years, note the increasing trend for both CCSM4. CCSM4 trends are higher due to more favorable

1981–2018 conditions with LSEFs noted in Chapter III, Section D.1. With this positive trend into the future with CCSM4 projections, it would be expected that there would be more TCs in the future with a higher TC formation probability than what was seen in the past results with CFSRV2 and CCSM4 historical results.

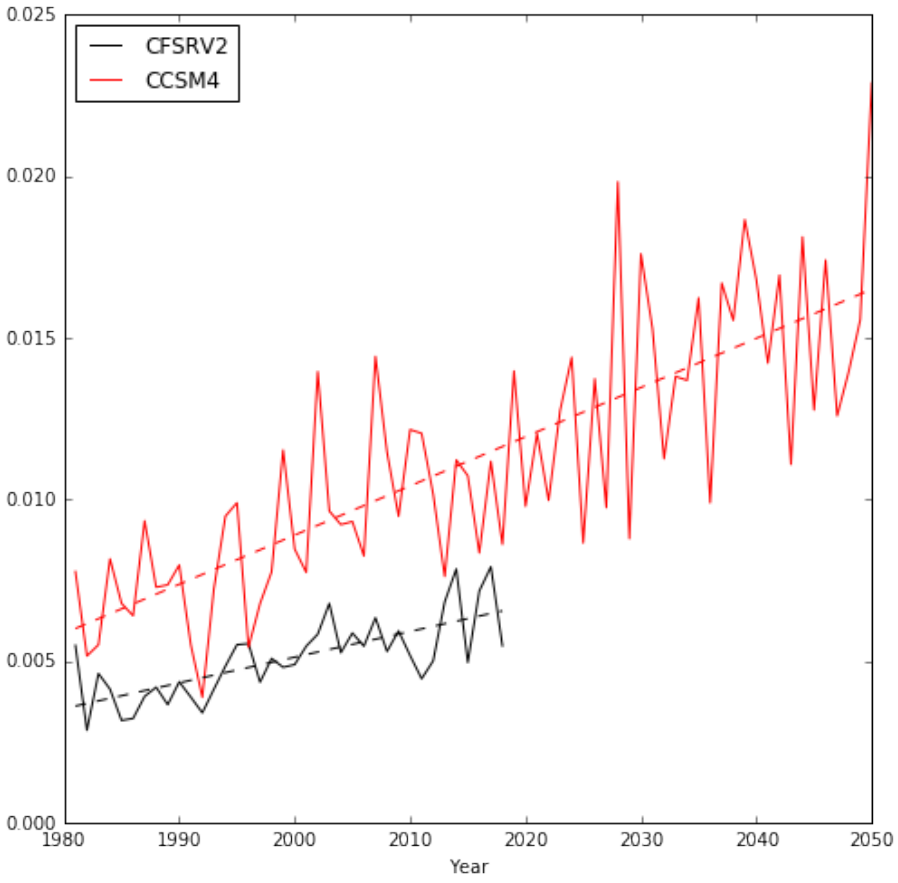

Figure 35. TC formation probabilities for the CFR for JASO 1981–2050 based on historical and projected information from CFSRV2 (black) and CCSM4 (red) with best fit trend lines (dashed).

G. PROJECTED LSEFS AND TC FORMATION PROBABILITIES 2021–2050

1. WNP CCSM4 2021–2030

a. LSEFs

Figure 36 shows the projected LSEFs for JASO 2021–2030 for the WNP based on the CCSM4 projection results.

Figure 36a shows the SST LSEF. The warmest SSTs in the WNP occur south of 20°N and west of 180°E, with SSTs exceeding 29°C in much of this area. Thus, the SSTs in much of this area are supportive of TC formation (see Chapter I, Section B.8).

Figure 36b shows the 200 hPa – 850 hPa vertical wind shear magnitude LSEF. Note the large area of low shear magnitude (0–8 ms^{-1}) that occurs in a southeast to northwest oriented area located between 120E°–150°W and 0°N–20N°. These low shear values are supportive of TC formations in this area (Meyer and Murphree 2015). The southern part of the SCS shows an area with relatively large vertical wind shear of 16–20 ms^{-1}. These values are unsupportive for TC formation.

Figure 36c shows the relative vorticity at 850 hPa LSEF. Note the large area of positive vorticity between 100°E–150°W and 10°N–20°N, especially in the SCS and Philippine Sea areas. These positive relative vorticity values are supportive for TC formations. Note that north of about 20°N, the relative vorticity values are negative, which is unsupportive of TC formation.

Figure 36d shows the divergence at 200 hPa LSEF. Note the large area of positive divergence south of 20°N, especially in the Philippine Sea. These positive divergence values are supportive for TC formation. Note that north of about 20°N, the divergence values are mainly negative, which is unsupportive of TC formation.

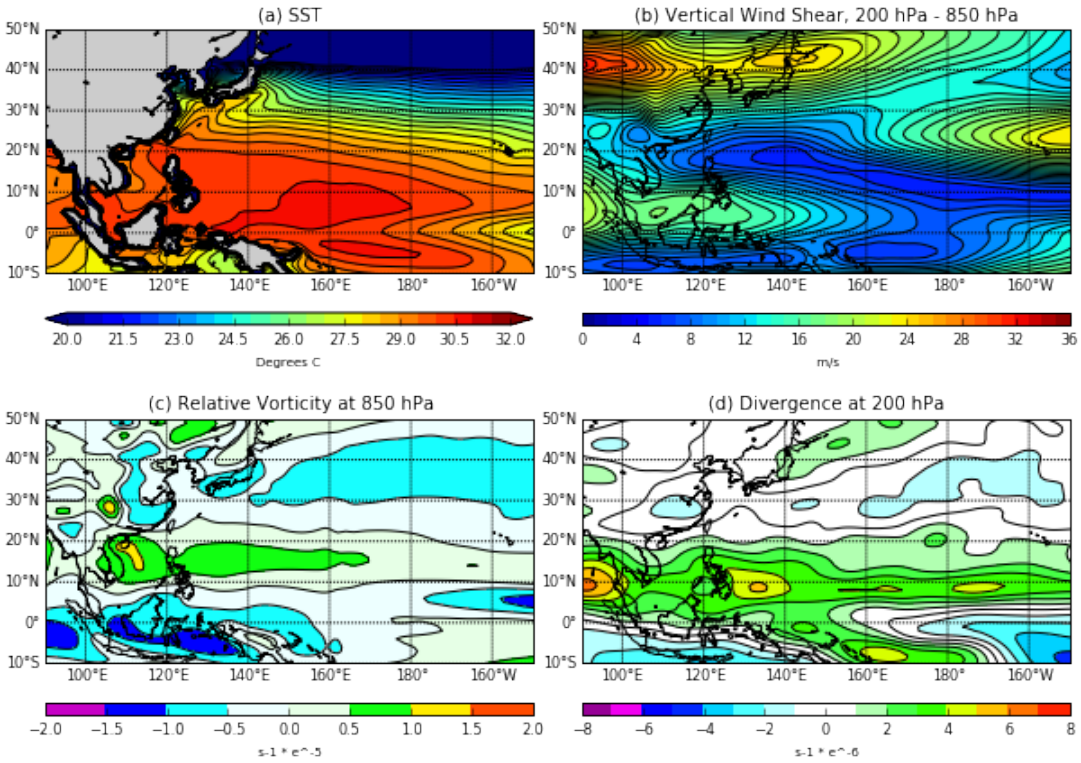

Figure 36. Projected LSEFs for the WNP for JASO 2021–2030 based on CCSM4 projection results. (a) SST (°C); (b) vertical wind shear (m s^{-1}); (c) relative vorticity (s^{-1}); (d) divergence (s^{-1}).

Overall, the CCSM4 projected LSEFs for 2021–2030 are favorable for TC formation in the area between about 100°E–150°W and 10°N–20°N. In this area, the projections are for generally high SST, low vertical wind shear, positive 850 hPa relative vorticity, and positive 200 hPa divergence. The projected LSEFs are unfavorable for TC formation north of about 20°N because the projections are for generally low SSTs, high vertical wind shear, negative 850 hPa relative vorticity, and negative 200 hPa divergence. A comparison of the projected LSEFs for 2021-2030 (Figure 36) to those for 1981-2018 derived from CFSRV2 data (Figure 28) and CCSM4 historical results (Figure 30) shows many similarities in spatial patterns but magnitudes that are more supportive of TC formations in much of the WNP, especially for the SST LSEF. Chapter III, Section G.1.c, provides more information about the differences between the projected 2021-2030 LSEFs and the 1981-2018 LSEFs.

b. TC Formation Probability

Figure 37 shows the projected TC formation probability for JASO 2021–2030 for the WNP based on CCSM4 projections of the LSEFs. The projected probabilities for 2021-2030 are two times greater than those in 1981–2018 in much of the WNP (see Chapter II, Section D.1). Note that the highest probabilities are located in the northern SCS, Luzon Strait, Philippine Sea and eastward to the dateline, and in the Kuroshio region near the Ryukyu Islands. The high probability area and magnitudes shown in Figure 37 are consistent with the favorable LSEFs shown in Figure 36. A comparison of the projected TC formation probabilities for 2021–2030 (Figure 37) to those for 1981–2018 derived from CFSRV2 data (Figure 29) and CCSM4 historical results (Figure 31) shows many similarities in spatial patterns but higher probabilities in much of the WNP. Chapter III, Section G.1.c, provides more information about the differences between the projected 2021–2030 probabilities and the 1981–2018 probabilities.

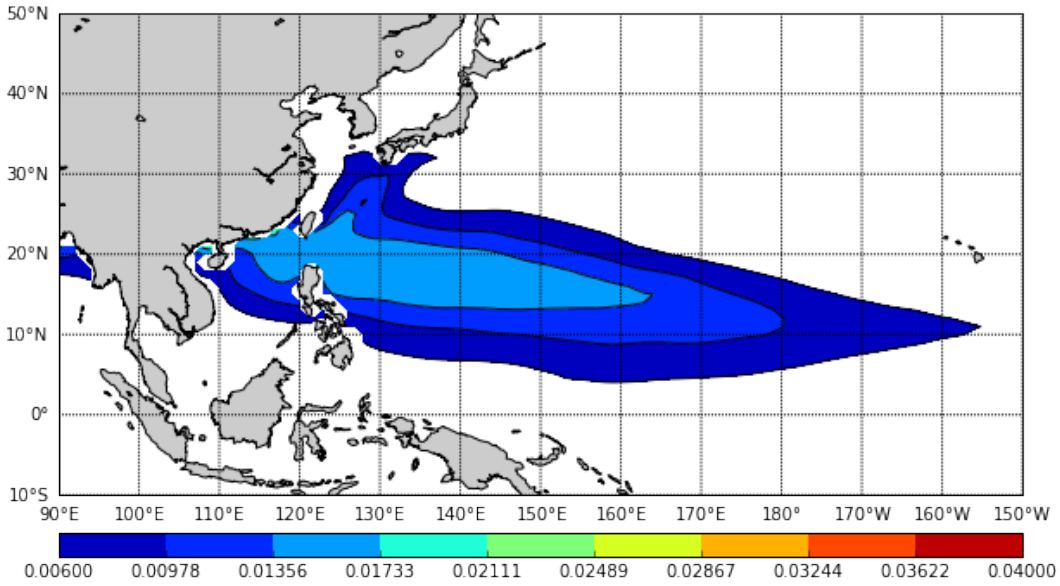

Figure 37. Projected TC formation probabilities for JASO 2021–2030 based on CCSM4 projected LSEFs.

c. Anomalies

Projected LSEF anomalies were calculated by subtracting the CCSM4 LSEFs for JASO 1981–2018 (Figure 30) from the CCSM4 projected LSEFs– for example, the CCSM4 projected LSEFs for JASO 2021–2030 (Figure 36) (for more information on our anomaly calculation methods, see Chapter II, Section C.2). Figure 38 shows the JASO of 2021–2030 projected LSEF anomalies for the WNP.

Figure 38a shows the projected SST anomaly. Note the positive projected SST anomaly in most of the WNP in 2021–2030 of about 0.5°C–1°C. This indicates that the SSTs in 2021–2030 are projected to be more supportive of TC formation than they were in 1981–2018.

Figure 38b shows the projected 200 hPa – 850 hPa vertical wind shear magnitude anomaly. Note the positive anomaly in the central and eastern portion of the WNP (130°E–180°E, 0°N–15°N), indicating that the wind shear is projected to be less supportive of TC formation in 2021–2030 than it was in 1981–2018.

Figure 38c shows the projected 850 hPa relative vorticity anomaly. Note the large positive anomaly with a southwest to northeast orientation located between 110°E–180°E and 10°N–30°N. These positive anomalies indicate that the vorticity in this area is projected to be more supportive of TC formation than it was in 1981–2018.

Figure 38d shows the projected 200 hPa divergence anomaly. Note the many small areas of weak anomalies located between 110°E–180°E and 05°N–20°N where TC formation has historically been high (see Figure 12). These weak anomalies indicate that in this area, 200 hPa divergence may be similar to what it was in 1981–2018, and thus as supportive of TC formation in 2021–2030 than it was in 1981–2018.

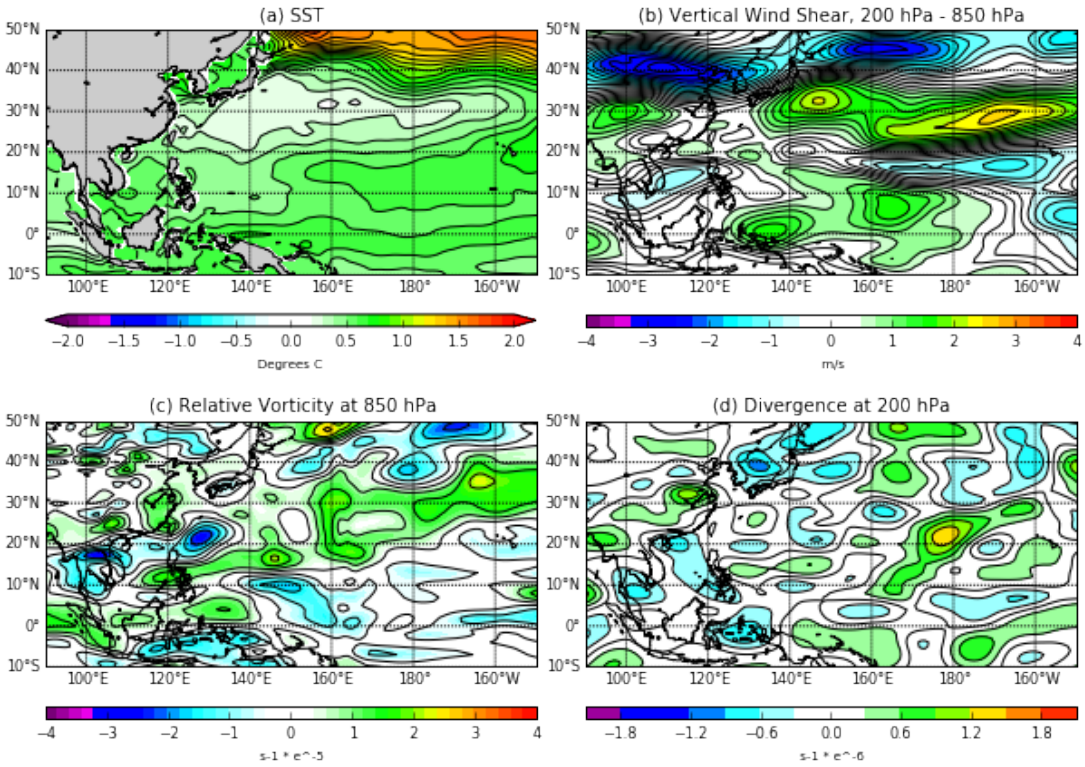

Figure 38. Projected LSEF anomalies for JASO 2021–2030 based on CCSM4 results. (a) SST (°C); (b) vertical wind shear (m s^{-1}); (c) relative vorticity (s^{-1}); (d) divergence (s^{-1}).

Overall, the CCSM4 projected LSEF anomalies for JASO of 2021-2030 indicate that more favorable conditions for TC formation in most of the WNP, especially between about 110°E–150°W and 10°N–20°N. The projected SST is especially pronounced and supportive of increased TC formations. But the other projected LSEF anomalies are also generally more supportive of increased TC formations. Thus, it would be expected to see that the corresponding projected TC formation probability anomalies are positive for most of the WNP, especially in the area where the projected SST anomalies are highest

Figure 39 shows the projected TC formation probability anomalies for JASO 2021–2030. Note the positive anomalies in TC formation probabilities across the WNP from 110°E–150°W and 05°N–20°N. These positive probability anomalies are consistent with the corresponding LSEF anomalies, especially the positive SST anomalies (Figure 38).

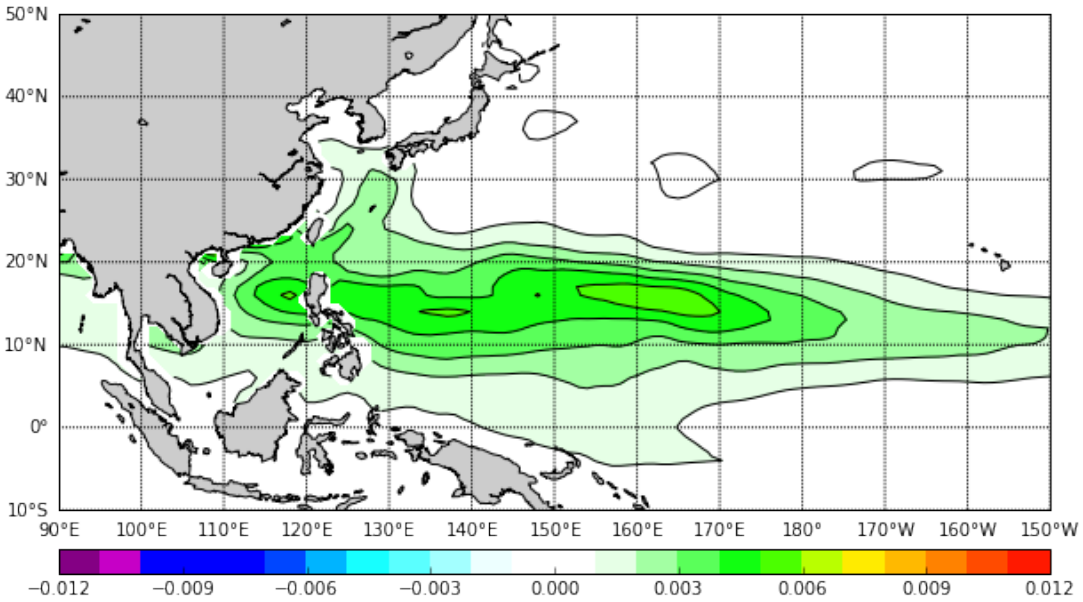

Figure 39. Projected TC formation probability anomalies for JASO 2021–2030 based on CCSM4 projected LSEFs.

Overall, the CCSM4 projections of LSEF and TC formation probability anomalies for JASO of 2021–2030 indicate that TC formations may be more probable over most of the WNP in the coming decade.

2. WNP CCSM4 2031–2040

a. LSEFs

Figure 40 shows the projected LSEFs for JASO 2031–2040 for the WNP based on the CCSM4 projection results.

Figure 40a shows the SST LSEF. The warmest SSTs in the WNP occur south 20°N and west of 180°E, with SSTs exceeding 30°C in much of the area. Thus, the SSTs in much of the area are supportive for TC formation (see Chapter I, Section B.8).

Figure 40b shows the 200 hPa – 850 hPa vertical wind shear magnitude LSEF. Note the large area of low vertical wind shear with a southeast to northwest orientation (120E°–150°W, 0N–20N°). This is an area that is expected to be favorable for TC formation with a shear magnitude between 0–8 ms^{-1}, below the threshold found by Meyer and Murphree

(2015). The SCS shows an unsupportive area for TC formation with vertical wind shear between 16–20 ms^{-1}.

Figure 40c shows the relative vorticity LSEF at 850 hPa. Note the large area of positive relative vorticity throughout the WNP (110°E–150°W, 10°–20°N). This is an area that is supportive for TC formation throughout the WNP. Note the area of negative relative vorticity to the east and west of Taiwan (100°E–150°W, 20°N–30°N) that is unsupportive of TC formation.

Figure 40d shows the divergence LSEF at 200 hPa. Note the large area of positive divergence throughout the WNP (100°E–150°W, 0N–20°N). This is an area that is supportive for TC formation throughout the WNP. Note the area of low positive and negative divergence to the east and west of Taiwan (100°E–150°W, 20°N–30°N) that is unsupportive of TC formation.

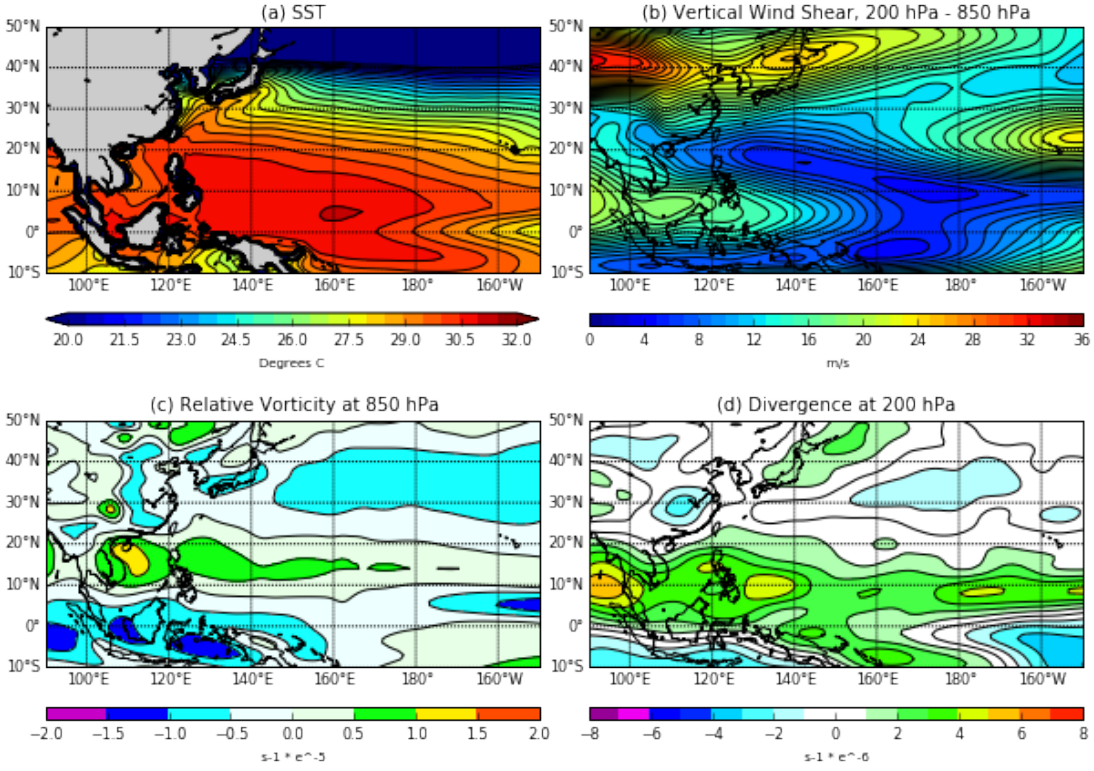

Figure 40. Projected LSEFs for JASO 2031–2040 based on CCSM4 projection results. (a) SST (°C); (b) vertical wind shear (m s^{-1}); (c) relative vorticity (s^{-1}); (d) divergence (s^{-1}).

Overall, the CCSM4 projected LSEFs for 2031–2040 are favorable for TC formation in the area between about 110°E–150°W and 10°N–20°N. In this area, the projections are for generally high SST, low vertical wind shear, positive 850 hPa relative vorticity, and positive 200 hPa divergence. The projected LSEFs are unfavorable for TC formation north of about 20°N because the projections are for generally low SSTs, high vertical wind shear, negative 850 hPa relative vorticity, and negative 200 hPa divergence. A comparison of the projected LSEFs for 2031–2040 (Figure 40) to those for 1981–2018 derived from CCSM4 historical results (Figure 30) and CCSM4 projection results from 2021–2030 (Figure 36) show many similarities in spatial patterns but magnitudes that are more supportive of TC formations in much of the WNP, especially for the SST LSEF. Chapter III, Section G.2.c, provides more information about the differences between the projected 2031–2040 LSEFs and the 1981–2018 LSEFs.

b. TC Formation Probability

Figure 41 shows the TC formation probability for JASO 2031–2040 for the WNP based on CCSM4 projections of the LSEFs . Note that the highest probabilities are located in the northern SCS, Luzon Strait, Philippine Sea and eastward to the dateline, and in the Kuroshio region near the Ryukyu Islands. The high probability area and magnitudes shown in Figure 41 are consistent with the favorable LSEFs shown in Figure 40. A comparison of the projected TC formation probabilities for 2031–2040 (Figure 41) to those for 1981–2018 derived from CCSM4 historical results (Figure 31) and CCSM4 future projection from 2021–2030 (Figure 37) shows many similarities in spatial patterns but higher probabilities in much of the WNP. Chapter III, Section G.2.c, provides more information about the differences between the projected 2031–2040 probabilities and the 1981–2018 probabilities.

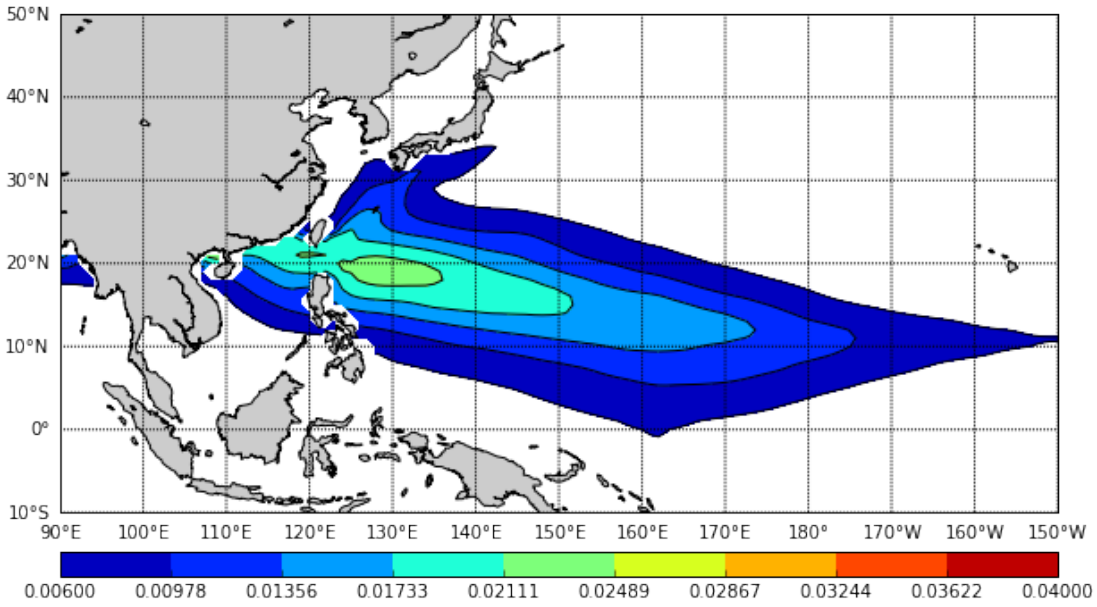

Figure 41. Projected TC formation probabilities for JASO 2031–2040 based on CCSM4 projected LSEFs.

c. Anomalies

LSEF anomalies were calculated by subtracting the CCSM4 LSEFs for JASO 1981–2018 (Figure 30) from the CCSM4 projected LSEFs– for example, the CCSM4 projected LSEFs for JASO 2031–2040 (Figure 40) (for more information on our anomaly calculation methods, see Chapter II, Section C.2). Figure 42 shows the JASO of 2031–2040 projected LSEF anomalies for the WNP.

Figure 42a shows the projected SST anomaly. Note positive projected SST anomaly in most of the WNP in 2031–2040 of about 0.75°C–1.5°C. This indicates that the SSTs in 2031–2040 are projected to be more supportive of TC formation than they were in 1981–2018.

Figure 42b shows the projected 200 hPa – 850 hPa vertical wind shear magnitude anomaly. Note the positive anomaly in the central and eastern portion of the WNP (130°E–180°E, 0°N–15°N), indicating that the wind shear is projected to as supportive of TC formation in 2031–2040 than it was in 1981–2018.

Figure 42c shows the projected 850 hPa relative vorticity anomaly. Note the large positive anomaly with a southwest to northeast orientation located between 120°E–150°E and 0°N–10°N. These positive anomalies indicate that the vorticity in this area is projected to be more supportive of TC formation than it was in 1981–2018.

Figure 42d shows the 200 hPa divergence anomaly. Note the large negative anomaly with a southwest to northeast orientation located between 130°E–160°E and 0°N–20°N. These negative anomalies indicate that the divergence in this area is projected to be less supportive of TC formation than it was in 1981–2018.

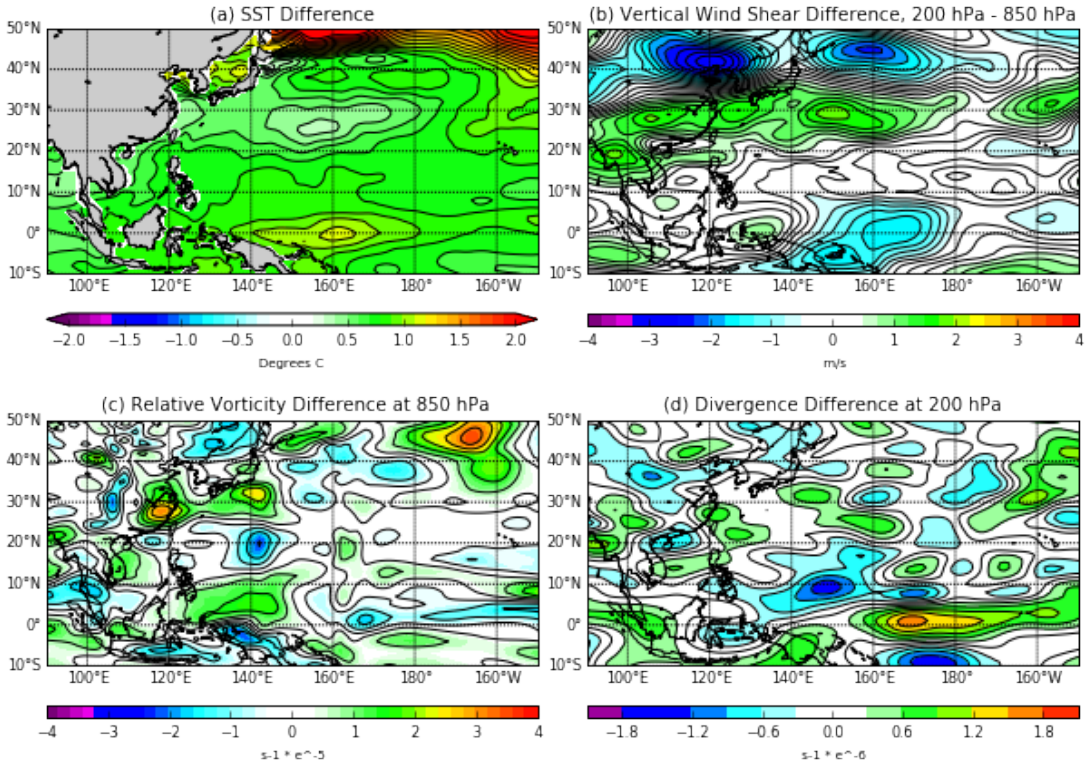

Figure 42. Projected LSEF anomalies for JASO 2031–2040 based on CCSM4 projection results. (a) SST (°C); (b) vertical wind shear (m s^{-1}); (c) relative vorticity (s^{-1}); (d) divergence (s^{-1}).

Overall, the CCSM4 projected LSEF anomalies for JASO of 2031–2040 indicate that more favorable conditions for TC formation in most of the WNP, especially between about 110°E–150°W and 10°N–20°N. The projected SST is especially pronounced and supportive of increased TC formations. But the other projected LSEF anomalies are also generally more supportive of increased TC formations. Thus, it would be expected to see that the corresponding projected TC formation probability anomalies are positive for most of the WNP, especially in the area where the projected SST anomalies are highest.

Figure 43 shows the projected TC formation probability anomalies for JASO 2031–2040. Note the positive anomalies in TC formation probabilities across the WNP from 110°E–150°W and 05°N–20°N. These positive probability anomalies are consistent with the corresponding LSEF anomalies, especially the positive SST anomalies (Figure 42).

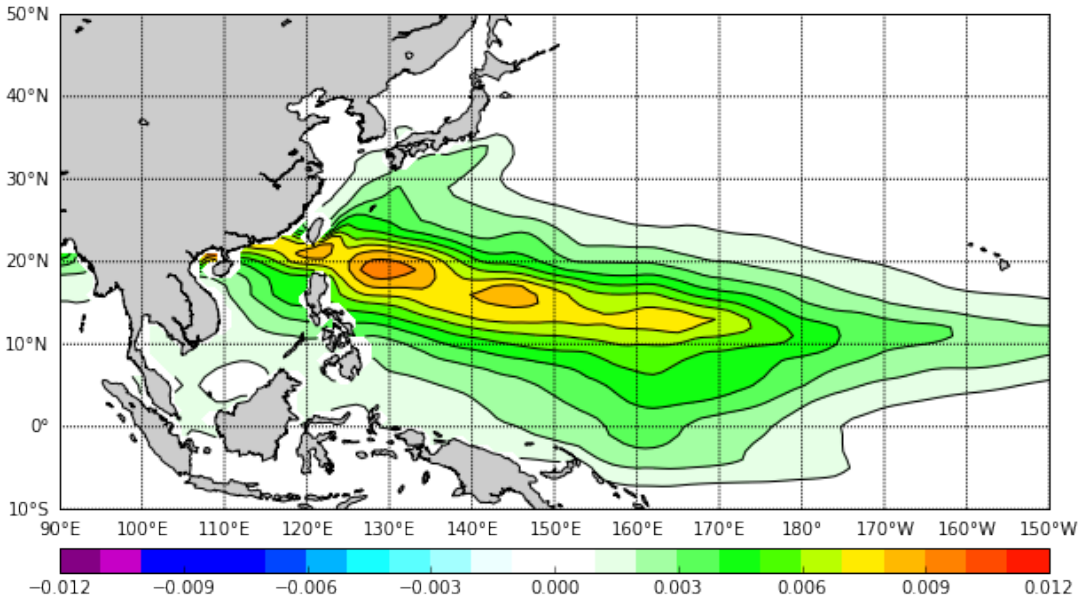

Figure 43. Projected TC formation probability anomalies for JASO 2031–2040 based on CCSM4 projected LSEFs.

Overall, the CCSM4 projections of LSEF and TC formation probability anomalies for JASO of 2031–2040 indicate that TC formations may be more probable over most of the WNP in the coming decades.

3. WNP CCSM4 2041–2050

a. LSEFs

Figure 44 shows the projected LSEFs for JASO 2041–2050 for the WNP based on the CCSM4 results.

Figure 44a shows the SST LSEF. The warmest SSTs in the WNP occur south of 20°N and west of 180°E, with SSTs exceeding 30.5°C in much of this area. Thus, the SSTs in much of this area are supportive of TC formation (see Chapter I, Section B.8).

Figure 44b shows the 200 hPa – 850 hPa vertical wind shear magnitude LSEF. Note the large area of low shear magnitude (0–8 ms^{-1}) that occurs in a southeast to northwest oriented area located between 120E°–150°W and 0N–20°N. These low shear values are supportive of TC formations in this area (Meyer and Murphree 2015). The southern part of the SCS shows an area with relatively large vertical wind shear of 16–20 ms^{-1}. These values are unsupportive for TC formation.

Figure 44c shows the relative vorticity LSEF at 850 hPa. Note the large area of positive relative vorticity throughout the WNP (100°E–150°W, 10°–20°N). This is an area that is supportive for TC formation throughout the WNP.

Figure 44d shows the divergence at 200 hPa LSEF. Note the large area of positive divergence south of 20°N, especially in the Philippine Sea. These positive divergence values are supportive for TC formation. Note that north of about 20°N, the divergence values are mainly negative, which is unsupportive of TC formation.

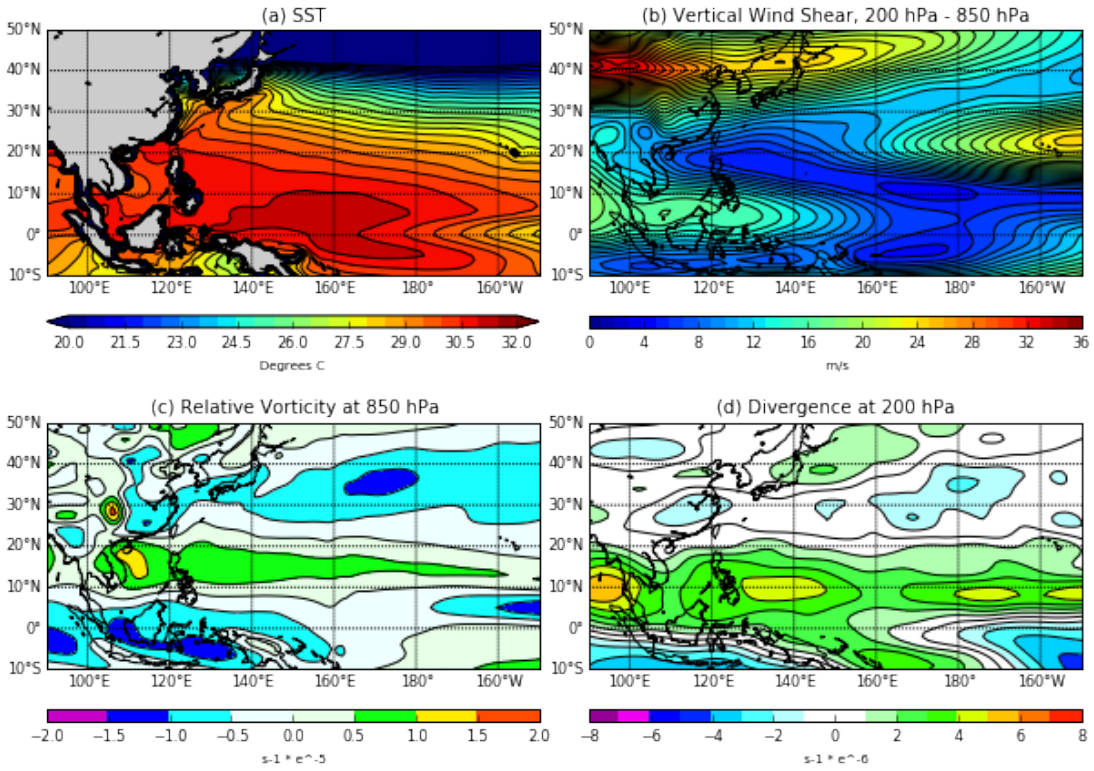

Figure 44. Projected LSEFs for JASO 2041–2050 based on CCSM4 projection results. (a) SST (°C); (b) vertical wind shear (m s^{-1}); (c) relative vorticity (s^{-1}); (d) divergence (s^{-1}).

Overall, the CCSM4 projected LSEFs for 2041–2050 are favorable for TC formation in the area between about 110°E–150°W and 10°N–20°N. In this area, the projections are for generally high SST, low vertical wind shear, positive 850 hPa relative vorticity, and positive 200 hPa divergence. The projected LSEFs are unfavorable for TC formation north of about 20°N because the projections are for generally low SSTs, high vertical wind shear, negative 850 hPa relative vorticity, and negative 200 hPa divergence. A comparison of the projected LSEFs for 2041–2050 (Figure 44) to those for 1981–2018 derived from CCSM4 historical results (Figure 30), CCSM4 projection results from 2021-2030 (Figure 36), and CCSM4 projection results from 2031–2040 (Figure 40) shows many similarities in spatial patterns but magnitudes that are more supportive of TC formations in much of the WNP, especially for the SST LSEF. Chapter III, Section G.3.c, provides more information about the differences between the projected 2041–2050 LSEFs and the 1981–2018 LSEFs.

b. TC Formation Probability

Figure 45 shows the TC formation probability for JASO 2041–2050 for the WNP based on CCSM4 projections of the LSEFs. Note that the highest probabilities are located in the northern SCS, in and east of the Luzon Strait, Philippine Sea and eastward to the dateline, and in the Kuroshio region near the Ryukyu Islands. The high probability area and magnitudes shown in Figure 45 are consistent with the favorable LSEFs shown in Figure 44. A comparison of the projected TC formation probabilities for 2041–2050 (Figure 45) to those for 1981–2018 derived from CCSM4 historical results (Figure 31), CCSM4 future projection from 2021–2030 (Figure 37), and CCSM4 future projection from 2031–2040 (Figure 41) shows many similarities in spatial patterns but higher probabilities in much of the WNP. Chapter III, Section G.3.c, provides more information about the differences between the projected 2041–2050 probabilities and the 1981–2018 probabilities.

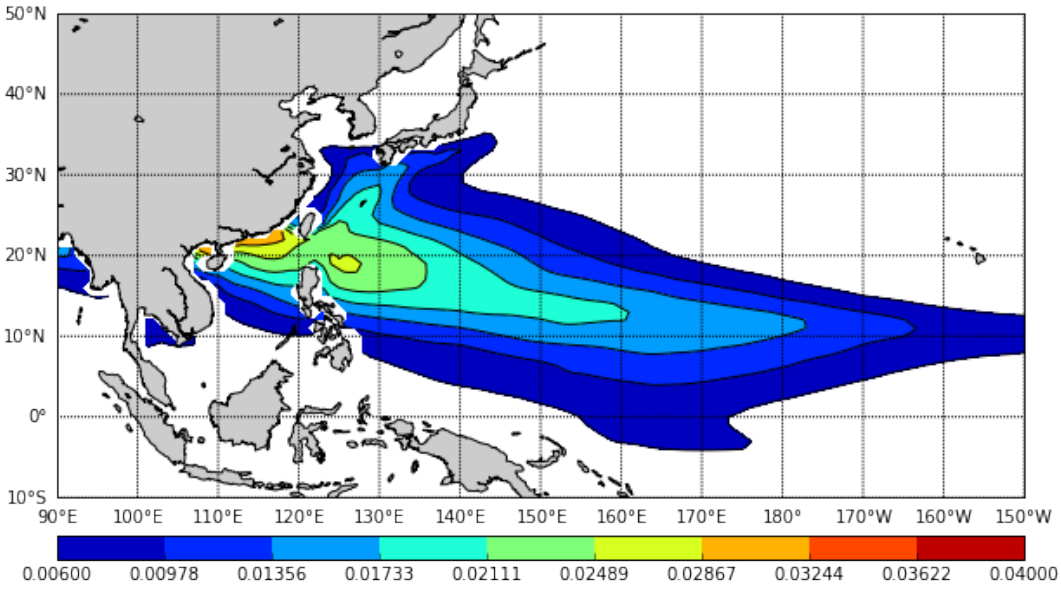

Figure 45. Projected TC formation probabilities for JASO 2041–2050 based on CCSM4 projected LSEFs.

c. Anomalies

LSEF anomalies were calculated by subtracting the CCSM4 LSEFs for JASO 1981–2018 (Figure 30) from the CCSM4 projected LSEFs- for example, the CCSM4 projected LSEFs for JASO 2041–2050 (Figure 44) (for more information on our anomaly calculation methods, see Chapter II, Section C.2). Figure 46 shows the JASO of 2041–2050 projected LSEF anomalies for the WNP.

Figure 46a shows the projected SST anomaly. Note the positive projected SST anomaly in most of the WNP in 2041–2050 of about 1°C–1.5°C warmer than the SST temperatures in 1981-2018. This indicates that the SSTs in 2041–2050 are projected to be more supportive of TC formation than they were in 1981–2018.

Figure 46b shows the projected 200 hPa–850 hPa vertical wind shear magnitude anomaly. Note the large negative anomaly with a southwest to southeast orientation located between 130°E–160°E and 0°N–20°N. These negative anomalies indicate that the shear in this area is projected to be more supportive of TC formation than it was in 1981–2018.

Figure 46c shows the projected 850 hPa relative vorticity anomaly. Note the large positive anomaly with a southwest to northeast orientation located between 110°E–170°W and 08°N–20°N. These positive anomalies indicate that the vorticity in this area is projected to be more supportive of TC formation than it was in 1981–2018.

Figure 46d shows the projected 200 hPa divergence anomaly. Note the many small areas of weak anomalies located between 110°E–180°E and 05°N–20°N where TC formation has historically been high (see Figure 12). These weak anomalies indicate that in this area, 200 hPa divergence may be similar to what it was in 1981–2018, and thus as supportive of TC formation in 2041–2050 than it was in 1981–2018.

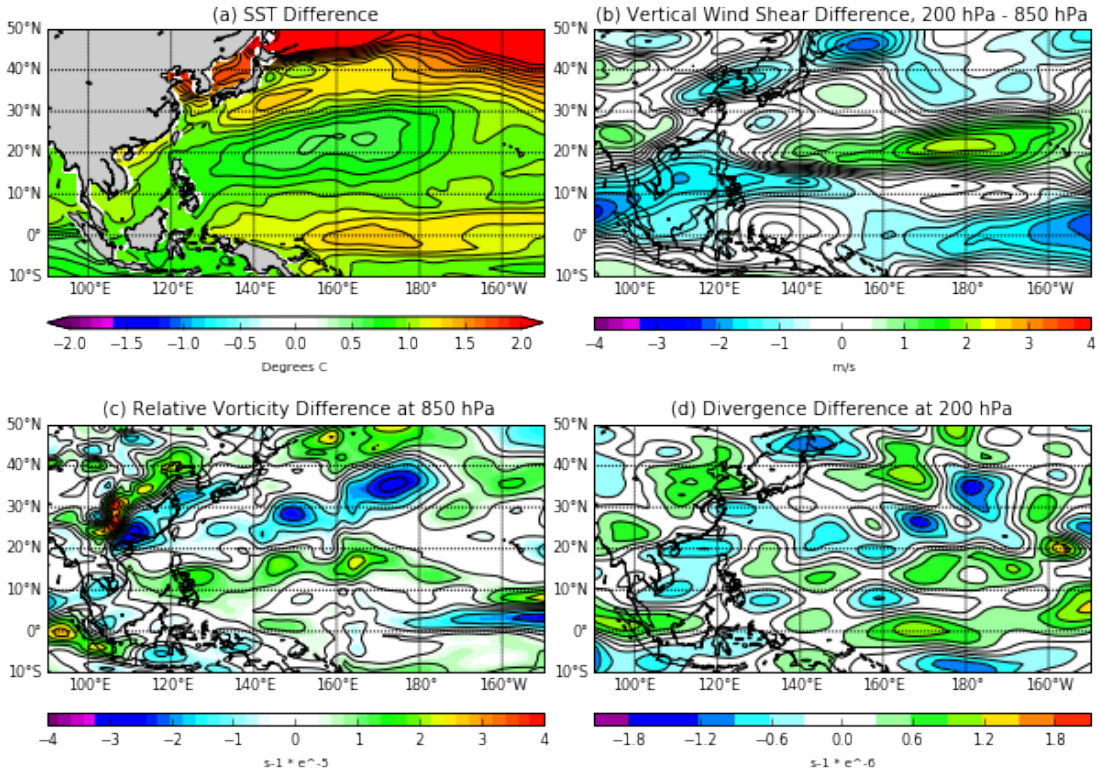

Figure 46. Projected LSEF anomalies for the WNP for JASO 2041–2050 based on CCSM4 projection results. (a) SST (°C); (b) vertical wind shear (m s^{-1}); (c) relative vorticity (s^{-1}); (d) divergence (s^{-1}).

Overall, the CCSM4 projected LSEF anomalies for JASO of 2041–2050 indicate that more favorable conditions for TC formation in most of the WNP, especially between about 100°E–150°W and 10°N–20°N. The projected SST is especially pronounced and supportive of increased TC formations. But the other projected LSEF anomalies are also generally more supportive of increased TC formations. Thus, it would be expected to see that the corresponding projected TC formation probability anomalies are positive for most of the WNP, especially in the area where the projected SST anomalies are highest

Figure 47 shows the projected TC formation probability anomalies for JASO 2041–2050. Note the positive anomalies in TC formation probabilities across the WNP from 110°E–150°W and 05°N–30°N. These positive probability anomalies are consistent with the corresponding LSEF anomalies, especially the positive SST anomalies (Figure 46).

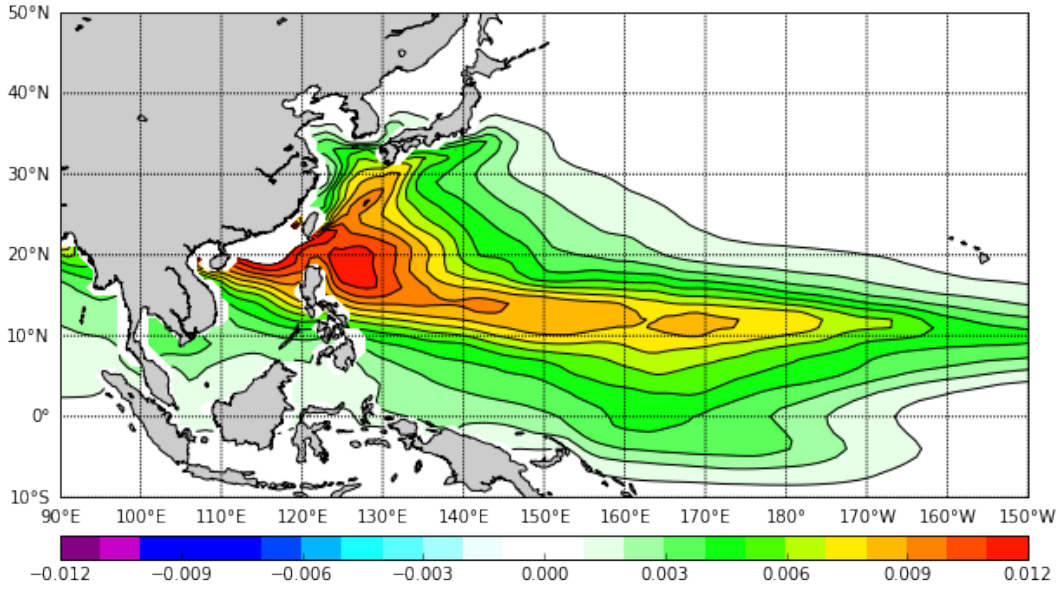

Figure 47. Projected TC formation probability anomalies for JASO 2041–2050 based on CCSM4 projected LSEFs.

Overall, the anomalies for CCSM4 projections results from JASO 2041-2050 show that SST and TC formation probability have increased when compared to CCSM4 results from JASO 1981-2018. Note the poleward shift for stronger TC formation probability northwards towards Japan (125°E–140°E, 20°N–30°N) along with a southward shift towards the southern Philippines (125°E–130°W, 8°N–10°N). These differences show that TC formations in the WNP in the future decade during JASO of 2041–2050 should increase and change the TC formation areas in the WNP when not only compared to JASO of 1981–2018, but also increase when compared the TC formation probability anomaly for JASO of 2021–2030 (Figure 39) and JASO of 2031–2040 (Figure 43).

As noted in prior sections, the statistical model limitation discussed in Chapter II, Section D, should be considered when assessing our results for future years.

THIS PAGE INTENTIONALLY LEFT BLANK

IV. SUMMARY AND CONCLUSIONS

A. KEY RESULTS AND CONCLUSIONS

This research investigated how climate change may impact TC formations in the WNP. Our overall goal was to achieve a better understanding of how LSEFs and TC formations may change in the WNP over the next 30 years. Our primary datasets were: (a) reanalysis data from CFSRV2; (b) historical and RCP 8.5 projection results from the CCSM4 climate model; (c) JTWC best track TC formations; and (d) HURDAT2 best track TC formations. Four LSEFs were analyzed: SST, 200 hPa – 850 hPa vertical wind shear, 850 hPa relative vorticity, and 200 hPa divergence. LSEF information was used from CCSM4 to force the HTCFS statistical model and produce TC formation probabilities for the WNP. This research was conducted to: (a) test LSEF and TC formation probability with CCSM4 results through the HTCFS for accuracy with known past events such as ENLN; (b) compare historical CCSM4 LSEF and HTCFS TC formation probability result trends to trends from a reanalysis data source CFSRV2, using time series analysis; (c) identify CCSM4 biases and assess bias correction methods; and (d) evaluate LSEF and HTCFS TC formation probability of CCSM4 projection results in future decades. Our main results included analyses of LSEFs and TC formation probabilities for JASO in the WNP using reanalysis data and climate model results for the most recent four decades (1981–2018) and climate model projections for the next several decades (2021–2050). Good agreement was found overall between the LTM reanalysis results and LTM climate model results for the recent past decades, but with a notable positive bias in the climate model SST LSEF values. For these past decades, generally good agreement was found between the ENLN reanalysis results and ENLN climate model results, but with a notable positive bias in the climate model SST LSEF values. For TC formation numbers in the WNP, a decreasing time series trend was found, and for TC formation numbers in the CFR, an increasing trend was found. For the future decades 2021–2050, an increase in TC formation probabilities across the WNP was found that was associated with large increases in SST, and a poleward shift in TC formation probability northwards towards Japan and southward towards the southern Philippines that is most evident in the decade 2041–2050.

The following variations were found in the CCSM4 LSEFs during EN(LN) with CCSM4 historical results: (1) a shift in the warmest SSTs to the east (west); (2) Stronger (weaker) vertical wind shear in western and central WNP; (3) Stronger (weaker) relative vorticity across the WNP; and (4) Stronger (weaker) divergence across the WNP.

The HTCFS was forced with these ENLN LSEFs to produce TC formation probabilities in the WNP. The following variations were observed in the TC formation probabilities during EN(LN): (1) an increase (decrease) in TC formation probability in the eastern portion of the WNP; and (2) a decrease (increase) in TC formation probability in the eastern portion of the WNP. The resulting ENLN TC formation probabilities were comapred with the JTWC and HURDAT2 best track TC formation datasets. It was visually observed that the TC formation probabilities for both ENLN were well corresponded with actual TC formations. This correspondence proved the HTCFS could accurately describe differences in ENLN with the use of LSEFs from CCSM4 historical results.

Time series on the LSEFs and TC formation probabilities were analyzed to compare CFSRV2 and CCSM4 results for JASO of 1981–2018. It was found that: (1) all LSEFs increased during this timeframe for CCSM4 results; and (2) TC formation probability increased for CCSM4. Overall, CCSM4 was more supportive of TC formation in the CFR than CFSRV2 with respect to all four LSEFs: SST, vertical wind shear, relative vorticity, and divergence in the CFR.

Additionally, TC formation numbers were calculated for the WNP and CFR for every year in JASO of 1981–2018. For the WNP there was a decrease of 0.25 TCs per decade, with a decrease of one TC over the entire period. For the CFR, there was an increase of 0.75 TCs per decade, with an increase of three TCs over the entire period. Overall, there was a decrease in TC formations in the WNP of 5% and an increase in the CFR TC formations of 33% for JASO of 1981–2018. These results indicated that TC formation locations may have shifted into the CFR from other sub-regions of the WNP.

The possibility of using the 1981–2018 differences between CFSRV2 and CCSM4 LSEFs and TC formation probabilities to develop bias corrections to the CCSM4 LSEF and TC formation probabilities was investigated. The objective was to determine if such

bias corrections could feasibly be used to improve the CCSM4 LSEF and TC formation probability projections for 2021–2050. Overall, LSEF bias correction was found to be complicated and did not improve the CCSM4 derived TC formation probabilities. Thus, no bias corrections were applied in this research.

The results concluded that the CCSM4 results were suitable for investigating past and projected changes in TC formations in the WNP. A future times series analysis was conducted with CCSM4 to determine future trends with the LSEFs along with TC formation probability for the years 2019-2050. The findings were: (1) LSEFs increase for both SST and relative vorticity for JASO of 2018-2050; (2) LSEFs stay relatively the same for both vertical wind shear and divergence in JASO of 2018-2050; and (3) TC formation probability increases for JASO of 2019-2050 according to the statistical model currently in use.

LSEFs and TC formation probabilities were analyzed for CCSM4 projections in future decadal data sets for JASO of 2021–2030, 2031–2040, and 2041–2050 while also comparing the changes in these decades to the LTM for JASO 1981–2018. For the LSEFs and TC formation probabilities for JASO of 2021–2030, the findings were: (1) An increase in SST throughout the WNP; (2) spatial and temporal similarities with the LSEFs 200 hPa – 850 hPa vertical wind shear, 850 hPa relative vorticity, and 200 hPa divergence; (3) an increasing trend throughout all three future decades of TC formation potential increasing each consecutive decade; and (4) a poleward shift in TC formation potential northwards towards Japan (125°E–140°E, 20°N–30°N) along with a southward shift towards the southern Philippines (125°E–130°W, 8°N–10°N).

In summary, the results showed:

1. By utilizing the LSEFs to predict TC formation probabilities, this research was able to analyze specifically which LSEFs influenced TC formation probabilities the most with all other variables remaining equal.

2. CCSM4 historical results were used to assess how well these results described anomalies in TC formation locations and formation probabilities associated with ENLN.

3. CCSM4 data, when used in conjunction with the HTCFS, showed that in the future TC formation probabilities in the WNP may increase and expand across the WNP with the understanding that as forcing data grows increasingly different than that used to build the HTCFS, the validity of the model becomes increasingly in doubt.

4. In a future warmer world, TC formation probability increases, meaning that the WNP should expect to see an increase in TC numbers given higher probabilities for formation. This is with the caveat being that model skill in HTCFS becomes increasingly questionable as the forcing data departs that used for model building of HTCFS.

B. AREAS FOR FURTHER RESEARCH

This research provided many insights into datasets and methods for inferring how climate change may affect TC activity. However, a number of questions remain, including:

1. What is the relationship between TC formation probability and TC formation numbers in the WNP?

2. How can bias correction be effectively used with CCSM4 projection results?

3. Is the TC season in the WNP getting longer due to climate change?

4. Is there a relationship between warming SSTs and rising atmospheric temperatures on TC formation numbers in WNP?

5. What would the climate change impacts look like in other sub-regions of the WNP?

To address these questions, the following additional research is recommended:

1. Repeat the analysis of TC formation probability using more recent climate projections, such as those from the newest CCSM5 results using the higher resolution coupled models that are part of CMIP6.

2. Conduct significance level and confidence level testing on LSEFs, TC formation probabilities, and TC formation number time series data.

3. Analyze future changes in the timing and duration of the TC season by investigating additional months of (e.g., May-June and November-December).

4. Conduct further analysis in other sub-regions of the WNP in addition to the CFR. The WNP is a very large region and very diverse in terms of its LSEFs and the climate scale variations in its LSEFs. For example, ENLN can cause large changes in the LSEFs for some parts of the WNP but not all parts of the WNP.

5. Address the statistical model limitation discussed in Chapter II, Section D. One approach would be to build the statistical model using only the most recent historical LSEF and TC formation data. This most recent data might be more representative of future LSEFs and TC formations than earlier data, given the trends shown in Figures 34 and 35. This approach is conceptually similar to the optimal climate normal approach used in S2S forecasting (van den Dool 2007).

6. Conduct testing and data analysis to translate future TC formation probabilities into future quantifiable numbers of TC formation numbers in the WNP.

7. Apply HTCFS and CCSM4 data to assessing future TC activity in other basins.

8. Investigate the relationship between warming SSTs and rising atmospheric temperatures on TC formation numbers in WNP.

9. Alter climate change research practices by making climate change projection outputs readily accessible to the broad scientific community. Additionally, organizations that generate climate model projections

provide those projections along with assessments of those projections, including reports of biases in the projections.

10. Continue to research possible climate change effects on TCs in the WNP, especially given the increase in TC formation probabilities moving towards US bases located in Japan and the Philippines.

APPENDIX. TC FORMATIONS IN THE WNP AND CFR FOR JASO 1981–2019

Table 3 shows the number of TC formations in the WNP and in the CFR based on data from the JTWC best track data for JASO 1981-2017 and from the NRL TC Page for JASO of 2018. This TC formation information is also represented in Figure 26 as a time series. Additionally, Table 3 shows the MEI values and ENLN state for September and October of 1981– 2018 where: (a) EN corresponds to a MEI value greater than or equal to 0.5; (b) LN corresponds to a MEI value less than or equal to -0.5; and (c) a neutral year is a value between -0.5 and 0.5. The CFR is a relatively small sub-region of the WNP (see Chapter II, Section A), but the CFR formations in JASO 1981–2018 were 51% of the total number of formations in the WNP in JASO of 1981–2018. 42% of the JASO periods with an above average number of formations in the CFR were EN periods, 26% were LN periods, and 32% were neutral periods. 26% of the JASO periods with a below average number of formations in the CFR were EN periods, 42% were LN periods, and 32% were neutral periods. This indicates that there is a tendency for EN (LN) to increase (decrease) the number of formations in the CFR during JASO.

Table 3. Number of TC formations in the WNP and CFR in JASO 1981–2018 based on JTWC best track data for 1981–2017 and NRL TC Page data for 2018, along with MEI and ENLN information for September–October of each year.

Year	TC Formations in JASO in WNP	TC Formations in JASO in CFR	% of WNP TCs in CFR	MEI for Sep-Oct	EN/LN State
1981	18	8	44.4%	-0.1	Neutral
1982	**19**	**14**	**73.7%**	1.9	EN
1983	17	8	47.1%	-0.4	Neutral
1984	25	11	44.0%	-0.1	Neutral
1985	18	7	38.9%	0.0	Neutral
1986	15	10	66.7%	0.6	EN
1987	17	11	64.7%	1.1	EN
1988	18	9	50.0%	-1.5	LN
1989	24	12	50.0%	-0.6	LN
1990	18	11	61.1%	-0.1	Neutral
1991	22	10	45.5%	1.1	EN
1992	**25**	7	**28.0%**	0.8	EN
1993	23	13	56.5%	0.9	EN
1994	30	13	43.3%	1.5	EN
1995	26	9	34.6%	-0.7	LN
1996	31	11	35.5%	-0.3	Neutral
1997	**22**	**2**	**9.1%**	2.0	EN
1998	20	11	55.0%	-1.2	LN
1999	21	7	33.3%	-1.3	LN
2000	27	9	33.3%	-0.6	LN
2001	20	11	55.0%	-0.3	Neutral
2002	22	11	50.0%	0.8	EN
2003	17	10	58.8%	0.3	Neutral
2004	17	10	58.8%	0.3	EN
2005	18	9	50.0%	-0.7	LN
2006	18	11	61.1%	0.7	EN
2007	19	11	57.9%	-1.1	LN
2008	16	7	43.8%	-1.1	LN
2009	**20**	**17**	**85.0%**	0.6	EN
2010	15	7	46.7%	-2.2	LN
2011	**16**	**13**	**81.3%**	-1.4	LN
2012	17	10	58.8%	-0.2	Neutral
2013	23	14	60.9%	-0.2	Neutral
2014	13	10	76.9%	0.1	Neutral
2015	19	13	68.4%	2.1	EN
2016	24	14	58.3%	-0.6	LN
2017	23	9	39.1%	-0.6	LN
2018	22	15	68.2%	0.4	Neutral

Year	TC Formations in JASO in WNP	TC Formations in JASO in CFR	% of WNP TCs in CFR	MEI for Sep-Oct	EN/LN State
Total Number of Formations in JASO 1981-2018	775	395	51.0%		
Mean Number of JASO Formations per Year	20.4	10.4			

THIS PAGE INTENTIONALLY LEFT BLANK

LIST OF REFERENCES

Bengtsson, L., K. I. Hodges, M. Esch, N. Keenlyside, L. Kornblueh, J.J. Luo, T Yamagata, 2007: How may tropical cyclones change in a warmer climate?. *Tellus A: Dynamic Meteorology and Oceanography*, **59A**, 539–561, https://doi.org/10.1111/j.1600-0870.2007.00251.x.

Bhatia, K., G. Vecchi, H. Murakami, S. Underwood, J. Kossin, 2018: Projected response of tropical cyclone intensity and intensification in a global climate model. *J. Climate*, **31,** 8281-8303, https://doi.org/10.1175/JCLI-D-17-0898.1.

Camargo, S.J., A.G. Barnston, P.J. Klotzbach, C.W. Landsea, 2007: Seasonal tropical cyclone forecasts. *WMO Bulletin*, **56**, 297-309.

Cheng, L., J. Abraham Z. Hausfather, K.E. Trenberth, 2019: How fast are the oceans warming? *Science Magazine*, **363**, 128–129.

City University of Hong Kong Laboratory of Atmospheric Research, 2019: Seasonal forecast of tropical cyclone activity. Accessed 28 May 2019, http://weather.cityu.edu.hk/tc_forecast/forecast.htm.

Climate Data Gateway at NCAR, 2018: CMIP5 output data for RCP. Accessed 22 August 2018, https://www.earthsystemgrid.org/dataset/ucar.cgd.ccsm4.cmip5.output.html.

Colbert, A.J., B.J. Soden, B.P. Kirtman, 2015: The impact of natural and anthropogenic climate change on western North Pacific tropical cyclone tracks. *J. Climate*, **28**, 1806–1823. https://doi.org/10.1175/JCLI-D-14-001100.1.

Colorado State University, 2019: Tropical meteorology project two-week forecast schedule. Accessed 24 May 2019, https://tropical.colostate.edu/forecasts/

Deser, C., A.S. Philips, M.A. Alexander, 2010: Twentieth century tropical sea surface temperature trends revisited. *Geophysical Research Letters*, **37**, 1–6, https://doi.org/10.1029/2010GL043321.

Dowdy, J.D., 2014: Long term changes in Australian tropical cyclone numbers. *Atmos. Sci. Let.*, **15**, 292–298, https://doi.org/10.1002/asl2.502.

Emanuel, K., R. Sundararajn, J. Williams, 2008: Hurricanes and global warming results from downscaling IPCC AR4 simulations. *Bull Am. Meteor. Soc.*, ***89,*** 347–367, https://doi.org/10.1175/BAMS-89-3-347.

European Centre for Medium-Range Weather Forecasts, 2019: Tropical Cyclones. Accessed 25 May 2019, https://www.ecmwf.int/en/forecasts/charts/latest-tropical-cyclones-forecast.

Ford, B. W., 2000: El Niño and La Niña effects on tropical cyclones: the mechanisms. M.S. thesis, Dept. of Meteorology, Naval Postgraduate School, 190 pp.

Friedman, L., M. Astor, 2019: We asked the 2020 democrats about climate change (yes, all of them). Here are their ideas. *New York Times*, 24 April 2019, https://www.nytimes.com/2019/04/18/us/politics/climate-change-democrats.html?rref=collection%2Fsectioncollection%2Fclimate&action=click&contentCollection=climate&region=rank&module=package&version=highlights&contentPlacement=1&pgtype=sectionfront.

Gent, P.R., and coauthors, 2011: The community climate system model version 4. *J. Climate*, **24**, 4973–4991, https://doi.org/10.1175/2011JCLI4083.1.

Gray, W. M., 1975: Tropical cyclone genesis. Dept. of Atmospheric Science, Colorado State University, 128 pp.

Gray, W.M., 1977: Tropical cyclone genesis in the western North Pacific. *J. of the Meteor. Society of Japan*, **55**, 465–482.

International Panel on Climate Change, 2019: Special Report: Global warming of 1.5° Celsius. Accessed 12 May 2019, https://www.ipcc.ch/sr15/chapter/chapter-1-pdf/.

International Panel on Climate Change DDC, 2019: Definition of terms used within the DDC pages. Accessed 29 May 2019, https://www.ipcc-data.org/guidelines/pages/glossary/glossary_r.html.

International Research Institute for Climate and Society, 2019: Climate and forecast products. Accessed 25 May 2019, https://iri.columbia.edu/our-expertise/climate/forecasts/.

Johnson, S.A., 2011. Modeling the impacts of interseasonal to interannual climate variations on tropical cyclone formations in the western North Pacific. M.S. thesis, Dept. of Meteorology, Naval Postgraduate School, 112 pp, http://hdl.handle.net/10945/5572.

JTWC, 2018: Western North Pacific Ocean best track data. Accessed 14 October 2018, https://www.metoc.navy.mil/jtwc/jtwc.html?western-pacific.

JTWC, 2019: Tropical cyclone support products and services. Accessed 14 May 2019, https://www.metoc.navy.mil/jtwc/jtwc.html?notices.

Knutson, T.R., and Coauthors, 2015: Global projections of intense tropical cyclone activity for the late twenty-first century from dynamical downscaling of CMIP5/RCP 4.5 scenarios. *J. Climate*, **28**, 7203–7224, https://doi.org/10.1175/JCLI-D-15-0129.1.

Knutson, T.R., R.E. Tuleya, 2008: Tropical cyclone and climate change: revisiting recent studies at GFDL, *Climate Extremes and Society*, H.F. Diaz, Cambridge University Press, 120-144.

Koneswaran, G., D. Nierenberg, 2008: Global farm animal production and global warming: impacting and mitigating climate change. *Environmental Health Perspectives*, **115**, 578-582, https://doi.org/10.1289/ehp.11034.

Kossin, J.P., K.A. Emanuel, S.J. Camargo, 2016: Past and projected changes in western north Pacific tropical cyclone exposure. *J. Climate*, 5725–5739, https://doi.org/10.1175/JCLI-D-16-0076.1.

Kuhn, A., 2018: The U.S. positions warships in tense Asia-Pacific waters. National Public Radio, accessed 13 January 2019, https://www.npr.org/sections/parallels/2018/03/02/589876233/the-u-s-positions-warships-in-tense-asia-pacific-waters.

Landsea, C.W., J.L. Franklin, 2013: Atlantic hurricane database uncertainty and presentation of a new database format. *Monthly Weather Review*, **141**, 3576–3592.

Meehl, G.A., and coauthors, 2012: Climate system response to external forcings and climate change projections in CCSM4. *J. Climate* ,**25**, 3661–3683, https://doi.org/10.1175/JCLI-D-11-00240.1.

Meyer, D.W., 2007: Relationships between global warming and tropical cyclone activity in the western North Pacific. M.S. thesis, Dept. of Meteorology, Naval Postgraduate School, 139 pp.

Meyer, D., T. Murphree, 2015: A dynamical-statistical approach to forecasting tropical cyclogenesis in the Western North Pacific. *Proceedings of the 2015 Cincinnati-Dayton INFORMS Symposium*, 1-12. http://hdl.handle.net/10945/48206.

Montgomery, M.T., B.F. Farrell, 1993: Tropical cyclone formation. *Am. Meteor. Society*, **50,** 285**–**310.

Mundhenk, B.D., 2009: A statistical-dynamical approach to intraseasonal prediction of tropical cyclogenesis in the western North Pacific. M.S. thesis, Dept. of Meteorology, Naval Postgraduate School, 190 pp.

Nakamura, J., and Coauthors, 2017: Western North Pacific tropical cyclone model tracks in present and future climates. *Journal of Geophysical Research: Atmospheres*, **122**, 9721–9744, https://doi.org/10.1002/2017JD027007.https://doi.org/10.1029/2009JD013058.

National Hurricane Center, 2019: Atlantic 5-day graphical tropical weather outlook. Accessed 25 May 2019, https://www.nhc.noaa.gov/gtwo.php.

NOAA CPC, 2019: Global Tropics Hazards and Benefits Outlook. Accessed 7 May 2019, https://www.cpc.ncep.noaa.gov/products/precip/CWlink/ghazards/.

NOAA ESRL, 2019: Multivariate ENSO Index Version 2. Accessed 10 February 2019, https://www.esrl.noaa.gov/psd/enso/mei/.

NOAA National Center for Environmental Information, 2018: Climate forecast system. Accessed 15 August 2018, https://www.ncdc.noaa.gov/data-access/model-data/model-datasets/climate-forecast-system-version2-cfsv2.

NOAA NHC, 2019: Northeast and north central Pacific hurricane database (HURDAT2) 1949–2017. Accessed 7 January 2019, https://www.nhc.noaa.gov/data/#hurdat.

NRL Monterey, 2019: NRL tropical cyclone page. Accessed 14 April 2019, https://www.nrlmry.navy.mil/tc-bin/tc_home2.cgi.

Overpeck, J.T., G.A. Meehl, S. Bony, D.R. Easterling, 2011: Climate data challenges in the 21st century. *Science Magazine*, **331,** 700–702.

Patricola, C., M. Wehner, 2018: Anthropogenic influences on major tropical cyclone events. *Nature*, **563**, 339–346, https://doi.org/10.1038/s41586-018-0673-2.

Saha, S. and Coauthors, 2006: The NCEP climate forecast system. *J. Climate*, **19,** 3483–3517. https://doi.org/ 10.1175/JCLI3812.1.

Saha, S. and Coauthors, 2010: The NCEP climate forecast system reanalysis. *Am. Meteor. Society*, 1016–1056. https://doi.org/10.1175/2010BAMS3001.1.

Saha, S. and Coauthors, 2014: The NCEP Climate Forecast System Version 2. *J. Climate*, **27**, 2185–2208, http://dx.doi.org/10.1175/JCLI-D-12-00823.1.

Sharmila, S., J.E. Walsh, 2018: Recent poleward shift of tropical cyclone formation linked to Hadley cell expansion. *Nature Climate Change*, **8,** 730–736.

Song, J.J., Y. Wang, L. Wu 2010: Trend discrepancies among three best track data sets of western North Pacific tropical cyclones. *Journal of Geophysical Research*: Atmospheres, **115**, 1-9.

Statistical Solutions LLC, 2019: Western North Pacific TC forecasts. Accessed 12 April 2019, http://www.statisticalsolutionsllc.com/western-north-pacific-formation-forecasts.html.

van den Dool, H., 2007: *Empirical methods in short-term climate prediction*, Oxford University Press, 215 pp.

Van Vuuren, D.P., and coauthors, 2011: The representative concentration pathways: An overview. *Climatic Change*, **109**, 5–31, https://doi.org/10.1007/s10584-011-0148-z.

Wang R., L. Wu, C. Wang, 2011: Typhoon track changes associated with global warming. *J. Climate*, **24**, 3748–3752, https://doi.org/10.1175/JCLI-D-11-00074.1.

THIS PAGE INTENTIONALLY LEFT BLANK

INITIAL DISTRIBUTION LIST

1. Defense Technical Information Center
   Ft. Belvoir, Virginia

2. Dudley Knox Library
   Naval Postgraduate School
   Monterey, California